Photovoltaic generation with energy storage integrated into the electric grid: Modelling, simulation and experimentation

Luis André Pereira Fialho

Tese apresentada à Universidade de Évora
para obtenção do Grau de Doutor em Engenharia Mecatrónica e Energia

ORIENTADOR: *Manuel Collares-Pereira*

EVORA, Fevereiro 2019

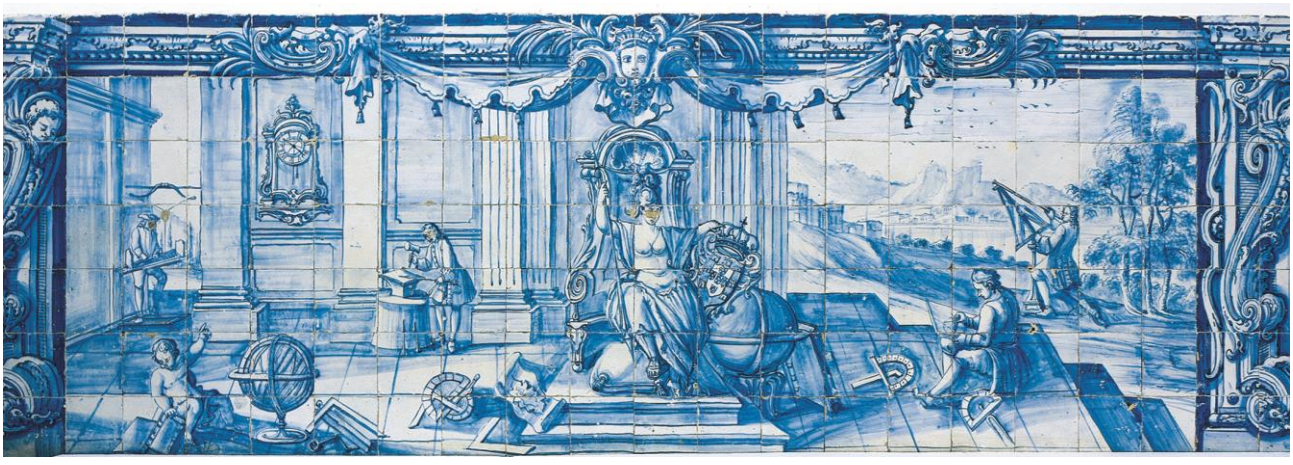

INSTITUTO DE INVESTIGAÇÃO E FORMAÇÃO AVANÇADA

Title | Photovoltaic generation with energy storage integrated into the electric grid: Modelling, simulation and experimentation

Photovoltaic generation with energy storage integrated into the electric grid: Modelling, simulation and experimentation

Luis André Pereira Fialho

Orientador | Manuel Collares Pereira

Tese apresentada à Universidade de Évora para obtenção do Grau de Doutor em Engenharia Mecatrónica e Energia

Évora, 2019

This page is intentionally left blank.

Acknowledgements

“No man is an island entire of itself”.

This work would not have been possible without the support of many people, to whom I owe special thanks.

First, to Carla, for the immense hours and patience to put up with me, trough the daily obstacles, but also for sharing the victories and happy moments.

To my parents, my sister and my family, for being always on my side, my support and my roots.

To my invaluable and patient advisor, Prof. Manuel Collares Pereira, for having always supported and encouraged me, keeping the bearing towards the sun. His guidance and mentoring are always an inspiration and without which none of this would be possible.

With a special mention to all the team of the Renewable Energies Chair. It is a fantastic opportunity to work in our facilities with you, sharing countless laughs and challenging moments. Thank you for teaching me so much.

I would also like to extend my thanks to the IIFA staff, for their complete availability to help me wherever it was needed.

Contents

Photovoltaic generation with energy storage integrated into the electric grid: Modelling, simulation and experimentation

Conversão fotovoltaica com armazenamento de energia integrado em rede elétrica: modelação, simulação e experimentação

Resumo

Esta tese apresenta o trabalho e resultados da investigação desenvolvida sobre conversão fotovoltaica com armazenamento de energia integrado em rede elétrica. Começa por apresentar a modelação, simulação e validação da conversão fotovoltaica e inversores com injeção para a rede. Descreve também seguidamente o processo de conceção, construção, comissionamento e desenvolvimento experimental das infraestruturas hoje existentes na Cátedra Energias Renováveis da Universidade de Évora, no que diz respeito às duas microgrids desenvolvidas no âmbito do projeto europeu PVCROPS. Estas microgrids são compostas, de forma geral, por um elemento de produção fotovoltaica, um elemento de armazenamento de energia, uma ligação à rede e um sistema de controlo e *datalogging*. Relativamente ao armazenamento de energia, esta tese aborda e caracteriza ainda as duas tecnologias instaladas: a bateria de iões de lítio e a bateria de fluxo redox de vanádio. Estas microgrids servem assim para implementação e validação de uma estratégia de gestão de energia tendo como objetivo a maximização do autoconsumo, cujos conteúdos são apresentados no capítulo 4. Depois das conclusões, no último capítulo, apontam-se ainda as linhas de investigação futuras de maior potencial, na sequência do trabalho desenvolvido e apresentado nesta tese.

Palavras-chave

Sistemas Fotovoltaicos, Armazenamento de energia, Bateria de Fluxo Redox de Vanádio, Bateria de Lítio, Estratégias de Gestão de Energia.

Photovoltaic generation with energy storage integrated into the electric grid: Modelling, simulation and experimentation

Abstract

This thesis presents the work and results of the research developed on photovoltaic conversion with energy storage integrated into the electric grid. It begins by presenting the modeling, simulation and validation of the photovoltaic conversion and inverters with injection into the electric grid. It also describes the process of design, construction, commissioning and experimental development of the existing infrastructures in the Renewable Energies Chair of the University of Évora, with respect to the two microgrids developed under the European project PVCROPS. These microgrids are generally composed by a photovoltaic production element, an energy storage element, a grid connection and a control and datalogging system. Regarding energy storage, this thesis also discusses and characterizes the two installed technologies: the lithium-ion battery and the redox-flow vanadium battery. These microgrids thus serve to implement and validate an energy management strategy with the objective of maximizing self-consumption, the contents of which are presented in Chapter 4. Following the conclusions, in the last chapter are pointed the future research lines of greater potential, following the work developed and presented in this thesis.

Keywords

Photovoltaic Systems, Energy Storage, Vanadium Redox Flow Battery, Lithium-Ion Battery, Energy Management Strategies.

List of scientific papers

This thesis includes the following papers:

L. Fialho, T. Fartaria, L. Narvarte, M. Collares-Pereira, “Implementation and Validation of a Self-Consumption Maximization Energy Management Strategy in a Vanadium Redox Flow BIPV Demonstrator”, Energies, Vol. 9, pp. 496, 2016. (**Chapter 4, Section 4.2**)
http://dx.doi.org/10.3390/en9070496

L. Fialho, R. Melício, V.M.F. Mendes, M. Collares-Pereira, "Simulation of a-Si PV system linked to the grid by DC boost and three-level inverter under cloud scope", Technological Innovation for Cloud-based Engineering Systems, DoCEIS 2015 Proceedings, Vol. 450, pp. 423-430, 2015. (**Chapter 2, Section 2.6**)
https://doi.org/10.1007/978-3-319-16766-4_45

L. Fialho, R. Melício, V.M.F. Mendes, A. Estanqueiro, M. Collares-Pereira, “PV systems linked to the grid: Parameter identification with a heuristic procedure”, Sustainable Energy Technologies and Assessments, Vol. 10, pp. 29-39, June 2015. (**Chapter 2, Section 2.2**)
http://dx.doi.org/10.1016/j.seta.2015.01.006

L. Fialho, R. Melício, V.M.F. Mendes, A. Estanqueiro, "Simulation of a-Si PV System Grid Connected by Boost and Inverter", International Journal of Renewable Energy Research, Vol.5, N°.2, pp. 443-451, May 2015. (**Chapter 2, Section 2.5**)
http://hdl.handle.net/10174/16472

L. Fialho, R. Melício, V. M. F. Mendes, J. Figueiredo, M. Collares-Pereira, "Amorphous Solar Modules Simulation and Experimental Results: Effect of Shading", Technological Innovation for Collective Awareness Systems, DoCEIS 2014 Proceedings, Vol. 423, pp. 315-323, 2014. (**Chapter 2, Section 2.3**)
http://link.springer.com/chapter/10.1007%2F978-3-642-54734-8_35

L. Fialho, R. Melício, V.M.F. Mendes, S. Viana, C. Rodrigues, A. Estanqueiro, "A simulation of integrated photovoltaic conversion into electric grid", Solar Energy, vol. 110, pp. 578-594, 2014. (**Chapter 2, Section 2.4**)
http://dx.doi.org/10.1016/j.solener.2014.09.041

Also published with blind peer review (not included in this thesis):

Ricardo Conceição, Hugo G. Silva, José Mirão, Michael Gostein, Luis Fialho, Luis Narvarte, Manuel Collares-Pereira, “Saharan dust transport to Europe and its impact on photovoltaic performance: A case study of soiling in Portugal”, Solar Energy, Vol. 160, pp. 94–102, 2018.
https://doi.org/10.1016/j.solener.2017.11.059

L. Fialho, R. Melicio, V.M.F. Mendes, “Poly-Si PV system grid connected and fuzzy controlled”, EUROCON 2015 - International Conference on Computer as a Tool (EUROCON), IEEE, Salamanca, pp. 1-6,

September 2015.
http://dx.doi.org/10.1109/EUROCON.2015.7313668

L. Fialho, R. Melício, V.M.F. Mendes, J. Figueiredo, M. Collares-Pereira, "Effect of shading on series solar modules: simulation and experimental results", Procedia Technology (Elsevier), Vol. 17, pp. 295–302, 2014.
https://doi.org/10.1016/j.protcy.2014.10.240

L. Fialho, R. Melício, V.M.F. Mendes, L. Rodrigues, S. Viana, and A. Estanqueiro, "Simulation of a-Si PV System Linked to the Grid by DC-DC Boost and Two-level Converter", 16th International Power Electronics and Motion Control Conference and Exposition – PEMC 2014, Antalya, Turkey, pp. 21-24, September 2014.
http://ieeexplore.ieee.org/xpl/articleDetails.jsp?arnumber=6980627%2F06980627

L. Fialho, R. Melício, V.M.F. Mendes, "PV system modeling by five parameters and in situ test", SPEEDAM International Symposium on Power Electronics, Electrical Drives, Automation and Motion, pp. 577-582, 2014.
http://ieeexplore.ieee.org/xpl/articleDetails.jsp?arnumber=6872097

Submitted papers (currently under peer review):

Ricardo Conceição, Hugo G. Silva, Luis Fialho, Francis M. Lopes, Manuel Collares-Pereira, “PV system design with the effect of soiling on the optimum tilt angle”, Renewable Energy, 2018.

List of conference posters

This thesis includes the following conference posters in the annexes:

Marios Theristis, Carolina Senabre, Emilio Gómez, Sonia Pinto, Luis Fialho, Emilio Muñoz, JonathanLeloux, “EU COST Action PEARL-PV: Performance and Reliability of Photovoltaic Systems: Evaluations of Large-Scale Monitoring Data WG5: PV in grids”, Conference 2018 NREL/SNL/BNL PV Reliability Workshop, USA.
https://doi.org/10.13140/RG.2.2.24190.48963

Luis Fialho, Tomás Fartaria, Manuel Collares Pereira, “Validation of a Energy Management Strategy for a BIPV System with a Vanadium Battery Demonstrator”, EU PVSEC 2015, European PV Solar Energy Conference and Exhibition, Hamburg, Germany.

Luis Fialho, Tomás Fartaria, Manuel Collares Pereira, Aitor Makibar, “Validation of a Energy Management Strategy for a BIPV System with a Lithium Ion Battery Demonstrator”, EU PVSEC 2015, European PV Solar Energy Conference and Exhibition, Hamburg, Germany.

Luis Fialho, Tomás Fartaria, Manuel Collares Pereira, “Performance Characterization of a Vanadium Redox Flow Battery”, EU PVSEC 2015, European PV Solar Energy Conference and Exhibition, Hamburg, Germany.

Submitted conference posters (currently under review):

A.B. Cristóbal, A. Martí, L. Navarte, I. Antón, G. Revuelta, L. Fialho, D. Hernández, R. Schwald, M. Ackermann, N. Tyutyundzhiev, I. Cuesta, E. Unger, B. Müller, R. Zilles and Carlos del Cañizo “Putting Open Science into Practice: The Photovoltaic Sector”. To be presented as a poster at the B-Debate “Open science: from values to practice. Building a roadmap for transformative change”. Barcelona, 4th-5th October 2018.

List of figures

Note: The figures of the scientific papers included in the chapters of this thesis are not included in this list to preserve all the formatting and numbering of the papers, presenting them as published in the journals.

Acronyms

AC	Alternating Current
BEV	Battery Electric Vehicle
BIPV	Building Integrated PhotoVoltaics
BoS	Balance of System
CAPEX	CAPital EXpenditure
CPV	Concentrating Photovoltaics
CSP	Concentrated Solar Power
DC	Direct Current
DOD	Depth of Discharge
DSM	Demand Side Management
DSO	Distribution System Operator
DSO	Distribution System Operator
EC	European Commission
EMS	Energy Management Strategy
EPC	Engineering, Procurement and Construction
ESS	Energy Storage System
EU	European Union
EV	Electric Vehicle
FIT	Feed-In Tariff
GPS	Global Positioning System
HMI	Human Machine Interface
IEEE	Institute of Electrical and Electronics Engineers
IGBT	Insulated-Gate Bipolar Transistor
IoT	Internet of Things
IT	Information Technology
KPI	Key Performance Index
LCoE	Levelized Cost of Energy (in €/kWh)
LIB	Lithium-Ion Battery
MPP	Maximum Power Point
MPPT	Maximum Power Point Tracking
NOCT	Normal Operating Cell Temperature
O&M	Operation and Maintenance
OPEX	OPerational Expenditure
PC	Personal Computer
PERC	Passivated Emitter and Rear Cell
PERL	Passivated Emitter Rear Locally-diffused solar cell

PHEV	Plug-in Hybrid Electric Vehicle
PID	Potential-Induced Degradation
PLC	Programmable Logic Controller
PPA	Power Purchase Agreement
PR	Performance Ratio
PV	Photovoltaic
PVCROPS	PhotoVoltaic Cost reduction, Reliability, Operational performance, Prediction and Simulation
PWM	Pulse Width Modulation
RES	Renewable Energy Sources
RMS	Root Mean Square
SCADA	Supervisory Control and Data Acquisition
SME	Small and Medium Enterprises
SMES	Superconducting Magnetic Energy Storage
SOC	State of Charge
STC	Standard Testing Conditions
TCO	Transparent Conductive Oxide
TCP/IP	Transmission Control Protocol / Internet Protocol
THD	Total Harmonic Distortion
TSO	Transmission System Operator
UEvora	University of Évora
UPS	Uninterruptible Power System
V2G	Vehicle to Grid
VRFB	Vanadium Redox Flow Battery

CHAPTER 1. Introduction

1.1 Motivation

In Greek mythology, Prometheus defies the gods by stealing fire and giving it to humanity, an act that enabled progress and civilization. Throughout history, humankind has been able to utilize energy in ways that other species have failed to attain, differentiating us as the dominant species on the planet. Developments in the production and use of energy have improved the economic and social aspects of our lives, influencing everything from quality of life and health to science and research.

However, the growth of humanity and the use of energy has left us in an increasingly fragile equilibrium with our planet. The use of non-renewable resources, at a rapid rate of acceleration since the industrial revolution, for the energy production of the growing world population places us facing a critical problem. These finite resources are being depleted and carbon emissions continue to cause large-scale environmental impacts. [1]

The extraction, transport and burning of fossil fuels often have negative impacts not visible in our daily lives. The extraction and transport of natural gas, for example, is often accompanied by important leaks of its main component, methane. Methane is a much more potent greenhouse gas than carbon dioxide, about 34 times more effective at trapping heat over a 100-year timescale and 86 times more effective over a 20-year timescale [2]. Also, the transport of these fossil fuels often has other disastrous environmental consequences for ecosystems such as the known examples of Exxon Valdez's spill of 262 000 barrels of oil in 1989 or the Prestige oil spill in 2002, releasing 64 000 tonnes of oil and affecting Portugal, Spain and France with this black tide. Also, burning fossil fuels emits several air pollutants as SO_2, NOx or particulate matter, increasing respiratory problems as asthma, pulmonary infections or other chronic respiratory diseases with direct consequences on human health and lifespan.

However, humanity is taking action and facing the energy challenge with sustainable energy resources. In the past decades, global perceptions of renewable energy changed considerably and is viewed today as a tool for improved energy security, mitigation for climate change and a secure investment. Declining costs in recent years played a significant role in this expansion, being today cost competitive with fossil energy sources. [3]

Renewable energies as wind, tidal, hydropower, geothermal or solar represent a sustainable alternative with added advantages. Solar energy in particular is a vast and clean resource, a real alternative to fossil fuels.

The total solar energy reaching our planet far exceeds mankind’s total primary energy needs. An indication of the abundance of solar energy is, paradoxically, the threat of climate change itself. Solar energy technologies are coming of age and are increasingly cost competitive with conventional fuels.

Active solar technologies use photovoltaics (PV), concentrated solar power (CSP), solar thermal collectors and convert solar radiation into useful outputs. Passive solar techniques include selecting materials with favourable thermal properties, passive solar heating and

cooling/ventilation for buildings, natural illumination, etc. Active solar technologies increase the supply of energy and are considered supply side technologies, while passive solar technologies reduce the need for alternate resources and are generally considered demand side technologies. Solar fuels production, as hydrogen or other fuels should also be considered a potential to be explored, being attractive candidates for research and development. [4]

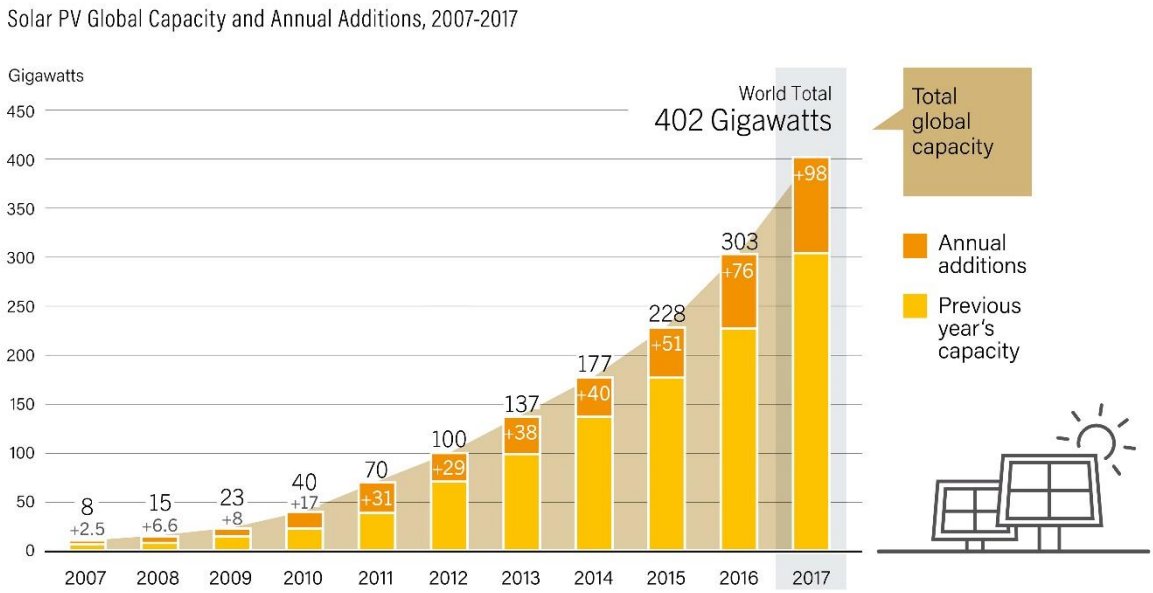

Figure 1: Global photovoltaic installed power evolution [5]

Global photovoltaic installed power in 2015 has reached 227 GW (Figure 1). Solar PV is a fast-growing market, with emerging countries starting to contribute to the global share. Rising demand for electricity and lower costs improve the market competitiveness for this technology. [5]

Solar PV already plays a substantial role in electricity generation in some countries. Once the share of electricity generated from variable renewable sources increases in our energy grids, it becomes necessary to compensate for generation shortages when resources are not available. Nonetheless, besides the need for storage technologies to replace parts of the power grid or support integration of large shares of variable solar power, a wide range of tasks are required today for the energy storage technologies to perform. There are numerous concepts today, from a decentralized approach where consumers consume, produce, and store their energy (prosumer) locally up to large grid support power storage facilities.

Storage technology is also now available at different stages of development, variable scale projects, and for meeting both short and long-term energy storage needs. Short-term storage technologies can compensate for output fluctuations ranging from milliseconds up to a few hours, whereas longer term or seasonal storage technologies can bridge the gap over several weeks (Figure 2) [6].

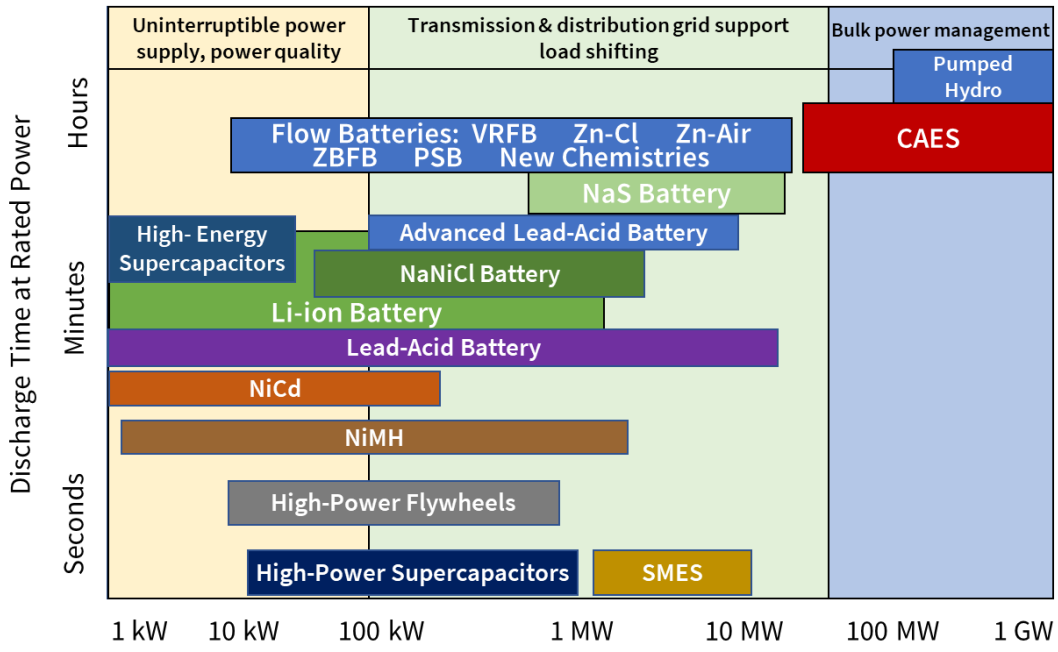

Figure 2: Positioning of different energy storage technologies [7]

Figure 2 legend: *Zn-Cl = zinc chlorine flow battery; Zn-Air = zinc air flow battery; ZBFB = zinc bromine flow battery; VRFB = vanadium redox flow battery; PSB= polysulfide bromine flow battery; NaS = sodium sulphur; NaNiCI = sodium nickel chloride; NiCd = nickel cadmium; NiMH = nickel–metal hydride; SMES = superconducting magnetic energy storage*.

Energy storage applications are increasing and range from bulk energy services as energy time shifting or on-site power, ancillary services as power quality and reliability (frequency, voltage regulation), black start, electric bill management or increased self-consumption, peak shaving, increased resilience of grids (e.g. stability of micro/minigrids), demand response, reliability of grid connected residential systems, the transport sector, etc.

In the transport sector, electric mobility still has a very marginal share, with electric vehicles (EV's) representing less than 0.1% of the global vehicle fleet [8]. Most electric vehicles are still hybrid electric, generating electricity from recovering braking energy and with small electrochemical batteries. In some countries such as China, the Netherlands, Norway and the United States, plug-in hybrid-electric vehicles (PHEV's) and battery-electric vehicles (BEV's) have increased their sales numbers in the last few years with some countries already stating their will to completely ban fossil fuels vehicles in the future. Norway's National Transport Plan 2018–2029 already states that all the new passenger cars and light vans sold in 2025 shall be zero-emission vehicles. [9]

In the last 20 years electrochemical storage facilities have grown significantly (Figure 3) due to investments stimulated by decreasing costs and improved performance.

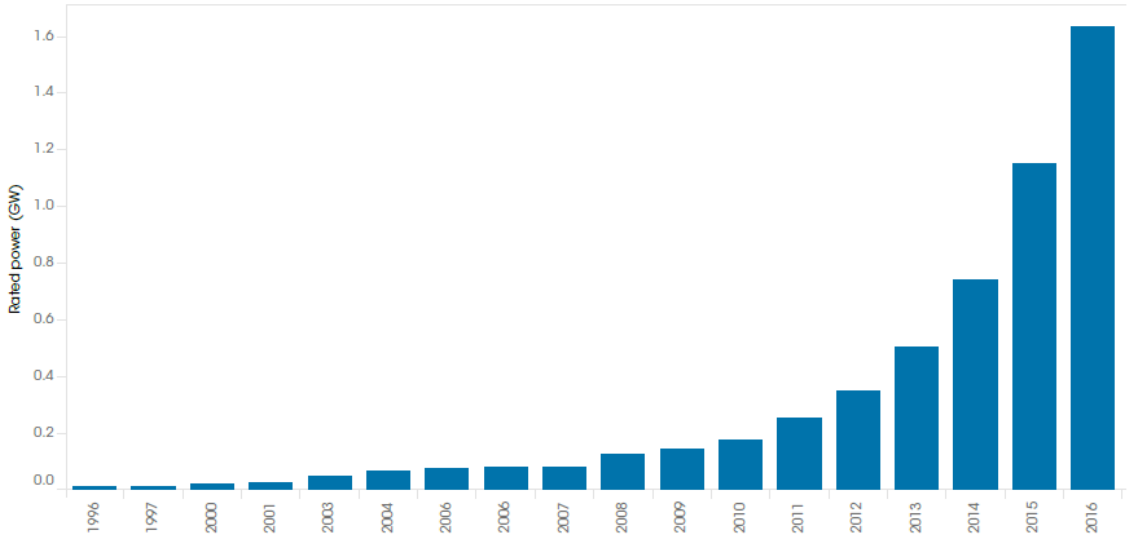

Figure 3: Global electrochemical storage installed power, 1996-2016 [10]

Massive investments in lithium-ion battery technology (also driven by the electric mobility market) have led to lower costs associated with greater experience and know-how in setting up ever-increasing scale projects. The current dominance of the market share on the electrochemical storage technology belongs to the lithium-ion technology. However, alternative electrochemical storage technologies offer advantages of great evolutionary potential. The two main flow battery technologies (vanadium redox flow and zinc bromine flow) offer valuable operational advantages, as they can operate at ambient temperatures, and their power and energy storage characteristics are independently scalable. [11]

The recent energy storage developments are driven by more favourable markets and regulation, increased access to financing and the aging energy grid infrastructure. Nevertheless, there is a long way to go for their uptake by the market and for them to achieve their full potential. Some issues still need to be addressed involving bankability and trust of traditional financiers; the need to develop codes, standards and regulations for novel battery types and the development of new commercial and industrial applications for the new storage technologies. [12]

The last years brought advances in enabling technologies, such as hardware and software to support the integration of renewable energy. These included management systems aimed to optimise performance and energy storage. In the last few years, new technological concepts have emerged, such as the Internet of Things (IoT), blockchain technology, smart grids, vehicles as non-stationary batteries - vehicle to grid (V2G), higher performance PV modules (PERC/PERL cells, heterojunction cells, rear contact cells), floating PV plants...

Solar energy is in constant state of innovation with energy storage capabilities under development that will enable renewable energy sources like solar to play a larger role on our electric grid. The excitement to discover new and forward-looking ways to think about the future in a sustainable way is the main driver behind this work.

1.2 Research questions

Solar energy is a very active field of research and development. This work intendeds to find answers to several questions not clearly solved by the state of the art. The work methodology of this thesis was to follow these questions, which, in turn, guided and also provided new interrogations.

- How to model and simulate the photovoltaic modules with limited data?
- How to model and simulate the PV module integrated with inverter and the grid?
- How to experimentally characterize and rehearse different battery technologies?
- How to model and develop an optimized energy management strategy for a BIPV and grid integration, maximizing self-consumption?
- How to experimentally validate an effective energy management strategy for a microgrid with BIPV and energy storage? Is it possible to replicate it and implement it with different ESSs?
- How to plan and design a smart microgrid with energy storage, demonstrating with real conditions and real scale environment? How to install and commission these systems? How to manage the operation and maintenance of these two different microgrids?

The results achieved lead to several papers with answers that, by no means are claimed to be neither definitive or complete, but can certainly be seen as an initial contribution.

1.3 Thesis structure

The work for this thesis began with an approach to the question related to the modelling and simulation of a photovoltaic conversion and inverter, injecting to the grid. How to accurately model and simulate the photovoltaic conversion with a similar I-V curve requiring only the usual limited data provided by the manufacturers? How to validate the simulation results? An initial model for the identification of the five key parameters of the one diode equivalent electric model is presented in the first two papers of Chapter 2. Also, a study about the usage of this model and its behaviour with a gradually shaded PV plant was done and presented in the second paper of this Chapter.

The model has then evolved to a more accurate one, presented and validated in the last three papers presented in Chapter 2. These papers also present the models, firstly for the two-level converter and secondly for three level inverters, developed and integrated with the previous PV model and injecting into the grid.

Chapter 3 presents the installation and commissioning of the UEvora microgrids within the scope of the PVCROPS project. It includes the technical specifications of the systems of the microgrids, details about their programming and communication scheme and the outcomes of these infrastructures as well as its current status. Chapter 3 was included in this thesis since the scientific papers cannot clearly express the majority of the work time spent for the experimental and validation results of this thesis. Chapter 3 contains and explains the substantial effort made to provide the Renewable Energies Chair with an important capacity for the study of the

interfaces in BIPV, including innovative electric storage solutions. Experimental work of this nature is, on one side, a quite time-consuming process, implying unforeseen technical issues and inflating research costs. On the other side, it provides a higher control level enabling to replicate natural settings at faster speeds and providing real validation results. The work in question offered a valuable in-depth knowledge and experience on smart microgrid challenges and on how to overcome them. This chapter also presents the commercial and scientific outcomes for the project partners such as new product designs.

Chapter 4 presents the results of the characterization and performance tests as well as the energy management strategy rehearsal and validation. The EMS was modelled and developed taking into account real characterization parameters from the VRFB and LIB initial tests. The objective of the EMS within the paper presented is to maximize the self-consumption of PV energy. Several merit factors are introduced and used to assess the EMS results. Additional performance tests for the VRFB and LIB and EMS validation results with the LIB are presented in three conference posters, included in the annexes.

Chapter 5 points overall conclusions synthesizing the various issues and pointing a general work assessment. Intermediate and specific conclusions are drawn in each paper presented.

Chapter 6 discuss briefly future research lines regarding photovoltaic solar energy, PV systems as well as the integration of new electrochemical energy storage. Research opportunities and technology challenges are discussed envisaging a future powered by photovoltaic energy.

Where appropriate the thesis has its main body incorporating directly the scientific papers produced with relevance to each chapter, keeping in full the citation and bibliographic styles of the journals. Additional published papers (previously indicated) were also published with blind peer review on topics related to this thesis, but for simplicity and clarity sake were not included here. The published conference posters were included in the annexes.

References

[1] Comprehensive Energy Systems, Vol. 1, Part A, Energy Fundamentals, Ibrahim Dincer, Elsevier 2018.

[2] Myhre, G., D. Shindell, F.-M. Bréon, W. Collins, J. Fuglestvedt, J. Huang, D. Koch, J.-F. Lamarque, D. Lee, B. Mendoza, T. Nakajima, A. Robock, G. Stephens, T. Takemura and H. Zhang (2013), Anthropogenic and Natural Radiative Forcing. In: Climate Change 2013: The Physical Science Basis. Contribution of Working Group I to the Fifth Assessment Report of the Intergovernmental Panel on Climate Change.

[3] IRENA, IEA and REN21 (2018), 'Renewable Energy Policies in a Time of Transition'. IRENA, OECD/ IEA and REN21.

[4] International Energy Agency, Cédric Philibert (2005), The present and future use of solar thermal energy as a primary source of energy, Paris, France.

[5] IEA PVPS (2018), 2018 Snapshot of global photovoltaic markets.

[6] REN21 (2017), Renewables Global Futures Report: Great debates towards 100% renewable energy.

[7] US DOE/EPRI (2015), DOE/EPRI Electricity Storage Handbook 2015, Sandia National Laboratories.

[8] OECD/IEA (2017), Global EV Outlook 2017. Two million and counting, International Energy Agency [Online]. Available at https://www.iea.org/publications/freepublications/publication/GlobalEVOutlook2017.pdf (Accessed 1 October 2017).

[9] Norwegian Ministry of Transport and Communications, 2016-2017, National Transport Plan 2018–2029 [Online]. Available at https://www.regjeringen.no/contentassets/7c52fd2938ca42209e4286fe86bb28bd/en-gb/pdfs/stm201620170033000engpdfs.pdf (Accessed 14 May 2018).

[10] US DOE Global Energy Storage Database (2018) [Online]. Available at http://www.energystorageexchange.org/projects (Accessed 14 May 2018).

[11] IRENA (2017), Electricity Storage and Renewables: Costs and Markets to 2030, International Renewable Energy Agency, Abu Dhabi.

[12] Paul Robson and Davide Bonomi (2018), Growing The Battery Storage Market 2018: Exploring Four Key issues, DUFRESNE – ENERGY STORAGE WORLD FORUM.

CHAPTER 2. PV conversion and Inverters – modelling, simulation and validation

2.1 Introduction

This chapter presents the initial work done for this thesis. Five scientific published papers are presented in this chapter about the PV conversion modelling and obtaining the I-V and P-V curves with two different models with unknown parameters identification. These papers also show the modelling of the power electronic converters and injection to the grid. All the models are then validated and compared with experimental results. Partial shading is also simulated in the second paper (Section 2.3) within this chapter. Additional papers were also published on these topics but were not included in this thesis for clarity sake and improved readability. All the papers were published with blind peer review.

2.2 PV systems linked to the grid: parameter identification with a heuristic procedure

L. Fialho[1], R. Melício[2,3], V.M.F. Mendes[3,4], A. Estanqueiro[5], M. Collares-Pereira[1]

In Journal Sustainable Energy Technologies and Assessments, Vol. 10, pp. 29-39, 2015.
http://dx.doi.org/10.1016/j.seta.2015.01.006.

Abstract
This paper focuses on a PV system linked to the electric grid by power electronic converters, identification of the five parameters modeling for photovoltaic systems and the assessment of the shading effect. Normally, the technical information for photovoltaic panels is too restricted to identify the five parameters. An undemanding heuristic method is used to find the five parameters for photovoltaic systems, requiring only the open circuit, maximum power, and short circuit data. The I-V and the P-V curves for a monocrystalline, polycrystalline and amorphous photovoltaic systems are computed from the parameters identification and validated by comparison with experimental ones. Also, the I-V and the P-V curves under the effect of partial shading are obtained from those parameters. The modeling for the converters emulates the association of a DC-DC boost with a two-level power inverter in order to follow the performance of a testing commercial inverter employed on an experimental system.

Keywords: **PV system; Power electronics; Parameter identification; Shading effect; Modeling, Simulation and experimental results.**

[1] Renewable Energies Chair, Universidade de Évora, 7002-554 Évora, Portugal
[2] IDMEC/LAETA, Instituto Superior Técnico, Universidade de Lisboa, Lisbon, Portugal
[3] Department of Physics, Universidade de Évora, Largo dos Colegiais 2, 7004-516 Évora, Portugal
[4] Department of Electrical Engineering and Automation, Instituto Superior de Engenharia de Lisboa, R. Conselheiro Emídio Navarro, 1950-062 Lisbon, Portugal
[5] National Laboratory of Energy and Geology, Estrada do Paço do Lumiar, 1649-038 Lisbon, Portugal

1. Introduction

The demand for sources of sustainable energy, the shortage of fossil fuels and the need for carbon footprint reduction have resulted in a global awareness of the importance of alternative energy sources and efficiency in the use of energy [1]. Renewable energy sources are likely to have a significant role in the world energy supply in the upcoming future. Among the renewable energy sources, solar energy has ubiquity and abundance [2,3]. Hence, if technology find is way through the development of cheaper converts of solar into electric energy and with better efficiency, solar energy will eventually be the most important source of sustainable energy for power supply, delivering energy in the neighborhood of where it is needed [4,5].

Apart from the solar thermal exploitation, the spreading of PV systems is being encouraged by delivering energy in the neighborhood of where it is needed tariffs and by the price drop in crystalline cells [6]. At present, significant photovoltaic (PV) deployment has occurred, particularly in Germany, Spain and Japan [7]. PV energy has exceptional conditions in Portugal to be exploited, because this European country has significant levels of solar radiation to go into exploitation. Sunshine hours in the mainland of Portugal vary between 1800 and 3100 hours per year [8]. Hence, the country has a huge potential for solar energy exploitation, the biggest PV system is in Moura, with an installed capacity of 46 MWp.

A PV system directly converts solar energy into direct electric current energy. Solar cells are made of several types of semiconductors using different manufacturing processes [9]. The energy converted by a solar cell depends on the substrate properties, on the temperature of the junction and on the incoming solar radiation [10], known as irradiation. The solar radiation is composed of photons with different levels of energy. But not all photons are useful in order to originate the photo current, the remainder energy passes by or is adsorbed as thermal agitation, contributing to the definition of the temperature on the solar cell [11].

A PV array may be either a panel or a set of panels connected to form large PV systems with or without tracking systems. But, even with tracking systems a correct consideration of the space for the operational neighborhood have to be assessed to avoid mutual shading.

Power-electronic converters are usually used to process the direct electric current coming from PV system, for instance, are used as inverters to deliver an alternate current and may be used to: regulate the voltage and current at the load, control the power flow in grid-connected systems and implement maximum power point tracking (MPPT) [12,13]. Generally, the energy conversation by a PV system is assumed to be in a tight neighborhood of the maximum power point due to the MPPT. Hence, the normal useful working portion on I-V characteristic is in the neighborhood of maximum power, so the tuned curve should have higher precision at this portion [13]. Hence, this is an important point to be considered in the identification of the equivalent parameters of a model for the I-V characteristic.

The shading on the PV panel, for instances, due to a passing cloud or neighboring buildings causes not only energy loss in the conversion, but also further non-linearity on the I-V characteristics [14,15]. A non-protected shaded panel of a non-uniform illuminated PV system can be submitted to a negative voltage. If there is no protection, cells breakdowns can happen during non-uniform illumination. Hence, normally in order to protect the cells an extra *p-n* junction is implemented as a bypass diode. For instance, one bypass diode connected in parallel with each set of 18 cells [16] or with a panel is common practice as a compromise between protection and increase on the cost due to the extra *p-n* junction.

Also shading pattern with hasty change is not easy for the tracking of the maximum power point (MPP), because with non-uniform illumination usually there will be multiple local MPPs and they will change as fast as does the illumination. Under shadowing conditions a PV system can have large energy losses and even small shadows can noticeably affect the energy yield [17].

Modeling is an important part of engineering design. The use of computers and powerful software has allowed to predict the performance of complex systems and to assist the almost near optimal design for better systems. Not only simulation is possible, but also performance can be predicted and monitored in real time. In what regards PV modeling, researchers have used equivalent electrical circuits to model the characteristics of a solar cell when subjected to environmental variations, i.e., irradiance and temperature. The equivalent electrical circuit of a solar cell with its parameters has been a tool to emulate the I-V characteristics of PV systems [7,18–20]. The equivalent circuit parameters of solar cells are intimately related to the internal solid-state physics acting within the solar cell [21,22]. The equivalent circuit parameters accessing is an important aspect for PV system applications in what regards the design and the simulation of those modules in order to uncover their behavior.

A PV system linked or not to the utility grid consists not only on solar cells, but also on several other apparatus, for instance: storage elements; power converters; control blocks. Hence, to have a correct evaluation is necessary that all models have enough accuracy in what regards the real behavior influencing the overall system performance [23].

By far, the simplest equivalent electrical circuits approach for a PV system is a current source in parallel with a diode [24]. Some authors state as a fact that the solution with a single diode model, i.e., current source in parallel with only one diode, for modeling a PV system integrated into the electric grid is enough to obtain satisfactory results [25]. But it seems to be dependent on what one considers by satisfactory results and what one wants to uncover about the reality in order to take proper action and avoid malfunction problems with the PV systems integration into the electric grid. An improved version for equivalent circuits is the five parameter modeling of the photovoltaic system, with the additional inclusion of a shunt and a series resistance. The shunt resistance accounts for the cell linkage current losses. The series resistance accounts for the joule losses. This version is justified for better accuracy and is the object of analysis in this paper in order to find a simple as possible parameter identification.

Typically, the parameters provided by the PV manufacturers are the open circuit voltage, the short circuit current, the current and voltage at maximum power, the temperature coefficients at open circuit voltage, short circuit current and the NOCT [26–28], but these parameters provide limited operational data for the five parameters modeling.

Power electronic converters have been developed for integrating renewable energy sources with the electric grid. The use of power electronic converters, i.e., inverters are particularly indispensable in PV systems, the inverter is necessary for two accomplishments: the accomplishment of adjusting the low DC voltage of the PV module to the voltage level of the electric grid using a two power converter topology, a DC-DC topology and a DC-AC topology; the accomplishment of the Maximum Power Point (MPP) tracking due to the fact of the power delivered by the modules being very sensitive to the point of operation in the I-V curve, the inverter is able to comply with functionality to circumvent this fact [29,30].

This paper focuses on the five parameters identification for the modeling of photovoltaic systems, using three solar cell technologies as a case study for the simulation of the I-V, shading characteristics and PV system implemented with a DC-DC boost and a two-level inverter topology. Experimental results are considered in this paper to allow a comparison with the ones

given by the modeling. The paper is organized as follows. Section II presents the solar cell model, the iterative procedure for the identification of the five parameters, the PV system with a DC-DC boost and a two-level inverter topology and the main expressions used in the modeling. Section III presents the control strategy, consisting in pulse width modulation (PWM) by space vector modulation (SVM) associated with sliding mode (SM) for controlling the converter. Section IV presents the case studies respectively the simulation and the comparison with the experimental results of the PV system linked to the electric grid by a commercial inverter. Finally, the conclusions are drawn in Section V.

2. Modeling

2.1 PV module

An improved parameter identification procedure of a photovoltaic module in order to acquire the I-V characteristics with the usual data given by the PV system industry is presented by the authors in [31]. The equivalent circuit model for a solar module simulation consisting on a current controlled generator, single-diode D_1, shunt and series resistances, bypass protection diode D_2 is shown in Fig. 1.

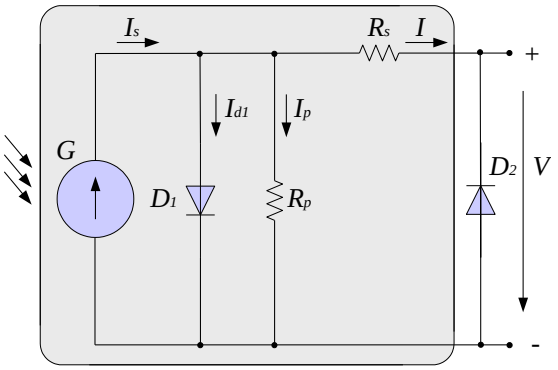

Fig. 1. Equivalent circuit model for a solar module.

Also the equivalent circuit model can be used to simulate an individual cell. But if all cells of a module, a panel or array are subjected to the same irradiance, then the equivalent circuit with the bypass protection diode is also the one shown in Fig. 1, where G is the common solar irradiance, R_p is the equivalent shunt resistance, R_s is the equivalent series resistance, I is the output current, D_2 is the bypass diode and V is the output voltage, I_S is the photo generated electric current, I_{d1} is the current at diode D_1 and I_p is the leakage current.

The thermal voltage of the solar cell is given by:

$$V_T = \frac{kT}{q} \tag{1}$$

where q is the electron charge, k is the Boltzman's constant and T is the cell p-n junction temperature in [K]. The I-V characteristic associated with the equivalent circuit model shown in Fig. 1 is given by:

$$I = I_S - I_0\left(e^{\frac{V+I\,R_S}{mV_T}} - 1\right) - \frac{V + I\,R_S}{R_p} \tag{2}$$

where I_0 is the diode reverse bias saturation current. Equation (2) is an implicit equation, implying the use of an iterative method to determine for instance the output current in function

of the output voltage, considering (2) at short-circuit conditions the expression for I_S is given by:

$$I_S = \frac{I_{SC}\left(R_s + R_p\right)}{R_p} + I_0\left(e^{\frac{I_{sc}R_s}{mV_T}} - 1\right) \tag{3}$$

The second term of (3) is usually small in comparison with the first term [13,32]. So, the approximation considered for I_S is given by:

$$I_S \approx \frac{I_{SC}\left(R_s + R_p\right)}{R_p} \tag{4}$$

From (2), considering the open circuit conditions, I_S is given by:

$$I_S = I_0\left(e^{\frac{V_{oc}}{mV_T}} - 1\right) + \frac{V_{oc}}{R_p} \tag{5}$$

Substituting (4) into (5) and due to the fact that the exponential is much greater than one, I_0 is given by:

$$I_0 \approx \frac{I_{SC}\left(R_s + R_p\right) - V_{oc}}{R_p} e^{-\frac{V_{oc}}{mV_T}} \tag{6}$$

The MPP of a PV system varies with solar irradiance and temperature [33]. An I-V characteristic curve has a unique operating point at a particular solar irradiance and temperature where energy is delivered at maximum possible power, known as the MPP. At this point the PV system operates at highest efficiency [33,34]. At condition of MPP holds the necessary following condition given by:

$$\left(\frac{\partial P}{\partial V}\right)_{MP} = I_{MP} + V_{MP}\left(\frac{\partial I}{\partial V}\right)_{MP} = 0 \tag{7}$$

This condition is also sufficient to identify the MPP, if there is no shading. The derivative of the current in (2) in order to the output voltage at MPP is given by:

$$\left(\frac{\partial I}{\partial V}\right)_{MP} = -\frac{V_{MP} - I_{MP}R_s}{V_{MP}}\left(\frac{I_0 e^{\frac{V_{MP}+I_{MP}R_s}{mV_T}}}{mV_T} + \frac{1}{R_p}\right) \tag{8}$$

Using (7) and (8), I_{MP} satisfy the implicit expression given by:

$$I_{MP} = \left(V_{MP} - I_{MP}R_s\right)\left(\frac{I_0 e^{\frac{V_{MP}+I_{MP}R_s}{mV_T}}}{mV_T} + \frac{1}{R_p}\right) \tag{9}$$

Substituting (4) into (2) at MPP condition and due to the fact that the exponential term is much greater than one, I_0 is approximated by the expression given by:

$$I_0 \approx \frac{\left(I_{sc} - I_{MP}\right)\left(R_s + R_p\right) - V_{MP}}{R_p} e^{-\frac{V_{MP}+I_{MP}R_s}{mV_T}} \tag{10}$$

Substituting (10) into (9) [13,32] I_{MP} is approximated by implicit expression given by:

$$I_{MP} \approx \left(V_{MP} - I_{MP}R_s\right)\frac{\left(I_{sc} - I_{MP}\right)\left(R_s + R_p\right) - V_{MP} + mV_T}{mV_T R_p} \tag{11}$$

Assuming (11) as a good approximation [32], R_p is approximated by the expression given by:

$$R_p \approx \frac{(V_{MP} - I_{MP}R_s)V_{MP} - mV_T V_{MP}}{(V_{MP} - I_{MP}R_s)(I_{sc} - I_{MP}) - mV_T I_{MP}} - R_s \tag{12}$$

and R_s from (6) of [32] is implicit given by:

$$R_s = \frac{1}{I_{MP}}\{V_{oc} - V_{MP} - mV_T \ln[\frac{V_{MP} + mV_T - I_{MP}R_s}{mV_T}\frac{I_{sc}(R_s + R_p) - V_{oc}}{I_{sc}(R_s + R_p) - 2V_{MP}}]\} \tag{13}$$

An initial value for R_s is derived assuming in (13) that $V_{MP} + mV_T - I_{MP}R_s \approx V_{MP}$ and R_p has a significant greater value, then holds the approximation given by:

$$\frac{I_{sc}(R_s + R_p) - V_{oc}}{I_{sc}(R_s + R_p) - 2V_{MP}} \approx 1 \tag{14}$$

Hence, from (13) and (14) the initial value for R_s [13,32] is given by:

$$R_s^0 \approx \frac{1}{I_{MP}}[V_{oc} - V_{MP} - mV_T \ln(\frac{V_{MP}}{mV_T})] \tag{15}$$

The ideality factor can be evaluated from (2) at maximum power point, replacing I_S given by (4), I_0 given by (6) and taking logarithms [32]. Hence *m* is given by:

$$m \approx \frac{V_{oc} - V_{MP} - I_{MP}R_s}{V_T \ln[\frac{I_{sc}(R_s + R_p) - V_{oc}}{(I_{sc} - I_{MP})(R_s + R_p) - V_{MP}}]} \tag{16}$$

Three values are defined in order to determine the initial value for *m*. The first is derived from (16) on the following assumptions $R_P \to \infty$ and $I_{MP}R_S \approx V_T$. Hence the first value [32] is given by:

$$m_g^0 = \frac{V_{oc} - V_{MP} - V_T}{V_T \ln\frac{I_{sc}}{I_{sc} - I_{MP}}} \tag{17}$$

Because $R_S > 0$, (13) has to satisfy the following implicit relation given by:

$$m < \frac{V_{oc} - V_{MP}}{V_T \ln\frac{V_{MP} + mV_T - I_{MP}R_s}{mV_T}\frac{I_{sc}(R_s + R_p) - V_{oc}}{I_{sc}(R_s + R_p) - 2V_{MP}}} \tag{18}$$

The second value is obtained from (18) assuming $V_{MP} + mV_T - I_{MP}R_s \approx V_{MP}$ and (14). The second value is given by:

$$m_S^0 = \frac{V_{oc} - V_{MP}}{V_T \ln[\frac{V_{MP}}{V_T}]} \tag{19}$$

To assure that $R_P < \infty$, then the denominator in (12) must be greater than zero [32]:

$$m < \frac{(V_{MP} - I_{MP}R_s)(I_{sc} - I_{MP})}{I_{MP}V_T} \tag{20}$$

Hence, a weighting factor less than one should be considered in the right side of (20) to set up an equality, the factor assumed [32] is given by:

$$I_{MP} / I_{sc} \tag{21}$$

Finally, $I_{MP}R_s$ in (20) is considered equal to V_T to establish the last value [32] given by:

$$m_P^0 = \frac{(V_{MP} - V_T)(I_{sc} - I_{MP})}{I_{sc}V_T} \tag{22}$$

The value for the initialization is considered to be the minimum of the above three values.

2.2 MPP algorithm

The data needed for the algorithm are: the MPP data, i.e., voltage V_{MP} and the current I_{MP}; the open circuit voltage V_{oc} and the short circuit current I_{sc} at STC. The initial values m_g^0, m_s^0, m_p^0, R_s^0, R_p^0 are respectively given by (17), (19), (22), (15) and (12). The ideality factor value [32] is given by:

$$m^k = min(m_g^k, m_s^k, m_p^k) \tag{23}$$

The calculation sequence to obtain an initial value of *m* is (17), (19), and (22) and (23).
The goal of the algorithm is to find, for the five parameters model, the values of the parameters m, R_s, R_p, I_0 and I_s in order to give an approximation of the I-V curve, using information of the I-V curve given by the: short circuit point, maximum power point and open circuit point. Meaningless negative series resistance and infinite shunt resistance are avoided from this approach [32]. After the initialization, the values for m_g^k, m_s^k, m_p^k, R_s^k, R_p^k are respectively computed from (16), (18) and (20) assumed as an equality, (13) and (12). It is used the difference between consecutive R_s values as a stopping criteria for the iterative process [32]. As soon as the difference between two consecutive R_s values is below a certain tolerance ε_{Rs}, the cycle ends.
Plotting the I-V characteristic curves requires solving (2) for $I \in [0, I_{sc}]$ or $V \in [0, V_{oc}]$, considering the impossibility of having an explicit formulation, i.e., $I = f(V, I)$ is an implicit equation, numerical methods as for instance the Newton-Raphson have to be used to solve a set of equation of the form $g(V, I) = I - f(V, I) = 0$ for a set of discrete values *V* included in $[o, V_{oc}]$. This method is known by having the ability to overcome undesired behaviors [26].
The algorithm to adjust and plot the I-V curve characteristic of the solar cell is shown in Fig. 2.

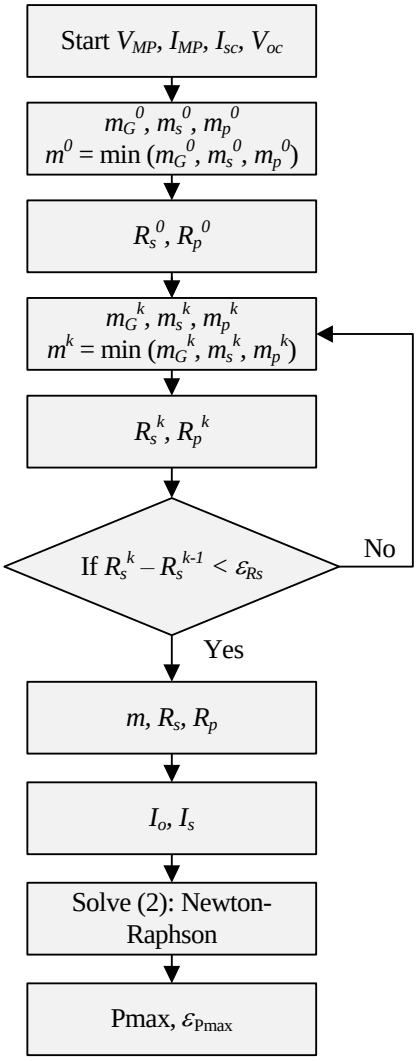

Fig. 2. Algorithm to adjust the I-V output characteristics of the solar cell.

2.3 DC-DC boost converter

The configuration of DC-DC boost converter in the simulated PV system is shown in Fig. 3.

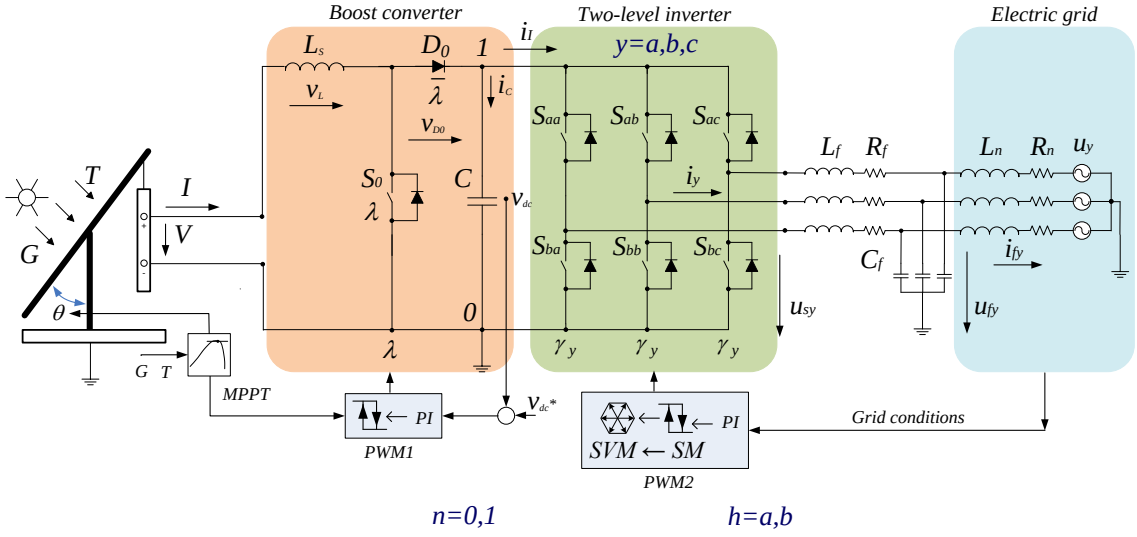

Fig. 3. PV system model with DC-DC boost and two-level inverter.

The DC-DC boost converter has one unidirectional commanded IGBT S_0. The switching function of the DC-DC boost converter is described by the switching variables λ, $\bar{\lambda}$ used to identify the state of the IGBT S_0 and to identify the state of the diode D_0 of the boost converter, respectively. The constraints on the switching variable of the DC/DC boost converter [15] are given by:

$$\begin{cases} \lambda = 1 \text{ and } \bar{\lambda} = 0 \ (S_0 = 1 \text{ and } D_0 = 0) \\ \lambda = 0 \text{ and } \bar{\lambda} = 1 \ (S_0 = 0 \text{ and } D_0 = 1) \end{cases} \tag{24}$$

The array current i_S is modeled by the state equation given by:

$$\frac{di_S}{dt} = \frac{1}{L_s}[v_A - \bar{\lambda}\,(v_{D0} + v_{dc})\,] \tag{25}$$

where $\mathrm{v_A}$ is the voltage at the PV array terminals, $\mathrm{v_{D0}}$ is the diode forward voltage at direct current, v_{dc} is the capacitor voltage.
The capacitor voltage $\mathrm{v_{dc}}$ is modeled by the state equation given by:

$$\frac{dv_{dc}}{dt} = \frac{1}{C}(\bar{\lambda}\,\mathrm{i_S} - i_I) \tag{26}$$

where i_I is the current injected at the inverter. At steady state the mean value of the voltage at the inductance terminals $\mathrm{v_L}$ is null, given by:

$$v_L = \frac{1}{T}\,[\int_0^{\lambda T} v_A\,dt + \int_{\lambda T}^{T}(v_A - v_{dc})\,dt\,] = 0 \tag{27}$$

Hence, the DC-DC boost converter can be modeled by (24) to (27).

2.4 Two-level inverter

The two-level inverter is a DC-AC converter, with six unidirectional commanded IGBTs, S_{hy} has shown in Fig. 3. The inverter is connected between a capacitor bank and a second order filter, which in turn is connected to an electric grid. The groups of two IGBTs linked to the same phase constitute a leg y of the converter. The two-level converter modeling assumes that: 1) the IGBTs are ideal and unidirectional and are never subject to reverse voltages, this is assured by the connection of an anti-parallel diode to each IGBT; 2) the diodes are ideal, i.e., in conduction state the voltage between their terminals is null, and in blockade the current that passes through diodes is null; 3) the voltage at the output of the boost converter is $v_{dc} > 0$; 4) each leg y of the converter always has one IGBT on a conduction state. The switching function of each IGBT is described by the switching variable γ_y, identifying the state of the IGBT h in the leg y of the converter. The index h with $h \in \{a,b\}$ identifies the IGBT. The index y with $y \in \{a,b,c\}$ identifies a leg of the inverter. The two conditions [35] for the switching variable of each leg y are given by:

$$\gamma_y = \begin{cases} 1, & (S_{ay} = 1 \text{ and } S_{by} = 0) \\ 0, & (S_{ay} = 0 \text{ and } S_{by} = 1) \end{cases} \qquad y \in \{a,b,c\} \tag{28}$$

The topological restriction for the leg y is given by:

$$\sum_{h=a}^{b} S_{hy} = 1 \qquad y \in \{a,b,c\} \tag{29}$$

Hence, each switching variable depends on the conduction and blockade states of the IGBTs. The current injected at the inverter i_I is given by:

$$i_I = \sum_{y=a}^{c} \gamma_y i_y \tag{30}$$

where i_y is the phase current at the output of the inverter.

2.5 Electric grid

The phase currents injected into the electric grid i_{fk}, considering the grid as an equivalent circuit given by a three-phase active symmetrical circuit as shown in Fig. 3, is given by:

$$\frac{di_{fy}}{dt} = \frac{1}{L_n}(u_{fy} - R_n i_{fy} - u_y) \qquad y \in \{a,b,c\} \tag{31}$$

Hence, the electric grid is modelled by (31).

3. Control strategy

A maximum power point tracking (MPPT) is used to extract the maximum power from a PV system which is under varying weather conditions [5]. The DC-DC Boost converter is used to implement maximum power operation of the PV system, controlling the voltage at the array terminals. The calculation of PV array output power requires solar irradiance and ambient temperature records, and therefore, records of these variables have been obtained for the adopted site [36]. The control of the boost converter includes the MPPT, using the $\partial P/\partial V$ algorithm to implement MPPT on the P-V curve of the array for each pair (*G, T*) [37]. The controllers used in the converters are classical PI controllers. PWM by SVM associated with SM control is used for controlling the converters. The SM control strategy presents attractive features such as robustness to parametric uncertainties of the PV array as well as to electric grid disturbances [34]. Sliding mode control is particularly interesting in systems with variable structure, such as power converters, guaranteeing the choice of the most appropriate space vectors. The aim of the sliding mode control is to let the system slide along a predefined sliding surface by changing the system structure. The control strategy of the PV system with DC-DC boost and two-level power converter topology using classical PI controllers has the diagram in box PWM1 and in box PWM2 shown in Fig. 3. The convenient vector selection to ensure stability for the converters, after being processed by the hysteresis comparator in the block of SM control and SVM are given in [35]. The SM control is a lower level of control as is normally implemented with the classical PI controller, for triggering the converters transistors is used PWM by SVM supplemented with SM.

Power semiconductors have physical limitations to be considered during design phase and during simulation. Particularly, the switch frequency has to be a finite value, for instances, switching frequencies of 2 kHz, 5 kHz or 10 kHz are normally reported. The switch frequency finite value implying that an error $e_{\alpha\beta}$ has to be tolerated on the electric current, i.e., an error between the reference value and the control value of the current. The error trajectory in order to guarantee that the system follows the sliding surface $S(e_{\alpha\beta},t)$, based on the Concordia transformation ($\alpha-\beta$), has to be in a convenient neighboring of this sliding surface, implying the satisfaction of stability conditions [35] given by:

$$S(e_{\alpha\beta},t)\ \frac{dS(e_{\alpha\beta},t)}{dt}<0 \tag{32}$$

The sliding surface in current practice is chosen in way to allow a small error $\varepsilon>0$ for $S(e_{\alpha\beta},t)$ has to be accepted due to power semiconductors switching only at finite frequency. Consequently, the switching strategy implemented by hysteresis comparators performing accordingly to the condition given by:

$$-\varepsilon<S(e_{\alpha\beta},t)<+\varepsilon \tag{33}$$

The outputs of the hysteresis comparators are the integer variables $\sigma_{\alpha\beta}=(\sigma_\alpha,\sigma_\beta)$ for the two-level converter take the values [35] given by:

$$\sigma_{\alpha\beta}\ \text{ with }\ \sigma_\alpha,\sigma_\beta\in\{-1,0,1\} \tag{34}$$

The integer variables values indicate whether the error is within or outside the sliding surface. If the error is within the sliding surface, given by $\sigma_\alpha=0$ and $\sigma_\beta=0$, the converter IGBTs do not switch, maintaining the actual voltage vector, but if the error is outside of the sliding surface, the voltage vector that meets the $\sigma_{\alpha\beta}$ coordinates is chosen, forcing the converter transistors to switch, in order to bring the error back into the sliding surface. For the two-level converter there are eight possible IGBTs combinations, which correspond to eight output voltage vectors and two voltage levels, lying between level $n=0$ and level $n=1$, vector a_0 and h_0 are the vectors for level 0 and vectors from b_1 trough h_1 are the vectors for level1. The IGBTs switching state combinations with corresponding output voltage vectors and levels are shown in Table 1.

Table 1. IGBTs switching state combinations with corresponding output voltage vectors

Vector	S_{aa}	S_{ba}	S_{ab}	S_{bb}	S_{ac}	S_{bc}	γ_a	γ_b	γ_c	$u_{s\alpha}/v_{dc}$	$u_{s\beta}/v_{dc}$	Level
a_0	0	1	0	1	0	1	0	0	0	0.0	0.0	0
b_1	1	0	0	1	0	1	1	0	0	0.8164	0.0	1
c_1	0	1	1	0	0	1	0	1	0	-	0.7071	1
d_1	1	0	1	0	0	1	1	1	0	0.4082	0.7071	1
e_1	0	1	0	1	1	0	0	0	1	-	-	1
f_1	1	0	0	1	1	0	1	0	1	0.4082	-	1
g_1	0	1	1	0	1	0	0	1	1	-	0.0	1
h_0	1	0	1	0	1	0	1	1	1	0.0	0.0	0

The output voltage vectors in the $\alpha\beta$ plane for the two-level converter are shown in Fig. 4.

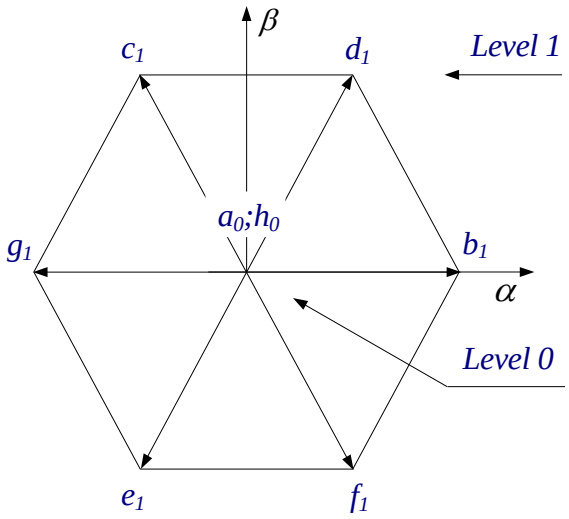

Fig. 4. Output voltage vectors for the two-level inverter.
The vector selection in order to ensure stability for the two-level converter is shown in Table 2.

Table 2. Output voltage vector selection for the two-level converter

$\sigma_\beta \setminus \sigma_\alpha$	**-1**	**0**	**1**
-1	e_1	e_1;f_1	f_1
0	g_1	a_0;h_0	b_1
1	c_1	c_1;d_1	d_1

Hence, the proposed control strategy for the power converters is given by (32) to (34).

4. Case studies

The mathematical modeling for the solar cell with single-diode, shunt and series resistances, for the MPPT algorithm and for the PV system with the DC-DC boost and the two-level power inverter topology is implemented in Matlab/Simulink. The simulation results were compared with experimental observation carried out for three different PV module technologies. The data measured from the PV modules were provided by [38], taken from a photovoltaic facility at the Laboratório Nacional de Energia e Geologia (LNEG) in Lisbon, Portugal. The coordinates for the PV modules site are: 38°46'18.50''N, 9°10'38.50''W. The tests were performed in clear sky days. Before experimental observation, the cover glass of each of the modules was cleaned in order to remove any residue that had been accumulated. Individual modules were unbolted and removed from the frame prior to testing. The module was then electrically disconnected from the remainder of the PV system and connected across the capacitive load test circuit in order to generate the I-V curve. To determine the module operating temperature, one thermocouple was attached to the back of the module near the center. The module was then replaced into the array frame and allowed to return to a steady-state temperature before the I-V curve was measured.

The experimental data provided, measured cell temperatures along with current and voltage values for three different photovoltaic cell technology types installed on an inclination angle of 30° for summer and an inclination angle of 50° for winter [38]. For each tested PV module, the characteristic curve is measured outdoors, quasi-simultaneously with the measurement of the reference unit I-V curve. The I-V curve is then translated to STC conditions by using the procedure described in IEC 60891 [39].
The capacitive load at PV module for I-V measurements procedure is implemented by a circuit capacitive load, presented in Fig. 5, being initially discharged, the capacitor is charged by the PV module current when S_1 is switched ON and S_2 remains OFF; R_1 is a very small resistance, just acting as a sensor current. Ideally, the charging process starts at the PV module short-circuit and ends when the voltage at the capacitor equals the open circuit voltage of the PV module. This way, the charging process takes over the full characteristic curve in the first quadrant. Later, the energy stored into the capacitor is dissipated through R_2, S_2 ON, S_1 OFF, in order to discharge the capacitor and prepare for the next measurement [40].

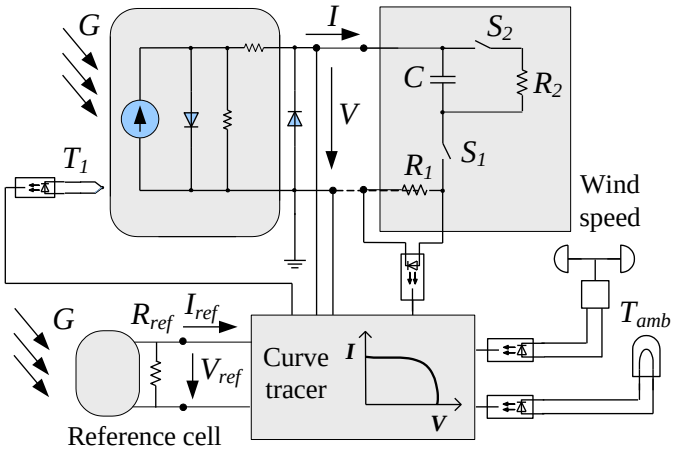

Fig. 5. The diagram of the system used to acquire the I-V curves.

The I-V curve tracer [38] is shown in Fig. 6.

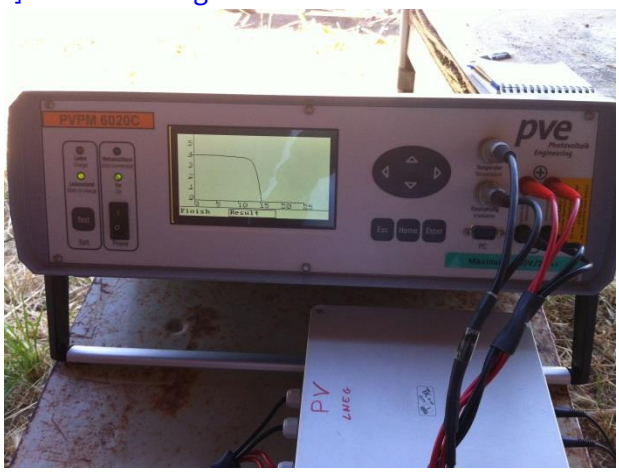

Fig. 6. The I-V curve tracer.

The I-V curves parameters were converted to STC, according with the usual procedure [36,41].

4.1 Case study 1 — Comparison between simulation and experimental results

This case study assesses the validity of the modeling of the PV systems for the three different PV module technologies tested. The three different PV module technologies tested are monocrystalline, polycrystalline and amorphous silicon solar modules. Table 3 summarizes the data given by the PV module manufacturers at STC [42–45].

Table 3. Data for the silicon solar modules at STC

Technology	V_m^*	I_m^*	V_{oc}^*	I_{sc}^*	Cells	β_{oc}	α_{sc}	NOCT
Monocrystalline Isofotón I53	17.4 V	3.05 A	21.65 V	3.27 A	36	-80 mV/ °C	1.748 mA/ °C	47 °C
Monocrystalline Siemens SP75	17 V	4.4 A	21.7 V	4.8 A	36	-77 mV/ °C	2.6 mA/ °C	-
Polycrystalline Photowatt PW500	17.2 V	2.9 A	21.6 V	3.2 A	36	-79 mV/ °C	0.95 mA/ °C	-
Amorphous Kaneka KA58	63 V	0.92 A	85 V	1.12 A	-	-206 mV/ °C	1.3 mA/ °C	-

The PV monocrystalline panel tested [38] is shown in Fig. 7.

Fig. 7. PV system formed by two monocrystalline solar modules connected in series.

The partial shading simulation was carried with six PV modules associating in parallel, i.e. two series of three modules. The partial shading is given by the following settings: $G = 1000$ W/m^2 and $T = 25$°C for the modules {1, 4}, $G = 800$ W/m^2 and $T = 20$°C for the modules {2, 5} and $G = 500$ W/m^2 and $T = 15$°C for the modules {3, 6}. Every cell of a module is assumed to be subjected to the same solar irradiance, i.e., uniform illumination is assumed over each module, but with different values. The equivalent electric circuit configuration for the partial shading is shown in Fig. 8.

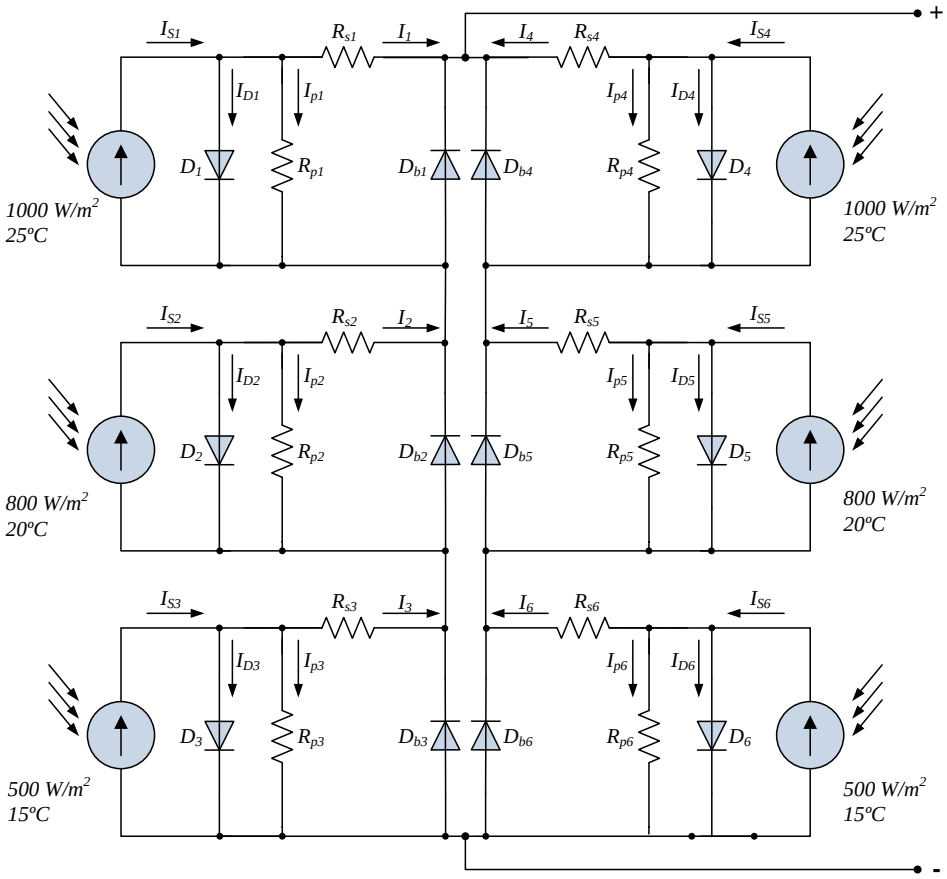

Fig. 8. Equivalent electric circuit with partial shading configuration.

For the monocrystalline technology two modules were tested, the Isofotón I53 and the Siemens SP75. In order to test the validity of the proposed model for the Isofotón I53, the simulated and the experimental curves at STC were carried out. The simulated and the experimental I-V curves without shading and simulated with shading are shown in Fig. 9.

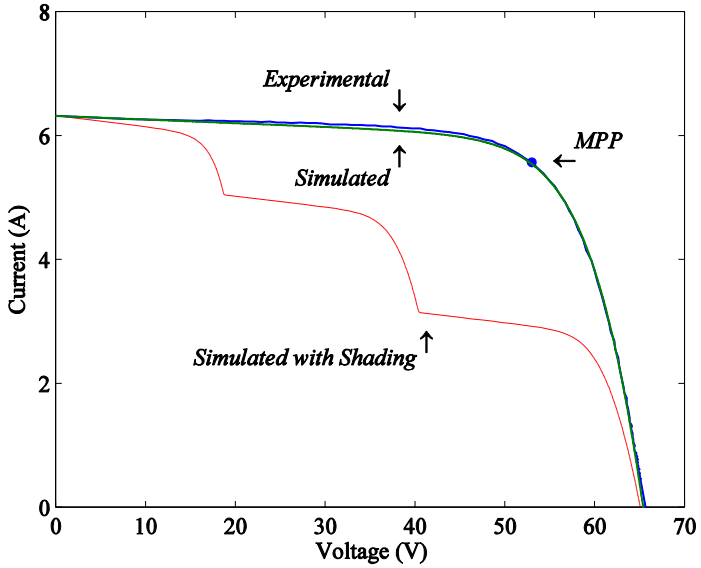

Fig. 9. Simulated and the experimental I-V curves without shading and simulated with shading (Isofoton I53).

The simulated and the experimental P-V curves without shading and simulated with shading are shown in in Fig. 10.

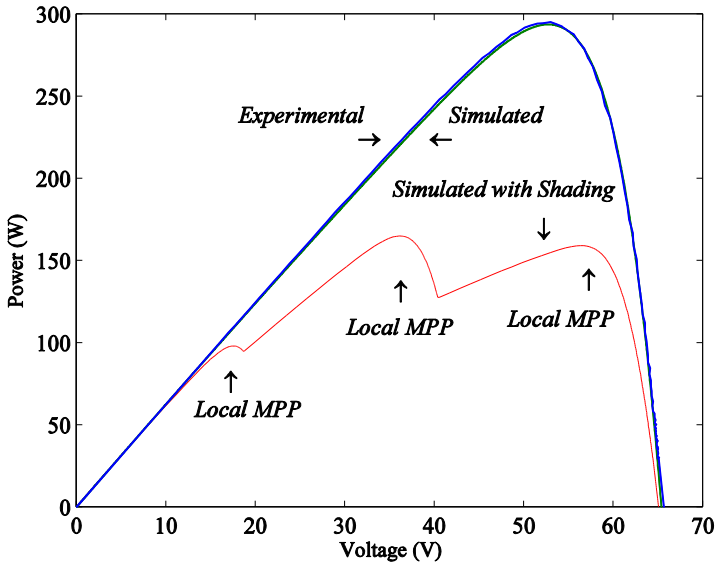

Fig. 10. Simulated and the experimental P-V curves without shading and simulated with shading, Isofoton I53.

For the Siemens SP75 monocrystalline module, the simulated and the experimental I-V curves without shading and simulated with shading is shown in Fig. 11 and the simulated and the experimental P-V curves without shading and simulated with shading is shown in Fig. 12.

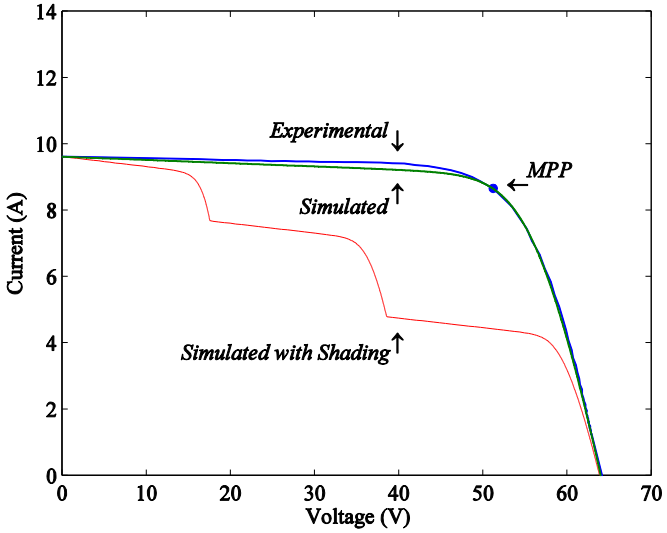

Fig. 11. Simulated and the experimental I-V curves without shading and simulated with shading, Siemens SP75.

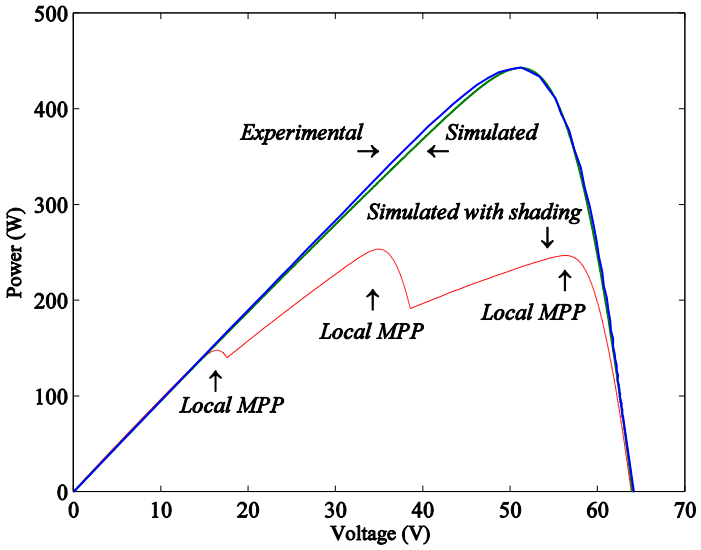

Fig. 12. Simulated and the experimental P-V curves without shading and simulated with shading, Siemens SP75.

For the polycrystalline technology one module was tested: the Photowatt PW500. The PV system formed by a silicon polycrystalline solar module [38] is shown in Fig. 13.

Fig. 13. PV system formed by one polycrystalline solar module, Photowatt PW500.

For the Photowatt PW500, the simulated and the experimental I-V curves without shading and simulated with shading are shown in Fig. 14 and the simulated and the experimental P-V curves without shading and simulated with shading is shown in Fig. 15.

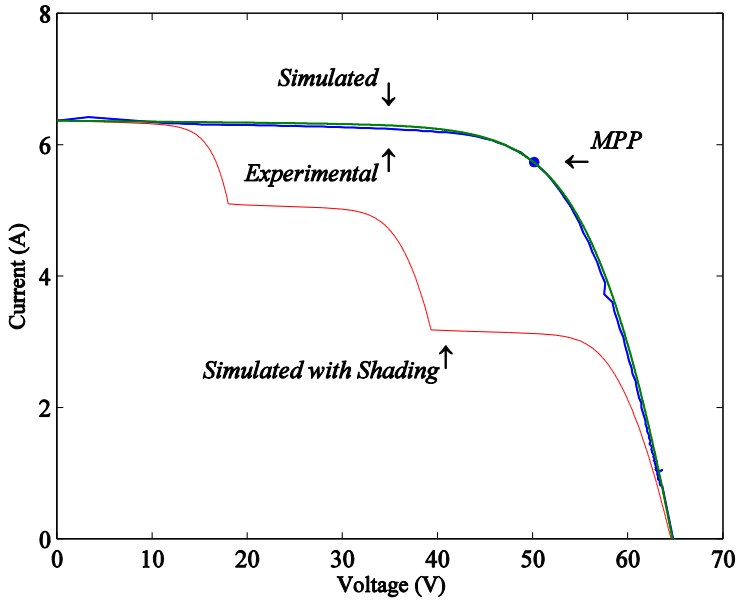

Fig. 14. Simulated and the experimental I-V curves without shading and simulated with shading, Photowatt PW500.

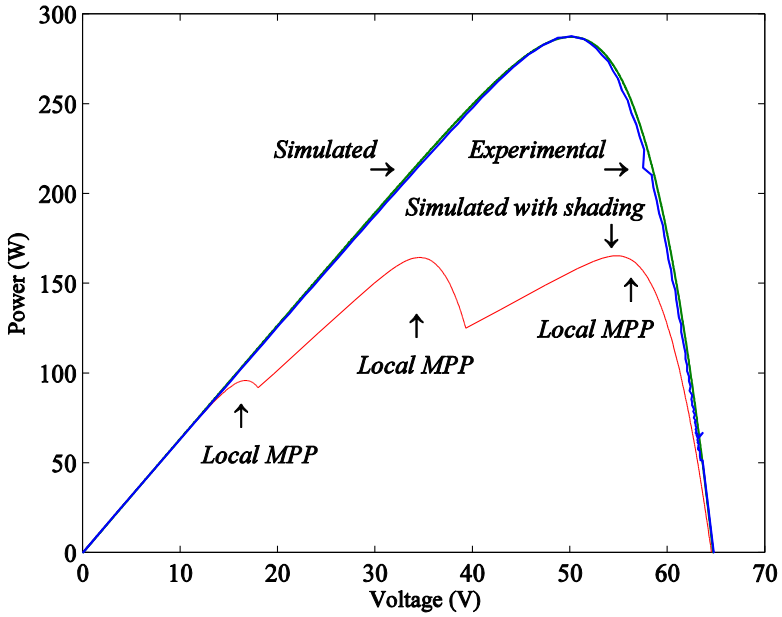

Fig. 15. Simulated and the experimental P-V curves without shading and simulated with shading, Photowatt PW500.

The PV system formed by a silicon amorphous solar module [38] is shown in Fig. 16.

Fig. 16. PV system formed by one amorphous solar module.

For the amorphous silicon technology one module was tested, the Kaneka KA58. The simulated and the experimental I-V curves without shading and simulated with shading are shown in Fig. 17 and the simulated and the experimental P-V curves without shading and simulated with shading is shown in Fig. 18.

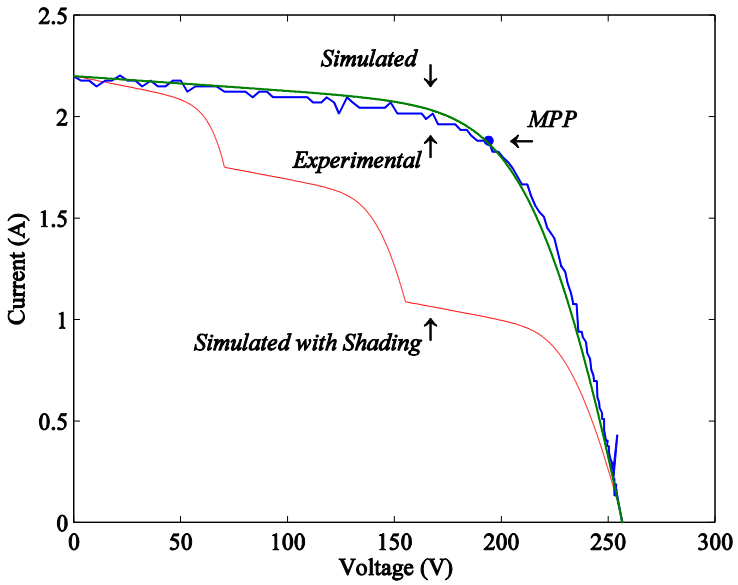

Fig. 17. Simulated and the experimental I-V curves without shading and simulated with shading, Kaneka KA58.

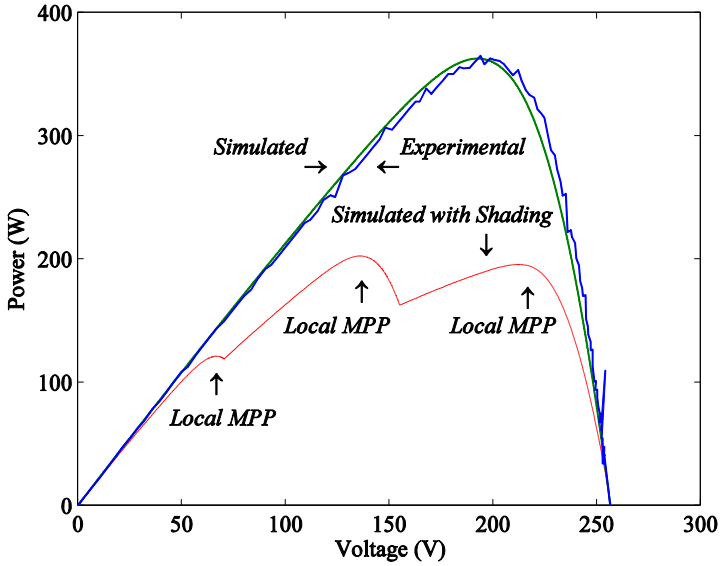

Fig. 18. Simulated and the experimental P-V curves without shading and simulated with shading, Kaneka KA58.

Table 4 summarizes the data results for the three different PV module technologies.

Table 4. Summarizes the data for three different module technologies (one solar cell module without shading)

Technology		Voltage at maximum power (V)	Maximum Power (W)	Current at maximum power (A)	Current Error (mA)
Monocrystalline Isofotón I53	Experimental	17.6567	49.1792	2.7853	-0.10
	Simulated	17.5200	48.8004	2.7854	
Monocrystalline Siemens SP75	Experimental	16.8882	72.6530	4.3020	-0.16
	Simulated	16.8800	72.6205	4.3022	
Polycrystalline Photowatt PW500	Experimental	16.6997	48.1353	2.8824	0.18
	Simulated	16.6700	48.0466	2.8822	
Amorphous Kaneka KA58	Experimental	64.6630	60.8479	0.9410	0.05
	Simulated	64.0900	60.3053	0.9409	

The I-V curves parameters were converted to STC, according with the usual procedure [36,41].

4.2 Case study 2 — Sinusoidal grid voltage waveform

This case study assesses the simulation results for the PV system linked to the electric grid. The PV systems are connected via the electrical switchboard to the electric grid at the level of domestic distribution, i.e., at a voltage of 230/400 V at 50 Hz.

The current injected into the electric grid, simulated in green and experimental in blue implementing the commercial inverter are shown in Fig. 19.

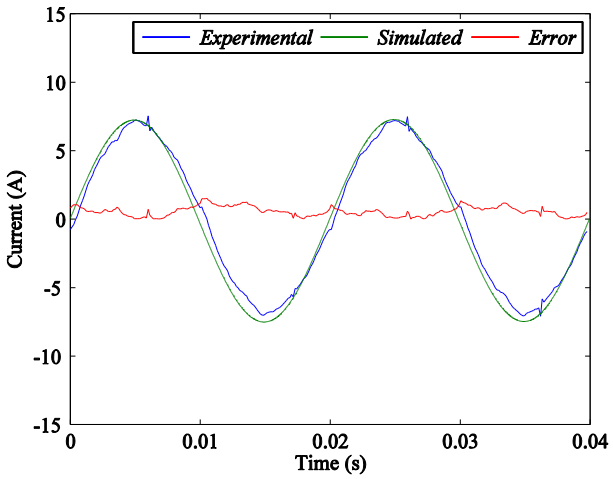

Fig. 19. Current injected in the electric grid simulated and experimental for the inverter.

Fig. 19 also shows in red the absolute error between the two currents.
Both RMSE are a small relative value of the respective rated values, showing that the modeling is appropriated for describing the PV system linked to the grid by the commercial inverter in this case study. The THD of the simulated voltage of the electric grid is 0.24% and the THD of the experimental voltage of the electric grid is 0.88% during normal operation of the PV system. The THD of the simulated current injected into the electric grid is 5.005% and the THD of the experimental current injected in the electric grid is 4.17% during normal operation of the PV system. The percentage of the fundamental component calculated by the DFT for the simulated current injected into the grid is 91.2% and for the experimental current injected into the grid is 79.5%. Those differences between the respective percentages are believed to happen impart due to the fact that the electric grid is not a perfect ideal source of voltage.
The PV system with DC-DC boost and two-level power inverter topology has an adequate performance in what regards the fact that the THD of the output current is lower than 5% limit imposed by IEEE-519 standard. The dominant harmonic of the current injected into the electric grid computed by the DFT for the simulated and the experimental PV systems is the 3rd harmonic with 0.7%. A comparison between simulated and the experimental results shows a satisfactory accomplishment in this modeling for the PV system at experimental testing.

5. Conclusions

A solar cell heuristic modeling over the equivalent circuit of one single-diode, shunt and series resistances, is used in this paper in order to achieve an acceptable approximation of the I-V curves at MPP. The simulated and experimental curves at STC are shown. The use of this modeling allows an easy use for assessing performance of a PV system, for instance, once the parameters identification is done, the simulation of the shading effects is possible. This simulation allows quantifying the effect of partial shading in reducing the energy obtained by a solar PV system, which should be taken into consideration during the economic evolution in the design phase. A comparison between the simulated and experimental curves shows that the method behaves satisfactorily in finding the parameters by adjusting the curves at three points: open circuit, maximum power and short circuit.

Simulation studies on PV systems are essential to assist the engineers in what regards extracting the maximum energy, anticipating performance and deciding convenient measures to avoid malfunctions.
A modeling for a PV system with DC-DC boost and two-level power inverter topology is proposed using the equivalent five parameters for PV modules; and DC-DC boost and two-level power inverter topology modeling, assuming a control strategy by classic PI controllers and pulse width modulation by space vector modulation associated with sliding mode.
The application of this modeling to a case study on a silicon PV system with a commercial inverter with a convenient filtering allows to anticipate a THD for the output current lower than the 5% limit imposed by IEEE-519 standard for the PV system with DC-DC boost and two-level power inverter topology.

Acknowledgments

This work was partially supported by Fundação para a Ciência e a Tecnologia, through IDMEC under LAETA, Instituto Superior Técnico, Universidade de Lisboa, Portugal and by Cátedra Novo Banco – Energias Renováveis, Universidade de Évora, Portugal. The authors gratefully acknowledge to Ms. L. Giacobbe for providing the measured data of PV modules at LNEG.

References

1. Schaefer L. Editorial. Sustainable Energy Technologies and Assessments 2013; 1:1–2.
2. Bouzidi B. New sizing method of PV water pumping systems. Sustainable Energy Technologies and Assessments 2013; 4:1–10.
3. Ismail MS, Moghavvemi M, Mahlia TMI. Design of an optimized photovoltaic and microturbine hybrid power system for a remote small community: case study of Palestine. Energy Conversion and Management 2013; 75:271–281.
4. Bhattacharjee S, Bhakta S. Analysis of system performance indices of PV generator in a cloudburst precinct. Sustainable Energy Technologies and Assessments 2013;4: 62–71.
5. Di Piazza MC, Pucci M, Vitale G. Intelligent power conversion system management for photovoltaic generation. Sustainable Energy Technologies and Assessments 2013; 2:19–30.
6. Spagnuolo G, Petrone G, Araújo SV, Cecati C, Madsenl FE, Gubía E, Hissel D, Jasinski M, Knapp W, Liserre M, Rodriguez P, Teodorescu R, Zacharias P. Renewable energy operation and conversion schemes. IEEE Industrial Electronics Magazine 2010; 4:38–51.
7. Spertino F, Akilimali JS. Are manufacturing I–V mismatch and reverse currents key factors in large photovoltaic arrays? IEEE Transactions on Industrial Electronics 2009; 56:4520–4531.
8. Presidency of the European Union. Renewable Energy in Portugal 2007. [Online]. Available: www.renewable.pt/pt/RE/.../Energias_Renov_PT.pdf.
9. Sedra AS, Smith KC. Microelectronic Circuits. London, U.K.: Oxford Univ. Press; 2006.
10. Eltawil MA, Zhao Z. Grid-connected photovoltaic power systems: Technical and potential problems—A review. Renewable and Sustainable Energy Reviews 2010; 14: 112–129.
11. Kininger F. Photovoltaic systems technology. Universitat Kassel, Kassel, Germany, 2003.
12. Villalva MG, Gazoli JR, Filho ER. Comprehensive approach to modeling and simulation of photovoltaic arrays. IEEE Transactions on Power Electronics 2009; 24:1198–1208.

13. Carrero C, Rodríguez J, Ramírez D, Platero C. Simple estimation of PV modules loss resistances for low error modelling. Renewable Energy 2010; 35:1103–1108.
14. Patel H, Agarwal V. MATLAB-based modelling to study the effects of partial shading on PV array characteristics. IEEE Transactions Energy Conversion 2008; 23:302–310.
15. Fialho L, Melício R, Mendes VMF, Viana S, Rodrigues C, Estanqueiro A. A simulation of integrated photovoltaic conversion into electric grid. Solar Energy 2014; 110:578–594.
16. Quaschning V, Hanitsch R. Numerical simulation of photovoltaic generators with shaded cells. In: Proc. 30th Universities Power Engineering Conference, London, UK 1995; 583–586.
17. Woyte A, Nijs J, Belmans R. Partial shadowing of photovoltaic arrays with different system configurations: literature review and field test results. Solar Energy 2003; 74:217–233.
18. Caracciolo F, Dallago E, Finarelli DG, Liberale A, Merhej P. Single-variable optimization for evaluating solar cell and solar module parameters. IEEE journal of Photovoltaics 2012; 2:173–180.
19. Lee MK, Wang JC, Horng SF, Meng HF. Extraction of solar cell series resistance without presumed current-voltage functional form. Solar Energy Materials & Solar Cells 2010; 94:578–582.
20. Kazem AH, Khatib T. Techno-economical assessment of grid connected photovoltaic power systems productivity in Sohar, Oman. Sustainable Energy Technologies and Assessments 2013; 3:61–65.
21. Yadir S, Benhmida M, Sidki M, Assaid E, Khaidar M. New method for extraction the model physical parameters of solar cells using explicit analytic solutions of current-voltage equation. In: Proc. International Conference on Microelectronics, Marrakech, Morocco 2009; 390–393.
22. Yordanov GH, Midtgård OM, Saetre TO. Series resistance determination and further characterization of c-Si PV modules. Renewable Energy 2012; 46:72–80.
23. Poullikkas A. A comparative assessment of net metering and feed in tariff schemes for residential PV systems. Sustainable Energy Technologies and Assessments 2013; 3:1–8.
24. Ishaque K, Salam Z, Taheri H. Simple, fast and accurate two-diode model for photovoltaic modules. Solar Energy Materials and Solar Cells 2011; 95:586–594.
25. Luque A, Hegedus S. Handbook of Photovoltaic Science and Engineering. West Sussex, U.K.: John Wiley and Sons, 2003.
26. Walker GR. Evaluating MPPT topologies using a Matlab PV model. Journal of Electrical & Electronics Engineering 2001; 21:49–56.
27. Photovoltaic devices - Part 3: Measurement principles for terrestrial photovoltaic (PV) solar devices with reference spectral irradiance data. IEC 60904-3:2008.
28. De Soto W, Klein SA, Beckman WA. Improvement and validation of a model for photovoltaic array performance. Solar Energy 2006; 80:78–88.
29. Kjaer SB, Pedersen JK, Blaabjerg F. Power inverter topologies for photovoltaic modules–a review. In: Proc. 37th IEEE Industry Applications Conf., Pittsburgh, USA 2002; 782–788.
30. Moradi MH, Tousi SMR, Nemati M, Basir NS, Shalavi N. A robust hybrid method for maximum power point tracking in photovoltaic systems. Solar Energy 2013; 94:266–276.
31. Fialho L, Melicio R, Mendes VMF. PV system modeling by five parameters and in situ test. In: Proc. 22th International Symposium on Power Electronics, Electrical Drives, Automation and Motion, Ischia, Italy 2014; 573–578.

32. Carrero C, Rodríguez J, Ramírez D, Platero C. Accurate and fast convergence method for parameter estimation of PV generators based on three main points of the I–V curve. Renewable Energy 2011; 36:2972–2977.
33. Varshni YP. Temperature dependence of the energy gap in semiconductors. Physica 1967;34: 149–154.
34. Jiang JA, Huang TL, Hsiao YT, Chen CH. Maximum power tracking for photovoltaic power systems. Tamkang Journal of Science and Engineering 2005; 8:147–153.
35. Melicio R, Mendes VMF. Simulation of power converters for wind energy systems. Información Tecnológica 2007; 18:25–34.
36. Photovoltaic devices - Part 1: Measurement of photovoltaic (PV) current-voltage characteristics. IEC 60904-1:2006.
37. Raj JSCM, Jeyakumar AE. A two stage successive estimation based maximum power point tracking technique for photovoltaic modules. Solar Energy 2014; 103:43–61.
38. Giacobbe L. Validação de modelos matemáticos de componentes de sistemas fotovoltaicos. Master Thesis. IST/DEEC, Portugal, 2005.
39. Procedures for temperature and irradiance corrections to measured I–V characteristics of crystalline silicon photovoltaic devices. IEC 60891.
40. Caamaño E, Lorenzo E, Zilles R. Quality control of wide collections of PV modules: lessons learned from the IES experience. Progress in Photovoltaics: Res. Applications 1999; 7:137–149.
41. Procedures for temperature and irradiance corrections to measured I-V characteristics of crystalline silicon photovoltaic (PV) devices. IEC 60891:1987 (Amendment 1: 1992).
42. Isofotón Photovoltaic Products Information [Online]. Available: http://www.isofoton.com.
43. Siemens Photovoltaic Products Information [Online]. Available: http://www.siemens.com.
44. Photowatt Photovoltaic Products Information [Online]. Available: http://www.photowatt.com.
45. Kaneka Photovoltaic Products Information [Online]. Available: http://www.pv.kaneka.co.jp.

2.3 Amorphous solar modules simulation and experimental results: effect of shading

L. Fialho[1], R. Melício[1,2], V.M.F. Mendes[1,3], J. Figueiredo[1,2], M. Collares-Pereira[1]

In the Proceedings of the 5th IFIP WG 5.5/SOCOLNET Doctoral Conference on Computing, Electrical and Industrial Systems, DoCEIS 2014, Technological Innovation for Collective Awareness Systems, Vol. 423, pp. 315-323, 2014.

http://link.springer.com/chapter/10.1007%2F978-3-642-54734-8_35

Abstract.
This paper focuses on the modeling of PV systems by the five parameters model, consisting on a current controlled generator, single-diode, a shunt and series resistances. An assessment for the identification of the parameters is used requiring data on open circuit, maximum power and short circuit tests. A simulation of a photovoltaic system on a parallel of two series connected amorphous solar modules under the effect of partial shading is presented. The estimated parameters are validated by a comparison with experimental measurements on photovoltaic modules.

Keywords
PV system, effect of shading, algorithm for parameter estimation, simulation, experimental results, shading on amorphous PV.

1 Introduction

The demand for energy, the foreseeable future scarcity and the price of fossil fuels coupled with the need for carbon footprint reduction turn out a political consciousness of the importance of energy savings and energy efficiency usage [1] and programs on the Demand-side Management have been developed in order to assist consumers on energy usage. Moreover, alternative sources of energy, for instance, wind and solar energy sources have turn out to be attractive for exploitation, not only for large scale systems, but also for micro and mini scale conversion systems [2], Disperse Generation owned by consumer. Disperse Generation significantly utilizes solar energy as a primary source of energy and have came into sight the utilization of Thermal and Photovoltaic (PV) systems. A PV system directly converts solar energy into electric energy. The main device of a PV system is a solar cell. Cells may be grouped to form arrays and panels. A PV array may be either a panel or a set of panels connected in series or parallel to form large PV systems without or with tracking systems in order to achieve higher values of energy conversion during sunny days due to the diverse perpendicular positions to collect the irradiation from the sun. The performance of a PV array depends on the operating conditions especially on solar irradiation, temperature, array configuration and shading. The shading on a PV array, for instances, due to a passing cloud or neighbouring buildings causes not only power losses, but also further non-linear effects on the array V-I characteristics [3]. In order to protect

[1] University of Évora, Évora, Portugal
[2] IDMEC/LAETA, Instituto Superior Técnico, Universidade de Lisboa, Lisbon, Portugal
[3] Instituto Superior of Engenharia de Lisboa, Lisbon, Portugal

the cells from destructive reverse voltages in case of shadowing or other abnormalities, a bypass diodes are utilized, for example, one bypass diode connected in parallel with each set of 18 cells [4] or with a panel is common practice as a compromise between protection and increase on the cost due to the extra pn-junction.
The impact of the shadow is important in case of large PV power system installations. Under partially shaded conditions, the PV characteristics of the system acquire complexity, appearing multiple peaks. Therefore, the importance to understand and to predict the shadow consequences in order not only to extract energy at the maximum possible power [3], but also to assess the protection on the systems.

2 Relationship to Collective Awareness Systems

Current trend in energy supply and usage are perceptibly economic, environmental and social unsustainable. There is a growing collective awareness of the urgent need to turn political statements and analytical work about the present unsustainable trend in energy supply and usage into concrete action in order to achieve what is anticipated as a sustainable development. The development of collective awareness platforms for a sustainable development allows the advancement not only of collective decision-making tools, but also of innovation mechanisms. These platforms allow individuals and groups to effectively react to environmental sustainability challenges, with an effective awareness of problems and possible solutions [5]. Solar energy is the most abundant form of energy on earth. PV systems are expanding due to supporting policies and cost reductions. Hence, PV systems are commercially available and a reliable technology with a potential for usage growth in almost everywhere. Although, can be argued that PV systems usage is not relevant in nowadays, PV systems are expected to be of relevant usage over the next decades [6].

3 Modeling

The equivalent circuit model used in this paper is the five parameters equivalent circuit, consisting in a current controlled generator, a single-diode, a shunt and series resistances as shown in Fig. 1.

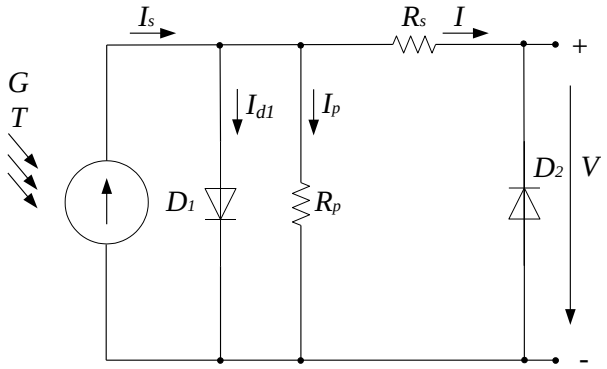

Fig. 1. Equivalent circuit of the solar module.

In Fig.1, although not a part of the equivalent circuit, the anti-parallel bypass diode D_2 is shown for connection illustration purpose. G is the solar irradiance, T is the cell *p-n junction* temperature in [K], R_p is the equivalent shunt resistance, R_s is the equivalent series resistance,

I is the output current, V is the output voltage, I_s is the photo generated electric current, I_{d1} is the current at diode D_1, I_p is the leakage current. If cells are associated in a module, an array or a panel and are equally subjected to the same irradiance, the junctions are at the same temperature T, then the circuit in Fig.1 is also the equivalent circuit for the association, but with a suitable transformation for the parameters. The thermal voltage of a solar cell V_T is given by:

$$V_T = kT / q \tag{1}$$

where k is the Boltzman's constant, q is the electron charge.

The I-V characteristic is given by the implicit function associated with the model shown in Fig. 1 for the solar cell and is given by:

$$I = I_S - I_0(e^{\frac{V+I R_S}{mV_T}} - 1) - \frac{V + I R_S}{R_p} \tag{2}$$

where I_0 is the diode reverse bias saturation current, and m is the diode ideality factor. (2). This equation has to be solved by an iterative method to determine for instance the output current in function of the output voltage. From (2), considering the short-circuit condition I_s is given by:

$$I_S = I_{SC}(1 + \frac{R_s}{R_p}) + I_0(e^{\frac{I_{sc}R_s}{mV_T}} - 1) \tag{3}$$

The second term of (3) is usually small in comparison with the first term [7,8]. So, the usual approximation considered for I_S is given by:

$$I_S \approx I_{SC}(1 + \frac{R_s}{R_p}) \tag{4}$$

Also from (2), considering the open circuit condition and due to the fact that the exponential at this condition is significant greater than one, I_S is given by:

$$I_S \approx I_0\, e^{\frac{V_{oc}}{mV_T}} + \frac{V_{oc}}{R_p} \tag{5}$$

Equating (4) to (5), I_0 is approximated by the expression given by:

$$I_0 \approx [I_{SC}(1 + \frac{R_s}{R_p}) - \frac{V_{oc}}{R_p}]e^{-\frac{V_{oc}}{mV_T}} \tag{6}$$

Hence, I_0 can be computed by (6), if the parameters R_p, R_s, T, m are known.

Substituting (4) into (2) at Maximum Power Point (MPP) condition and due to the fact that the exponential at this condition is significant greater than one, I_0 is approximated by the expression given by:

$$I_0 \approx [(I_{SC} - I_{MP})(1 + \frac{R_s}{R_p}) - \frac{V_{MP}}{R_p}]\, e^{-\frac{V_{MP}+I_{MP}R_s}{mV_T}} \tag{7}$$

The electric power output equation and (2) allow for the determination of the derivative of the I in order to V at MPP, respectively given by:

$$\left(\frac{\partial I}{\partial V}\right)_{MP} = -\frac{I_{MP}}{V_{MP}}, \qquad \left(\frac{\partial I}{\partial V}\right)_{MP} = -\frac{V_{MP} - I_{MP}R_s}{V_{MP}} \left(\frac{I_0}{mV_T} e^{\frac{V_{MP}+I_{MP}R_s}{mV_T}} + \frac{1}{R_p}\right) \tag{8}$$

Considering (7) and (8) I_{MP} is approximated by the implicit expression given by:

$$I_{MP} \approx \frac{(V_{MP} - I_{MP}R_s)}{mV_T}\left[(I_{SC} - I_{MP})\left(1 + \frac{R_s}{R_p}\right) - \frac{V_{MP} - mV_T}{R_p}\right] \tag{9}$$

Assuming (9) as having enough accurateness [8] for the parameter estimation R_p is approximated by the expression given by:

$$R_p \approx \frac{V_{MP} - I_{MP}R_s - mV_T}{(V_{MP} - I_{MP}R_s)(I_{sc}/I_{MP} - 1) - mV_T}\frac{V_{MP}}{I_{MP}} - R_s \tag{10}$$

and R_s from (6) of [8] is given by:

$$R_s \approx \frac{V_{oc} - V_{MP}}{I_{MP}} - \frac{mV_T}{I_{MP}} ln\left[\frac{V_{MP} - I_{MP}R_s + mV_T}{mV_T}\frac{I_{sc}(R_s + R_p) - V_{oc}}{I_{sc}(R_s + R_p) - 2V_{MP}}\right] \tag{11}$$

The ideality factor can be evaluated by (2) at maximum power point, replacing I_s given by (4), I_0 given by (6) and taking logarithms [8]. Hence m is given by:

$$m \approx \frac{1}{V_T}\frac{V_{oc} - V_{MP} - I_{MP}R_s}{ln[I_{sc}(R_s + R_p) - V_{oc}] - ln[(I_{sc} - I_{MP})(R_s + R_p) - V_{MP}]} \tag{12}$$

But $R_s > 0$, then (11) imposes the implicit relationship given by:

$$m < \frac{V_{oc} - V_{MP}}{V_T\, ln\left[\frac{V_{MP} - I_{MP}R_s + mV_T}{mV_T}\frac{I_{sc}(R_s + R_p) - V_{oc}}{I_{sc}(R_s + R_p) - 2V_{MP}}\right]} \tag{11}$$

Also to ensure that $R_p < \infty$, then the denominator in (10) imposes the relationship given by:

$$m < \frac{(V_{MP} - I_{MP}R_s)(I_{sc}/I_{MP} - 1)}{V_T} \tag{14}$$

The above expressions are capable of giving values for the five parameters equivalent circuit of a solar cell, using only data from open circuit, maximum power and short circuit tests. A Matlab/Simulink coding was carried out based on those expressions in order to simulate the behavior of PV systems.

4 Simulation

A simulation study concerning with the data measured from PV silicon amorphous solar modules Kaneka KA58 provided in [9] and placed in a photovoltaic facility at the Laboratório Nacional de Energia e Geologia (LNEG) in Lisbon, Portugal, is presented for illustration purpose. The coordinates for the PV modules site are: 38°46'18.50''N, 9°10'38.50''W.
The data for the silicon amorphous solar module Kaneka KA58 at STC [10] are shown in Table 1.

Table 1. Data for the Kaneka KA58 solar module at STC

Technology	V_m^*	I_m^*	V_{oc}^*	I_{sc}^*	β_{oc}	α_{sc}
Amorphous	63 V	0.92 A	85 V	1.12 A	-206 mV/ °C	1.3 mA/ °C

The characteristic curve for each tested PV module is measured outdoors quasi-simultaneously with the measurement of the reference unit I-V curve. The I-V curve is then converted to STC conditions by using the procedure described in IEC 60891 [11]. The I-V curve and the tracer used is shown in Fig. 2.

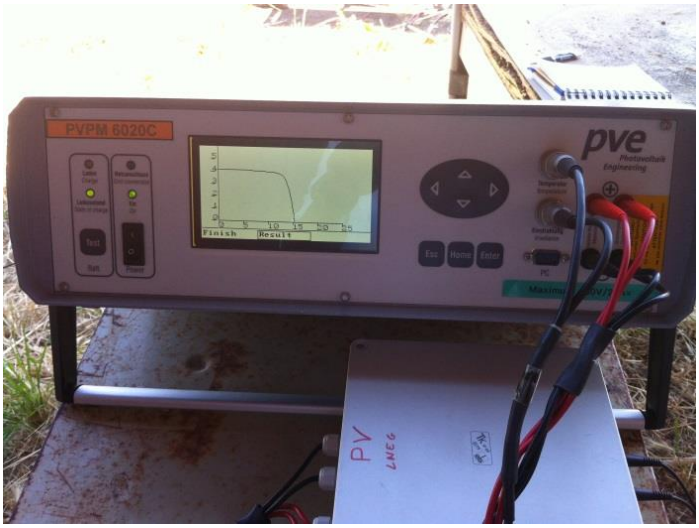

Fig. 2. Experimental I-V curves.

The simulation results are compared with experimental observation carried out for an amorphous PV module technology with two modules connected in series.
The I-V curves simulated and experimental without shading are shown in Fig. 3.

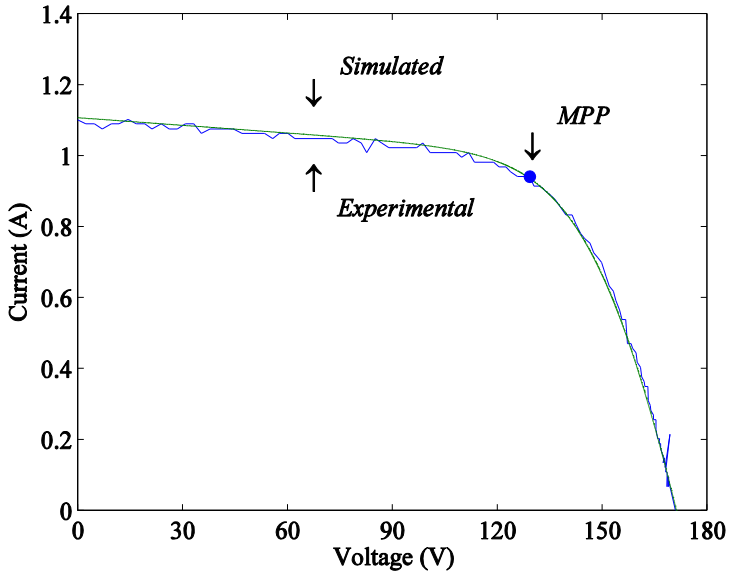

Fig. 3. I-V curves simulated and the experimental.

The partial shading simulation was carried with twelve PV modules associating in parallel two series of six modules. The configuration in study with partial shading is shown in Fig. 4.

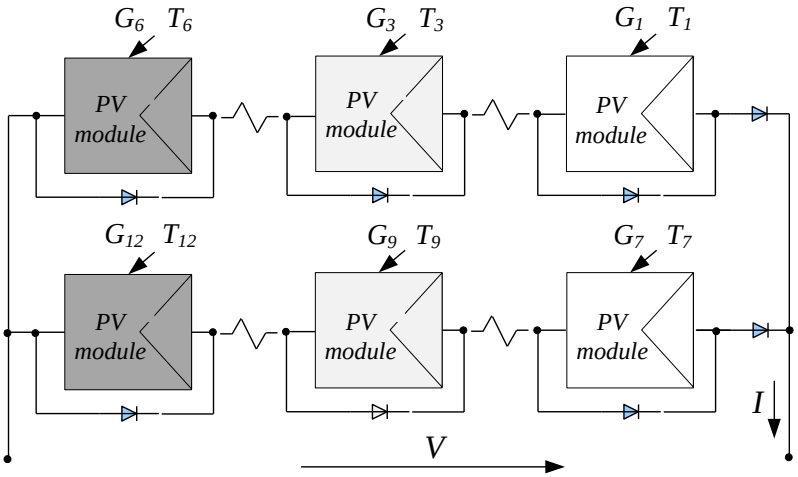

Fig. 4. Configuration for the simulation with partial shading.

In Fig. 4, the partial shading is given by the following condition: $G = 1200W/m^2$ for the modules $\{1,2,4,5,7,8,10,11\}$; $G = 1000W/m^2$ for the modules $\{3,9\}$ and $G = 700W/m^2$ for the modules $\{6,12\}$. The I-V and P-V curves obtained by simulation of partial shading are respectively shown in Fig. 5 and Fig. 6.

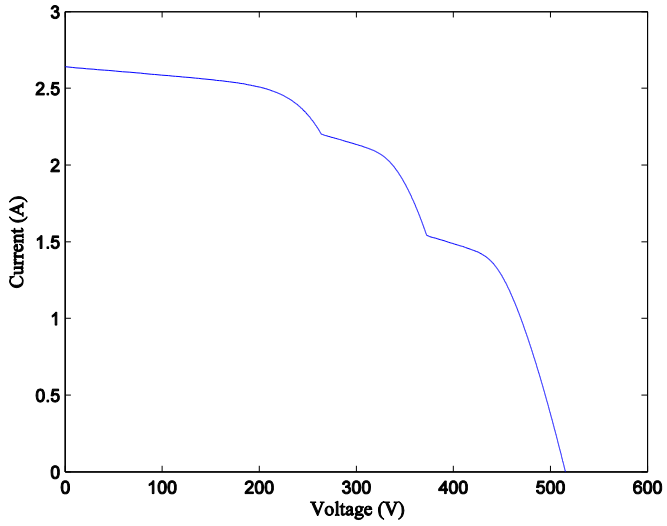

Fig. 5. I-V curve simulated for the PV modules with partial shading.

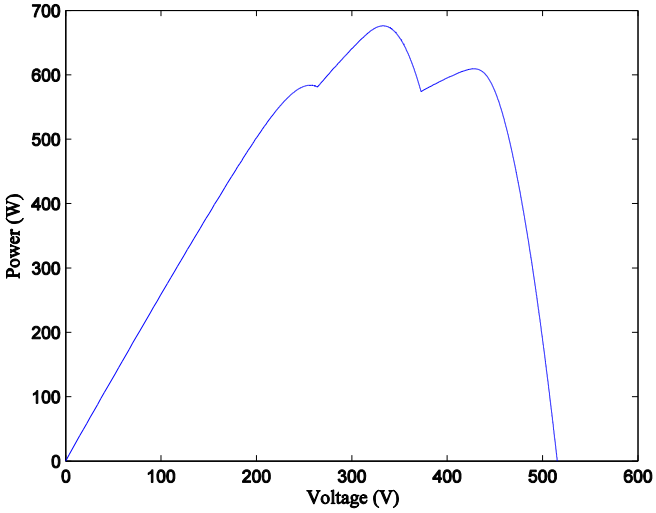

Fig. 6. P-V curve simulated for the PV modules with partial shading.

Fig. 5 and Fig. 6 reveal the implication in the I-V and P-V curves due to the shading, i.e., due to the non-uniform illumination on the modules there are local MPPs, which can pose a difficult to the MPP tracking (MPPT) system and there is a loss on the expected energy conversion.

5 Conclusions

The five parameters solar cell equivalent circuit is used in this paper in order to acquire analytically I-V curves. The five parameters are estimated by a method using a set of equations and requiring information on open circuit, maximum power and short circuit tests. A simulation study using the five parameters estimation is reported for illustration purpose, presenting the simulate performance of a PV system before installation in sitú in what regard shading conditions on a parallel of two series connected amorphous solar PV modules technology, assessing the performance given by the I-V and P-V curves due to a partial shading simulation. The shading curves show multiple local MPPs, which can pose a difficult to the MPPT algorithm. The knowledge of these curves can be useful to minimize power losses and avoid damage to the solar cells due to hot spots during high power losses. This shading simulation is handy to help the designer in what regards extracting the maximum energy and protection of the system. A comparison between simulated and the experimental results shows that the estimation is a satisfactory approximation method.

Acknowledgments.
This work was partially supported by Fundação para a Ciência e a Tecnologia, through IDMEC under LAETA, Instituto Superior Técnico, Universidade de Lisboa, Portugal. The authors gratefully acknowledge to Ms. L. Giacobbe for providind the measured data of amorphous PV modules at LNEG.

References

1. Seixas, M., Melicio, R., and Mendes, V.M.F. “A simulation for acceptance of two-level converters in wind energy systems”. Proc. of JIUE’ 2013 - 3ª Jornadas de Informática da Universidade de Évora, Évora, Portugal, pp. 75-79. (2013)
2. Blaabjerg, F., Chen, Z., and Kjaer, S.B. “Power electronics as efficient interface in dispersed power generation Systems”. IEEE Trans. Power Electron, Vol. 19, No. 5, pp. 1184-1194. (2004)
3. Patel, H., and Agarwal, V. “MATLAB-based modeling to study the effects of partial shading on PV array characteristics”. IEEE Trans. Energy Conversion, Vol. 23, No. 1, pp. 302-310. (2008)
4. Quaschning, V., Hanitsch, R.: Numerical Simulation of Photovoltaic Generators with Shaded Cells. In: 30th Universities Power Engineering Conference, pp. 583--586. London, UK (1995)
5. European Commission: Collective Awareness Platforms for Sustainability and Social Innovation. Europe 2020 Initiative, retrieved, http://ec.europa.eu/digital-agenda/en/collective-awareness-platforms-sustainability-and-social-innovation (2013)
6. International Energy Agency: Technology roadmap, solar photovoltaic energy (2010)
7. Carrero, C., Rodríguez, J., Ramírez, D., Platero, C.: Simple estimation of PV modules loss resistances for low error modelling. Renewable Energy. 35, 1103--1108 (2010)
8. Carrero, C., Rodríguez, J., Ramírez, D., Platero, C.: Accurate and fast convergence method for parameter estimation of PV generators based on three main points of the I–V curve. Renewable Energy. 36, 2972--2977 (2011)
9. Giacobbe, L.: Validação de modelos matemáticos de componentes de sistemas fotovoltaicos. Master Thesis (in Portuguese), DEEC/IST (2005)
10. Kaneka Photovoltaic Products Information, http://www.pv.kaneka.co.jp
11. IEC 60891: Procedures for temperature and irradiance corrections to measured I–V characteristics of crystalline silicon photovoltaic devices (2009)

2.4 A Simulation of Integrated Photovoltaic Conversion into Electric Grid

L. Fialho[1], R. Melício[1,2], V.M.F. Mendes[1,3], S. Viana[4], C. Rodrigues[4], A. Estanqueiro[4]

In Journal Solar Energy, Vol. 110, pp. 578-594, 2014.
http://dx.doi.org/10.1016/j.solener.2014.09.041

Abstract

This paper presents a systemic modeling for a PV system integrated into an electric grid. The modeling includes models for a DC-DC boost converter and a DC-AC two-level inverter. Classical or fuzzy PI controllers with Pulse width modulation by space vector modulation associated with sliding mode control is used for controlling the PV system and power factor control is introduced at the output of the system. Comprehensive performance simulation studies are carried out with the modeling of the DC-DC boost converter followed by a two-level power inverter in order to compare the performance with the experimental results obtained during in situ operation with three commercial inverters. Also, studies are carried out to assess the quality of the energy injected into the electric grid in terms of harmonic distortion. Finally, conclusions regarding the integration of the PV system into the electric grid are presented.

Keywords: Modeling; Power converters; Photovoltaic power generation; Power quality; Harmonic content

1. Introduction

Electricity market restructuring brought a different running set to the energy power system business, not only at the level of energy conversion, but also at the level of energy use (Cucchiella and D'Adamo, 2013). Since restructuring and the environmental concern on anthropogenic emission has arrived at this business, developments in distributed power generation systems (PGSs) allowed for the integration of renewable energy conversion, allowing a never seen before incentive to profit from renewable energy and an increment of mixed conversion into energy power systems (Peças Lopes et al., 2007, Liu et al., 2014). Nowadays, distributed PGSs are a reality on, for instances: solar energy exploitation by photovoltaic, concentrator solar and integrated solar combined cycle systems; wind energy exploitation by onshore and offshore wind turbines. A report on hardware and on control, including grid synchronization for distributed PGSs are given in (Blaabjerg et al., 2004) and in (Blaabjerg et al., 2006), respectively.

[1] Department of Physics, Universidade de Évora, R. Romão Ramalho 59, 7002-554 Évora, Portugal
[2] IDMEC/LAETA, Instituto Superior Técnico, Universidade de Lisboa, Avenida Rovisco Pais, 1049-001 Lisbon, Portugal
[3] Department of Electrical Engineering and Automation, Instituto Superior de Engenharia de Lisboa, R. Conselheiro Emídio Navarro, 1950-062 Lisbon, Portugal
[4] National Laboratory of Energy and Geology, Estrada do Paço do Lumiar, 1649-038 Lisbon, Portugal

Nomenclature

G	Solar irradiance.
T	Common cell *p-n* junction temperature.
θ	PV module tilt angle.
α_{sc}	Short-circuit current temperature coefficient.
β_{oc}	Open circuit voltage temperature coefficient.
D	Diode of the equivalent circuit for the PV module.
R_p	Module equivalent shunt resistance.
R_S	Module equivalent series resistance.
I_j	Output current of the PV module.
V_j	Output voltage of the PV module.
I_s	Photo generated electric current.
i_{Dj}	Current through diode *D*.
m	Diode ideality factor.
V_T	Thermal voltage.
V_{oc}	Open circuit voltage.
I_{sc}	Short-circuit current.
V_{mx}	Voltage at MPP.
I_{mx}	Current at MPP.
j	Operation conditions index ($j = oc$ open circuit, $j = sc$ short circuit, $j = mx$ MPP).
I_0	Diode reverse bias saturation current.
λ	IGBT switching variables at DC-DC boost converter.
$\overline{\lambda}$	Diode D_0 switching variables at DC-DC boost converter.
I	PV array current.
v_A	Voltage at the PV array terminals.
v_{D0}	Diode D_0 forward voltage at direct current at DC-DC boost converter.
v_{dc}	Capacitor voltage at DC-DC boost converter.
i_I	Current injected into the inverter.

v_L	Voltage at the inductance terminals.
v_{dc}	Voltage at the capacity bank C, i.e. continuous inverter input voltage.
C	DC-DC boost capacity bank.
S_{hy}	Unidirectional commanded IGBTs at DC-AC converter.
y	Index to identify the converter legs with $y \in \{a,b,c\}$.
h	Index to identify the IGBT with $h \in \{a,b\}$.
γ_y	IGBT switching variables of each leg *y* at DC-AC converter.
i_y	Phase current at the output of the converter.
u_{sy}	Converter voltage.
$x(n)$	Output inverter signal.
$X(k)$	Complex, amplitude and phase of the different sinusoidal components of $x(n)$.
X_H	Root mean square (RMS) value of the harmonic *H*.
X_F	RMS value of the fundamental component.
i_{fy}	Phase currents injected into the electric grid.
u_{fy}	Filter voltage.
L_f	Inductance of the filter.
R_f	Resistance of the filter.
C_f	Capacity of the filter.
L_n	Inductance of the electric grid.
R_n	Resistance of the electric grid.
u_y	Electric grid voltage.
$S(e_{\alpha\beta},t)$	Sliding surface on sliding mode control.
$e_{\alpha\beta}$	Error on the stator electric current in the $\alpha\beta$ plane.
ε	Error allowed for the sliding surface $S(e_{\alpha\beta},t)$.
$\sigma_{\alpha\beta}$	Voltage output of hysteresis comparators in the $\alpha\beta$ plane.

The increasing integration of distributed PGSs will change considerably the dynamic behavior of the energy power system in comparison with the forerunner one (Erlich et al., 2007). Actions have to be envisaged against this change to eventually circumvent the reduction of power system frequency regulation capabilities (Almeida and Peças Lopes, 2007) and to ensure that consumer power quality is not compromised (Salas et al., 2007). The harmonic problem, as one of the power quality issues, requires that the harmonic distortion is kept as low as possible on the energy following through the grid. Some standards have been established, for instance, IEEE Standards 519 and 1547 impose limits on voltage harmonics, on current harmonics and on total harmonic distortion (THD) of the energy injected into electric grids (Edwin et al., 2012; Spertino et al., 2012). The harmonic problem at the level of design is an example that different PGSs need different design considerations, namely: wind turbines and PV systems (Hasanzadeh et al., 2012; Tsang and Chan, 2014). Hence, new technical challenges emerge due to the increased renewable energy penetration and one challenge is on the research for more realistic models (Spertino et al., 2014).

The environmental concern is a relevant one for the energy power system business due to fact that the set of rules on anthropogenic emission is turning out to be more demanding and the acknowledgment on the environmental impact of this emission spreads, for instance, the greenhouse effect is said to be able of being slowed down only with a drastically reduction on CO_2 emissions (Dersch et al., 2004; Morales-Acevedo, 2006; Razkov et al., 2011). The European Commission has put forward a set of directives to create a new Energy Policy for Europe, for instance, imposing the reduction on CO_2 emissions by at least 20% by 2020 and 50% until 2050, increasing the share of renewable energy in the overall mixed conversion of energy power systems (Tyukhov, 2010). Hence, one should expect that distributed PGSs will turn out to be an important part of the future European Energy Policy. Among the distributed PGSs, the use of photovoltaic energy conversion in recent years is a reality not to be discarded, for instance, in locations where the connection with the electric grid is not economically feasible. Moreover, photovoltaic energy conversion is foreseen as eventually in parity with the conventional fossil-fueled thermal one in the future due to the foreseen technological developments in the solid state physics and due to the importance in what regards the environmental concern (Ismail et al., 2013; Kazem and Khatib, 2013; Ding et al., 2014). Also, the European Commission considers that the smart grid concept is a development on the path towards a higher consumer empowerment, higher integration of renewable energy conversion into the grid and higher energy use efficiency, contributing to the reduction of the anthropogenic emission and to the job creation and technological development in the European Union.

Photovoltaic energy conversion directly converts the solar energy into electric energy by the use of a solar cell. This is basically a p-n semiconductor junction with increasing in power output with the increase on solar irradiation and declining as temperature increases (Alami, 2014). Solar cells may be grouped to form modules. A PV array is a set of modules connected in series or parallel to form large PV systems with or without tracking systems in order to achieve higher values of energy conversion during sunny days due to the adjustment of the collecting plane so that it remains perpendicular to sunbeam throughout the day. But, even with tracking systems a correct consideration of the space for the operational neighborhood has to be assessed to avoid mutual shading (Fartaria and Pereira, 2013). Hence, the performance of a PV array depends on the operating conditions, i.e., depends not only on solar irradiation and

temperature, but also on the array configuration and shading effects. The shading effects, for instances, due to a passing cloud or neighboring buildings cause not only power losses, but also further non-linear effects on the I-V characteristics (Fialho et al., 2014a; Carrillo et al.; Díaz-Dorado et al., 2014). A solar cell is manufactured from several types of semiconductors and by several industrial processes (Sedra and Smith, 2006). The ideal photovoltaic cell equivalent circuit, a constant current source, with the electric current proportional to the irradiance level, in shunt with an ideal Shockley diode, which results from the theory of solid state physics is not enough suitable to represent the behavior of photovoltaic conversion. Observation on photovoltaic conversion data under different test conditions led to the inclusion of even more diodes and resistances, for instance, a very useful equivalent circuit (Rauschenbach, 1980) is the constant current source in shunt with a single-diode, with the ideality factor adjusted to the real characteristic data, and a parallel resistance followed by a series resistance (Khan et al., 2013). This inclusion is the one followed in this paper and allows a better practical representation, having five parameters to be identified in order to have a voltage and current characteristic resembling the behavior of the I-V characteristic of photovoltaic conversion (Rauschenbach, 1980; Duffie and Beckman, 2006). Data from Standard Test Conditions (STC) supply performance parameters for PV systems under the standard solar spectral distribution AM1.5 with an irradiance level of 1000 W/m^2 and *p-n junction* temperature of 25 ºC (IEC 60904–3, 2008; Marion, 2002; Rus-Casas et al., 2013). Additionally to STC parameters, performance parameters under nominal operating cell temperature (NOCT) are also provided by manufacturers. NOCT is the cell *p-n junction* temperature under ambient temperature of 20 ºC, solar spectral distribution AM1.5 with an irradiance level of 800 W/m^2 and wind speed of 1 m/s (IEC 60904–3, 2008). But all of these parameters, open circuit voltage, the short circuit current, the current and voltage at maximum power, the temperature coefficients at open circuit voltage and short circuit current, and the NOCT, provide not enough data for the identification of the five parameters equivalent circuit. Hence, particularly in the studies during the design phase there is a need to determine further experimental data, if experimentation is possible, or to introduce a method to evaluate a possible solution appropriated for the identification of the five parameters. The method used in this paper (Fialho et al., 2014b) postulates provision in order to circumvent the absence of enough data given by the producer of the PV module.

Power electronic converters have been developed for integrating renewable energy sources with the electric grid. The use of power electronic converters, namely inverters are particular indispensable in PV systems, allowing further for variable irradiance operation and enhanced power extraction, i.e., the inverter is indispensable for two accomplishments: the accomplishment of adjusting the low DC voltage of the PV module to the voltage level of the electric grid using a two power converter topologies, a DC-DC topology and a DC-AC topology; the accomplishment of the Maximum Power Point (MPP) tracking due to the fact of the power delivered by the modules being very sensitive to the point of operation in the I-V curve, the inverter is able to comply with functionality to circumvent this fact (Kjaer et al., 2002, Moradi et al., 2013). Historically, low power photovoltaic systems use single-phase inverters, but in three-phase grid connection, the use of only one single-phase inverters produce an imbalance between the phases due the injection of energy into only one phase of the grid. As reported in (Rampinelli et al., 2014) a maximum power of 4.6 kW, with 10% of tolerance, is possible to connect to only one phase of the three-phase grid. For power greater than 5 kW three single-

phase inverters are needed to ensure a balanced energy distribution between the three phases. The inverters used in grid connected photovoltaic systems use several circuits and there are a several options of transformer configurations. There are commercial inverters with high or low frequency transformers and even transformerless inverters. Each topology has its own characteristics and advantages and disadvantages (Kjaer et al., 2005; Patrao et al., 2011; Khatib et al., 2013; Rampinelli et al., 2014). The inverters used in grid-connected applications implant maximum power point tracker, anti-islanding operation, high conversion efficiency, automatic synchronization with the grid and have low level of harmonics distortion and power factor close to unity (Velasco et al., 2010; Patrao et al., 2011; Khatib et al., 2013; Rampinelli et al., 2014). The performance of the inverters connected to the grid depends largely on the control strategy applied (Zeng et al., 2013; Hassaine et al., 2014; Rampinelli et al., 2014). The DC-DC boost converter topology is a power converter with an output voltage greater than the input voltage. It is a class of switched-mode power supply (SMPS) containing at least two semiconductor switches (a diode and a transistor) and at least one energy storage element, a capacitor, inductor, or the two in combination. Filters made of capacitors or in combination with inductors are normally added to the output of the converter to reduce output voltage ripple (Kjaer et al., 2002). A two-level converter is an AC-DC-AC converter well suited for medium and high-power applications. Two-level converter generates an output voltage with two levels with respect to the ground terminal of the capacitor. Also, filters are normally added to the output of this converter to reduce output voltage ripple (Kjaer et al., 2002, Du et al., 2013).

This paper presents a study of mathematical models for a systemic modeling of a PV system including a DC-DC boost converter and a DC-AC two-level inverter. The paper is organized as follows. Section II presents the main expressions for the modeling of the solar cell, the PV system with DC-DC boost and two-level power inverter topologies. Section III presents the control strategies based on the use of classical PI controllers or fuzzy PI controllers, pulse width modulation (PWM) by space vector modulation (SVM) associated with sliding mode for controlling the converters, and we introduce power factor control at the output of the converters. Section IV presents the case studies with a comparison between simulation of a PV system model with classical or fuzzy PI controllers and experimental results obtained from three commercial inverters measured during their normal operation. Finally, concluding remarks are given in Section V.

2. Modeling

The PV system under study is constituted by a PV module, a DC-DC boost and a two-level power converter and is connected to an electric grid. The circuit model for the simulation of this PV system connected to the electric grid is shown in Fig. 1.

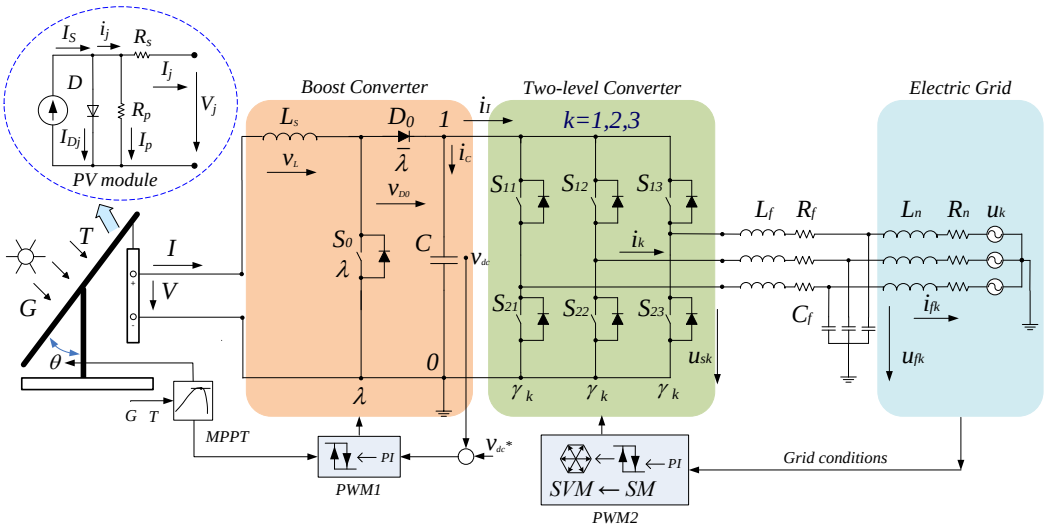

Fig. 1. The simulated PV system with DC-DC boost and two-level converter.

A three-phase active symmetrical independent voltage source in series with an inductive and resistive circuit models the electric grid. Power converters are on/off variable structure systems needing a particular description by switching functions as follows in 2.1 and 2.2.

2.1 PV module

The PV module equivalent circuit is shown in Fig. 1. The current i_j is given by (Fialho et al., 2014b):

$$i_j = I_j + \frac{V_j + R_s I_j}{R_p} \tag{1}$$

where *j* is an index associated with the operation conditions: $j = oc$ in open circuit conditions, $j = sc$ in short circuit conditions and $j = mx$ in MPP. From (1) at open circuit conditions, R_p is given by:

$$R_p = \frac{V_{oc}}{i_{oc}} \tag{2}$$

Also, from (1) at any operation conditions except for the open circuit conditions, R_s is given by (Fialho et al., 2014b):

$$R_s = \frac{R_p(i_j - I_j)}{I_j} - \frac{V_j}{I_j} \tag{3}$$

Eliminating R_s by equating (3) at short circuit and at MPP conditions and substituting R_p given by (2) holds the following equation:

$$V_{oc}\frac{i_{mx}-I_{mx}}{I_{mx}}-\frac{V_{mx}i_{oc}}{I_{mx}}-V_{oc}\frac{i_{sc}-I_{sc}}{I_{sc}}=0 \quad (4)$$

The diode current, i_{Dj}, is given by:

$$i_{Dj}=I_0 e_j \quad (5)$$

where e_j is defined by (Fialho et al., 2014b):

$$\ln(e_j+1)=\gamma(V_j+R_s I_j) \quad (6)$$

where γ is a parameter of the equivalent circuit defined by:

$$\gamma=\frac{1}{mV_T} \quad (7)$$

Hence, the current i_j is given by:

$$i_j=I_s-I_0 e_j \quad (8)$$

From (8), in open circuit conditions, in short circuit and in MPP holds the relations respectively given by:

$$I_s-I_0 e_{oc}-\frac{V_{oc}}{R_p}=0 \quad (9)$$

$$I_s-I_0 e_{sc}=i_{sc} \quad (10)$$

$$I_s-I_0 e_{mx}=i_{mx} \quad (11)$$

The system of equations (9) to (11) can be solved in order to I_s, I_0, i_{oc}, holding the solutions (12), (13) and (14) given by:

$$I_s=\frac{i_{sc}e_{mx}-i_{mx}e_{sc}}{e_{sc}^{mx}} \quad (12)$$

$$I_0=\frac{i_{mx}^{sc}}{e_{sc}^{mx}} \quad (13)$$

$$i_{oc}=\frac{i_{mx}e_{sc}^{oc}-i_{sc}e_{mx}^{oc}}{e_{sc}^{mx}}=\frac{V_{co}}{R_p} \quad (14)$$

where $e_j^{j'}$ and $i_j^{j'}$ are respectively defined by:

$$e_j^{j'} = e_{j'} - e_j$$
$$i_j^{j'} = i_{j'} - i_j \tag{15}$$

From (2), (9) to (11), holds the relations given by:

$$R_s I_{sc} < V_{mx} + R_s I_{mx} < V_{oc} = R_p i_{oc}$$
$$e_{sc} < e_{mx} < e_{oc} \tag{16}$$
$$i_{oc} < i_{mx} < i_{sc}$$

Taking the derivative of the current i_j given by (1) and (8) in order to the output voltage and equating both derivatives, holds the relation given by (Fialho et al., 2014b):

$$-\gamma R_p I_0 (1 + R_s \frac{dI_j}{dV_j}) e^{\gamma(V_j + R_s I_j)} = 1 + (R_p + R_s) \frac{dI_j}{dV_j} \tag{17}$$

If the derivative in (17) has null or positive values, then the relation does not hold. Hence as expected from experimental data, the derivative has to be a non-positive function, i.e., the PV module equivalent circuit is a non-ideal source of current. Also, in order to the relation (17) to be true hold the relations given by (Fialho et al., 2014b):

$$R_s < min\left\{-\frac{dV}{dI} : 0 \le V \le V_{oc}\right\} = -\left.\frac{dV}{dI}\right|_{oc}, \; R_p + R_s > max\left\{-\frac{dV}{dI} : 0 \le V \le V_{oc}\right\} = -\left.\frac{dV}{dI}\right|_{sc}$$

Hence hold the relations given by:

$$R_s < -\left.\frac{dV}{dI}\right|_{oc}, \; R_p > \left.\frac{dV}{dI}\right|_{oc} - \left.\frac{dV}{dI}\right|_{sc} \tag{18}$$

The MPP of a PV system depends on *G* and *T* (Dzimano, 2008), at the MPP conditions the conversion is attained at the highest efficiency (Dzimano, 2008; Beltran et al., 2008), implying the satisfaction of the relation given by:

$$-\left.\frac{dI}{dV}\right|_{mx} = \frac{I_{mx}}{V_{mx}} \tag{19}$$

Replacing the derivative of the current given by (19) into (17) at MPP, holds the relation given by:

$$\gamma R_p i_{mx}^{sc} (V_{mx} - R_s I_{mx})(e_{mx} + 1) + V_{mx} - I_{mx}(R_s + R_p) e_{sc}^{mx} = 0 \tag{20}$$

From (20), replacing R_p given by (2), $R_s I_{mx}$ given by (3) at MPP conditions, holds the relation given by (Fialho et al., 2014b):

$$\gamma V_{oc} i_{mx}^{sc} (I_{mx} - \delta)(e_{mx} + 1) - \delta i_{oc} e_{sc}^{mx} = 0 \tag{21}$$

where δ is defined by:

$$\delta = i_{mx} - 2\frac{V_{mx}}{V_{oc}} i_{oc} \tag{22}$$

From (21), δ is given by (Fialho et al., 2014b):

$$\delta = \frac{\gamma V_{oc} i_{mx}^{sc} (e_{mx} + 1)}{\gamma V_{oc} i_{mx}^{sc} (e_{mx} + 1) + i_{oc} e_{sc}^{mx}} I_{mx} \tag{23}$$

Hence, considering the last two inequalities of (16), (21) and (23), δ has to satisfy the relation given by:

$$0 < \delta < I_{mx} \tag{24}$$

From (1), i_j has to satisfy the relation given by:

$$i_j \geq I_j \tag{25}$$

Relation (25) allows to justify the initialization of the values for the unknowns i_{mx} and i_{sc} as near but not equal to the values I_{mx} and I_{sc}. Also, due to the relations (18), considering the relations and (2), (22), (24) the bounds for R_p and R_s are assumed to be respectively given by:

$$R_s \leq -\left.\frac{dV}{dI}\right|_{mx} \text{ and } R_p \geq -\left.\frac{dV}{dI}\right|_{mx} \tag{26}$$

The ideality factor, m, for a cell is assumed to be between 2/3 and 2. Hence from (7) the boundaries for γ are given by (Fialho et al., 2014b):

$$\frac{1}{2V_T} \leq \gamma \leq \frac{3}{2V_T} \tag{27}$$

The I-V characteristic for the PV module shown in Fig. 1 is given by:

$$I = I_S - I_0 (e^{\gamma(V + IR_S)} - 1) - (V + IR_S)/R_p \tag{28}$$

The five parameters associated with this I-V characteristic are identified by the solution of an optimization procedure. The General Algebraic Modeling System (GAMS) is used to code the mathematical programming problem (Fialho et al., 2014b) developed for the optimization procedure. The mathematical programming problem for photovoltaic module parameter identification is modeled by the equations (1), (4), (6), (14), (20) and the inequalities (16), (25), (26), (27). The optimization process computes the parameters R_p, R_s, γ, I_S and I_0.

2.2 DC-DC boost converter

The configuration of DC-DC boost converter in the simulated PV system is shown in Fig. 1. The DC-DC boost converter has one unidirectional commanded IGBT S_0. The switching function of the DC/DC boost converter is described by the switching variables λ, $\overline{\lambda}$ used to identify the state of the IGBT S_0 and to identify the state of the diode D_0 of the boost converter, respectively. The constraints on the switching variable of the DC/DC boost converter (Silva and Pinto, 2007) are given by:

$$\begin{cases} \lambda = 1 \text{ and } \overline{\lambda} = 0 \ (S_0 = 1 \text{ and } D_0 = 0) \\ \lambda = 0 \text{ and } \overline{\lambda} = 1 \ (S_0 = 0 \text{ and } D_0 = 1) \end{cases} \tag{29}$$

The array current *I* is modeled by the state equation given by:

$$\frac{dI}{dt} = \frac{1}{L_s}[v_A - \overline{\lambda}\ (v_{D0} + v_{dc})\ ] \tag{30}$$

The capacitor voltage v_{dc} is modeled by the state equation given by:

$$\frac{dv_{dc}}{dt} = \frac{1}{C}\ (\overline{\lambda}\ I - i_I) \tag{31}$$

At steady state the mean value of the voltage at the inductance terminals v_L is null, given by:

$$v_L = \frac{1}{T}\ [\int_0^{\lambda T} v_A\ dt + \int_{\lambda T}^{T} (v_A - v_{dc})\ dt\ ] = 0 \tag{32}$$

For an ideal boost converter the relationship between v_{dc} and v_A is given by:

$$\frac{v_{dc}}{v_A} = \frac{1}{(1 - \lambda(t))} \tag{33}$$

Hence, the DC-DC boost converter can be modeled by (29) to (33).

2.3 Two-level inverter

The two-level inverter is a DC-AC converter, with six unidirectional commanded IGBTs, S_{hy}, as shown in Fig. 1. The inverter is connected between a capacitor bank and a second order filter, which in turn is connected to an electric grid. The groups of two IGBTs linked to the same phase constitute a leg y of the converter. The two-level converter modeling assumes that: 1) the IGBTs are ideal and unidirectional and are never subject to reverse voltages, this is assured by the connection of an anti-parallel diode to each IGBT; 2) the diodes are ideal, i.e., in conduction state the voltage between their terminals is null, and in blockade the current that passes through diodes is null; 3) the voltage at the output of the boost converter is $v_{dc} > 0$; 4) each leg y of the converter always has one IGBT on a conduction state. The switching function of each IGBT is described by the switching variable γ_y, identifying the state of the IGBT h in the leg y of the converter. The index h with $h \in \{a,b\}$ identifies the IGBT. The index y with $y \in \{a,b,c\}$

identifies a leg of the inverter. The two conditions (Melício and Mendes, 2007) for the switching variable of each leg y are given by:

$$\gamma_y = \begin{cases} 1, \ (S_{ay} = 1 \ \text{and} \ S_{by} = 0) \\ 0, \ (S_{ay} = 0 \ \text{and} \ S_{by} = 1) \end{cases} \qquad y \in \{a,b,c\} \tag{34}$$

The topological restriction for the leg y is given by:

$$\sum_{h=a}^{b} S_{hy} = 1 \qquad y \in \{a,b,c\} \tag{35}$$

Hence, each switching variable depends on the conduction and blockade states of the IGBTs. The current injected into the inverter i_I is given by:

$$i_I = \sum_{y=a}^{c} \gamma_y i_y \tag{36}$$

Hence, the two-level converter is modeled by (34) to (36). The measure of the voltage and the current harmonic content at the output of the inverter is carried out by the discrete Fourier transform (DFT). The DTF is given by:

$$X(k) = \sum_{n=0}^{N-1} e^{-j2\pi k n/N} \ x(n) \quad \text{for} \quad k = 0,...,N-1 \tag{37}$$

The total harmonic distortion (THD) is given by:

$$\text{THD}\ (\%) = 100 \frac{\sqrt{\sum_{H=2}^{50} X_H^2}}{X_F} \tag{38}$$

2.4 Electric grid

The phase currents injected into the electric grid i_{fy}, considering the grid as an equivalent circuit given by a three-phase active symmetrical circuit as shown in Fig. 1, is given by:

$$\frac{di_{fy}}{dt} = \frac{1}{L_n}(u_{fy} - R_n i_{fy} - u_y) \qquad y \in \{a,b,c\} \tag{39}$$

Hence, the electric grid is modelled by (39).

3. Control strategy

A maximum power point tracking (MPPT) is used to extract the maximum power from a PV system which is under varying weather conditions. The DC-DC boost converter is used to implement maximum power operation of the PV system, controlling the voltage at the array

terminals. The calculation of PV array output power requires solar irradiance and ambient temperature records, and therefore, records of these variables have been obtained for the adopted site (Kazem and Khatib, 2013; Raj and Jeyakumar, 2014). The control of the boost converter includes the MPPT, using the $\partial P/\partial V$ algorithm to implement MPPT on the P-V curve of the array for each pair (*G, T*) and classical PI controllers or fuzzy PI controllers, as in (Viveiros et al., 2014; Viveiros et al., 2015).

PWM by SVM associated with sliding mode control is used for controlling the converters. The sliding mode control strategy presents attractive features such as robustness to parametric uncertainties of the PV array as well as to electric grid disturbances (Jiang et al., 2005). Sliding mode control is particularly interesting in systems with variable structure, such as power converters, guaranteeing the choice of the most appropriate space vectors. The aim of the sliding mode control is to let the system slide along a predefined sliding surface by changing the system structure. The control strategy of the PV system with DC-DC boost and two-level power converter topologies using classical or fuzzy PI controllers has the diagram in box PWM1 and in box PWM2 shown in Fig. 1. The convenient vector selection to ensure stability for the converters, after being processed by the hysteresis comparator in the block of SM control and SVM are given in (Seixas et al., 2014). The SM control is a lower level of control as is normally implemented with the classical or fuzzy PI controller, for triggering the converters transistors is used pulse width modulation (PWM) by SVM supplemented with SM.

Power semiconductors have physical limitations to be considered during design phase and during simulation. Particularly, the switch frequency has to be a finite value, for instances, switching frequency of 2 kHz, 5 kHz or 10 kHz are normally reported. The switch frequency finite value implying that an error $e_{\alpha\beta}$ has to be tolerated on the electric current, i.e., an error between the reference value and the control value of the current. The error trajectory in order to guarantee that the system follows the sliding surface $S(e_{\alpha\beta},t)$, based on the Concordia transformation ($\alpha-\beta$), has to be in a convenient neighboring of this sliding surface, implying the satisfaction of stability conditions (Silva and Pinto, 2007; Melício and Mendes, 2007) given by:

$$S(e_{\alpha\beta},t)\ \frac{dS(e_{\alpha\beta},t)}{dt}<0 \tag{40}$$

The sliding surface in current practice is chosen in way to allow a small error $\varepsilon>0$ for $S(e_{\alpha\beta},t)$. But, for the simulation studies, an implementation of the switching strategy considered may be implemented by hysteresis comparators performing accordingly to the condition given by:

$$-\varepsilon<S(e_{\alpha\beta},t)<+\varepsilon \tag{41}$$

The outputs of the hysteresis comparators are the integer variables $\sigma_{\alpha\beta}=(\sigma_\alpha,\sigma_\beta)$ for the two-level converter take the values (Silva and Pinto, 2007) given by:

$$\sigma_{\alpha\beta}\ \text{ with }\ \sigma_\alpha,\sigma_\beta\in\{-1,0,1\} \tag{42}$$

The integer variables values indicate whether the error is within or outside the sliding surface. If the error is within the sliding surface, given by $\sigma_\alpha=0$ and $\sigma_\beta=0$, the converter IGBTs do not switch, maintaining the actual voltage vector, but if the error is outside of the sliding surface,

the voltage vector that meets the $\sigma_{\alpha\beta}$ coordinates is chosen, forcing the converter transistors to switch, in order to bring the error back into the sliding surface. For the two-level converter there are eight possible IGBTs combinations, which correspond to eight output voltage vectors and two voltage levels, lying between level 0 and level 1. The IGBTs switching state combinations with corresponding output voltage vectors and levels are shown in Table 1.

Table 1. IGBTs switching state combinations with corresponding output voltage vectors

Vector	S_{aa}	S_{ba}	S_{ab}	S_{bb}	S_{ac}	S_{bc}	γ_a	γ_b	γ_c	$u_{s\alpha}/v_{dc}$	$u_{s\beta}/v_{dc}$	Level
a_0	0	1	0	1	0	1	0	0	0	0.0	0.0	0
b_1	1	0	0	1	0	1	1	0	0	0.8164	0.0	1
c_1	0	1	1	0	0	1	0	1	0	-	0.7071	1
d_1	1	0	1	0	0	1	1	1	0	0.4082	0.7071	1
e_1	0	1	0	1	1	0	0	0	1	-	-	1
f_1	1	0	0	1	1	0	1	0	1	0.4082	-	1
g_1	0	1	1	0	1	0	0	1	1	-	0.0	1
h_0	1	0	1	0	1	0	1	1	1	0.0	0.0	0

For the two-level converter the output voltage vector a_0 and h_0 are vectors for level 0 and vectors from b_1 to g_1 are vectors for level 1. The generic output voltage vectors in the $\alpha\beta$ plane for the two-level converter are shown in Fig. 2.

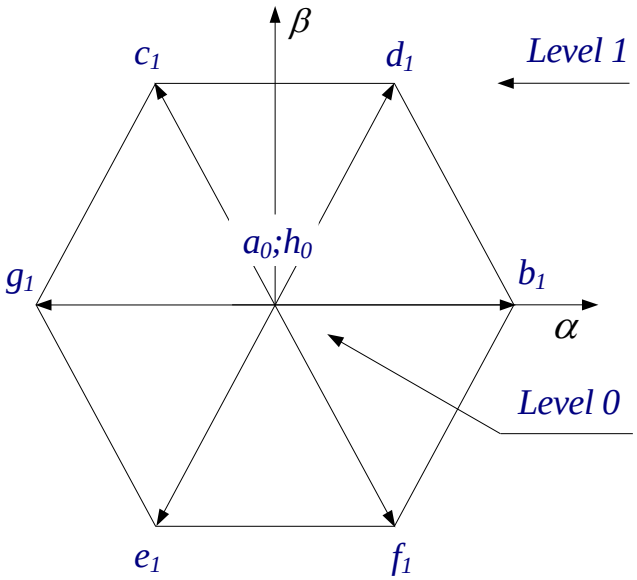

Fig. 2. Output voltage vectors for the two-level converter.

The generic vector selection in order to ensure stability for the two-level converter (Silva and Pinto, 2007; Melício and Mendes, 2007) is shown in Table 2.

Table 2. Output voltage vector selection for the two-level converter

$\sigma_\beta \setminus \sigma_\alpha$	**-1**	**0**	**1**
-1	e_1	e_1;f_1	f_1
0	g_1	a_0;h_0	b_1
1	c_1	c_1;d_1	d_1

Hence, the proposed control strategy for the power converters is given by (40) to (42).

4. Case studies

The cases studies are from a PV system (Giacobbe, 2005) situated in LNEG, Lisbon, Portugal, coordinates 38°46'18.50' N, 9°10'38.50' W. The mathematical model for the PV system with the five parameters cell equivalent circuit module, the DC-DC boost and the two-level power converter topologies as shown in Fig. 1 is implemented in Matlab/Simulink. The simulation is carried out for the four different PV module technologies at LNEG: monocrystalline, polycrystalline, amorphous and thin-film silicon solar modules.
The irradiation and module temperature for the three PV systems connected to the electric grid at the time of the experimental tests, i.e., February 02, 2012 is shown in Table 3.

Table 3. Data of the irradiance and module temperature

Irradiance and module temperature			
Test Parameters	System A	System B	System C
Irradiance (W/m^2)	780	730	800
Ambient Temperature (°C)	8	8.5	13
Date and Hour	03/02/2012 11:21	03/02/2012 11:53	08/02/2012 12:11

The experimental systems description and configurations are shown in Fig. 3.

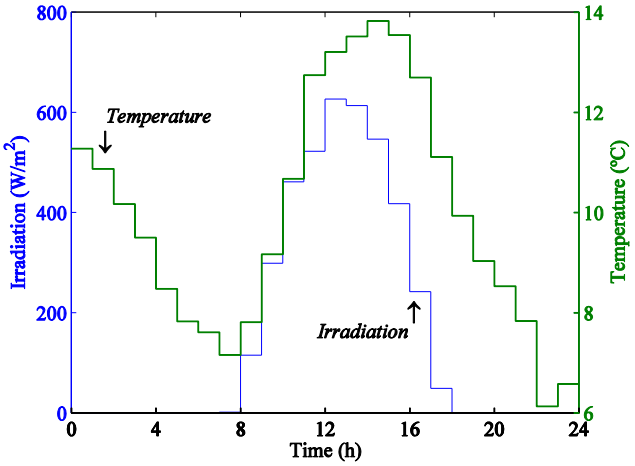

Fig. 3. Irradiation and module temperature at February 02, 2012.

The three PV systems connected to the electric grid studied are situated in LNEG, Lisbon, Portugal. The PV systems are connected via the electrical switchboard to the electric grid of

230/400 V at 50 Hz. The three experimental systems description and array configurations are shown in Table 4.

Table 4. The experimental systems description and configurations

Parameter	System A	System B	System C
Module capacity (Wp)	160	60	80
Module manufacturer/model	BP 3160	Kaneka GEA60	Schüco SPV 80-TF
Module Technology	Poly-Si	a-Si	CIS Thin-Film
Installed capacity (kWp)	3.840	3.000	3.920
String configuration	8 modules × 3 strings	5 modules × 10 strings	7 modules × 7 strings
Inverter manufacturer/model	Fronius IG40	SolarStocc PS4000HV	SMA SunnyBoy 3800/V
Inverter output rated capacity (kW)	3.500	3.300	3.680

The tests were performed in clear sky days. The relevant measures are the voltage and current inputs at power line as well as at harmonic frequencies. The power quality measurement equipment according to EN 50160 used is the Fluke 41 Power Harmonic Analyzer. The analyzer automatically calculates power and other measurements useful in determining harmonic distortion levels. This analyzer has a fundamental frequency measurements up to 100 Hz and harmonic frequency measurements up to about 1.5 kHz. Data acquisition harmonic components are up to the 31st harmonic order and their angle shift, with the phase angle of the fundamental voltage taken as reference.
The irradiation and the ambient temperature at the time of the experimental tests for the current and voltage waveform measurements are shown in Table 5.

Table 5. Data of the current and voltage waveform measurements

Current and Voltage Waveforms			
Test Parameters	System A	System B	System C
Irradiance (W/m^2)	880	400	800
Ambient Temperature (ºC)	15	13	13
Date and Hour	10/02/2012 14:40	31/01/2012 16:52	08/02/2012 12:08

Three single phase photovoltaic inverters where tested for the comparison with the results from the models and the evaluation of the power quality delivered to the electrical grid. The inverters are hereby named as inverter A, B and C, with a nominal AC power of 3.5 kW, 3.68 kW and 3.3 kW, respectively.

4.1 Case study 1 — Comparison between simulation and experimental results for a PV module

This case study assesses the validity of the modeling of the PV systems for the four different PV module technologies tested, monocrystalline, polycrystalline, amorphous and thin-film silicon.

Table 6 summarizes the data given by the producers of the PV modules at STC (Isofoton SA, Photowatt, Kaneka Solar Energy, Schüco).

Table 6. Data of the silicon solar modules at STC

Technology	V_m^*	I_m^*	V_{oc}^*	I_{sc}^*	Cells	β_{oc}	α_{sc}	NOCT
Monocrystalline Isofotón I53	17.4 V	3.05 A	21.65 V	3.27 A	36	-80 mV/ °C	1.748 mA/ °C	47 °C
Polycrystalline Photowatt PW500	17.2 V	2.9 A	21.6 V	3.2 A	36	-79 mV/ °C	0.95 mA/ °C	-
Amorphous Kaneka KA58	63 V	0.92 A	85 V	1.12 A	-	-206 mV/ °C	1.3 mA/ °C	-
Thin-film SPV 80-TF	41 V	1.95 A	56.5 V	2.26 A	-	-107.35 mV/ °C	0.904 mA/ °C	48 °C

The silicon monocrystalline module tested at STC (Isofotón I53) (IEC 60891, 2009) five parameters identification allows to draw the green curve, while the experimental results gives the blue curve shown for the I-V curves plotted in Fig. 4.

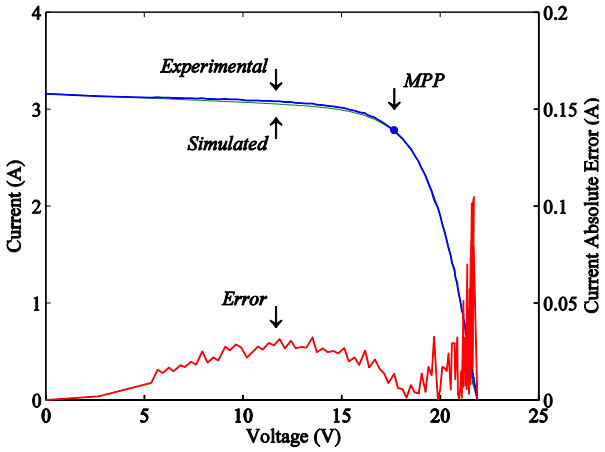

Fig. 4. I-V simulated and experimental curves at STC and current relative error (Isofotón I53).

Fig. 4 also shows the absolute error in red between the two curves. The equivalent plots but for the silicon polycrystalline module tested at STC (Photowatt PW500) (IEC 60891, 2009) five parameters identification and experimental results are shown in Fig. 5.

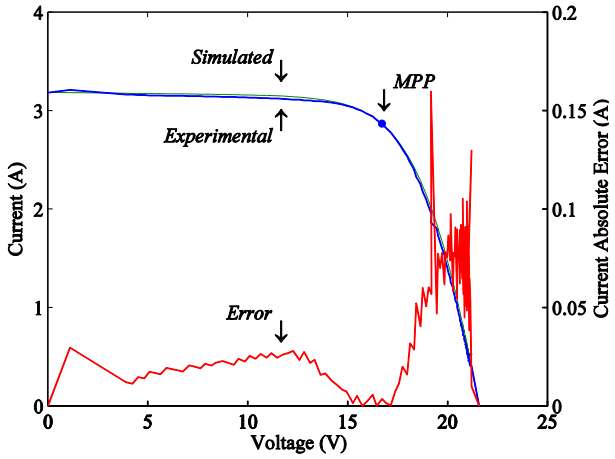

Fig. 5. I-V simulated and experimental curves at STC and current relative error (Photowatt PW500).

The equivalent plots for the silicon amorphous solar module tested at STC (Kaneka KA 58) (IEC 60891, 2009) five parameters identification and experimental results are shown in Fig. 6.

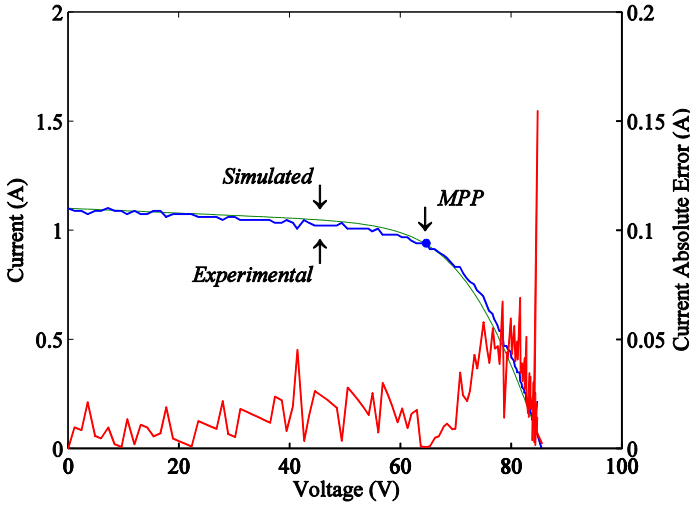

Fig. 6. I-V simulated and experimental curves at STC and current relative error (Kaneka KA 58).

The equivalent plots for the silicon thin-film solar module tested at STC (Schüco SPV 80-TF) five parameters identification and experimental results are shown in Fig. 7.

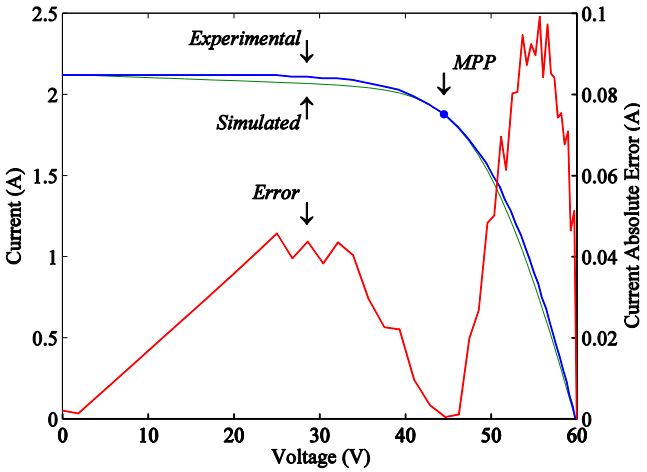

Fig. 7. I-V simulated and experimental curves at STC and current relative error (SPV 80-TF).

The observation of the errors in Fig. 5, Fig. 6 and Fig. 7 shows that the method for the five parameters identification in general has an acceptable error and allows neighborhoods where the normal operation is located, i.e., neighborhoods of maximum power point, with an exceptional small error. Hence, in case of non feasibility for the experimental testing, the five parameters identification method used in this paper is an acceptable one.

4.2 Case study 2 — Ideal Sinusoidal Grid Voltage Waveform

This case study assesses the simulation results for the PV system with the electric grid of the 230 V at 50 Hz. The current injected into the electric grid, simulated with classical PI controller in green and experimental in blue implementing the inverter A are shown in Fig. 8.

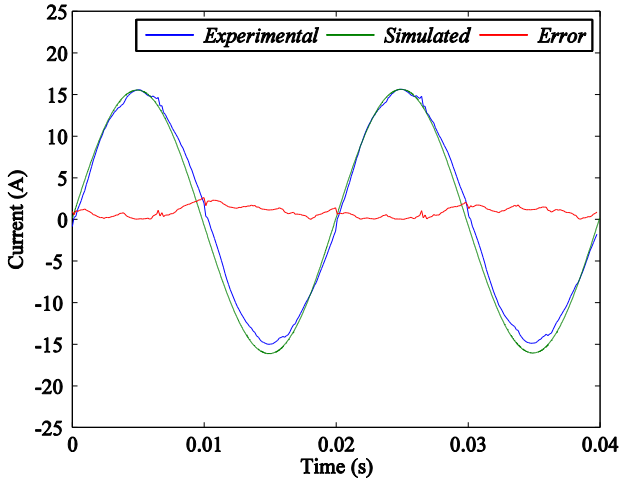

Fig. 8. Current injected into the electric grid simulated (ideal) and experimental for the inverter A.

Fig. 8 also shows in red the absolute error between the two currents. The correspondent figure for the current injected into the electric grid, simulated with classical PI controller and experimental results, implementing the inverter B are shown in Fig. 9.

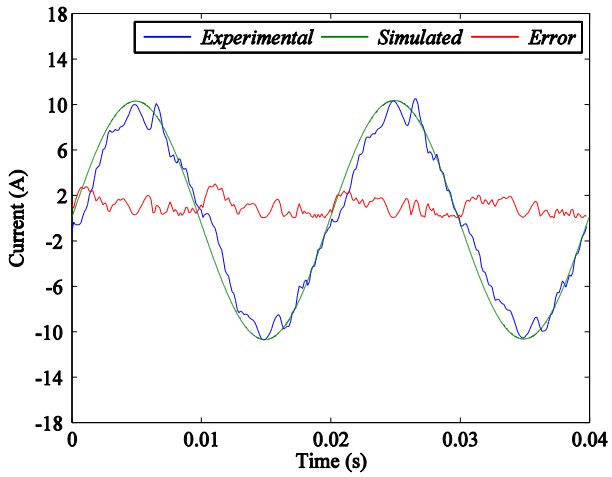

Fig. 9. Current injected into the electric grid simulated (ideal) and experimental for the inverter B.

The correspondent figure for the current injected into the electric grid, simulated with classical PI controller and experimental results, implementing the inverter C is shown in Fig. 10.

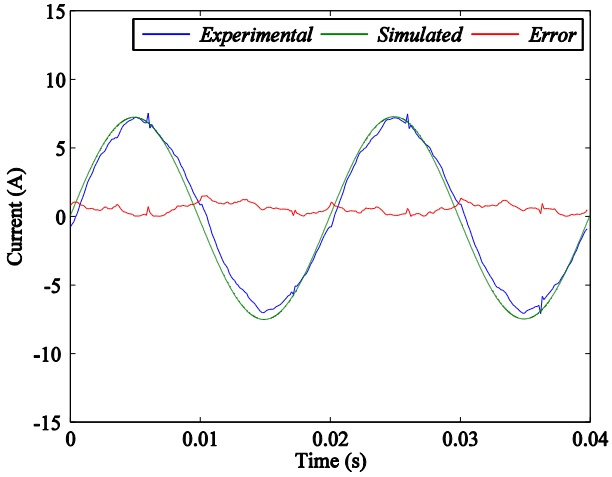

Fig. 10. Current injected into the electric grid simulated (ideal) and experimental for the inverter C.

The observation of the errors in Fig. 8, Fig. 9 and Fig. 10 is in favor of concluding that the PV system model has an acceptable behavior.
The harmonic behavior given by the DFT for the current injected into the electric grid, simulated with classical PI controller in blue and the experimental in green, implementing the inverter A is shown in Fig. 11.

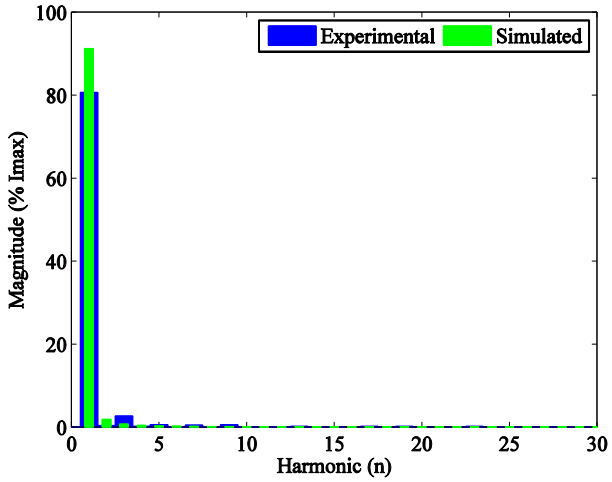

Fig. 11. DFT of the current injected into the electric grid simulated and experimental, inverter A.

The harmonic behavior for the current injected into the electric grid, simulated with classical PI controller in blue and the experimental in green, implementing the inverter B is shown in Fig. 12.

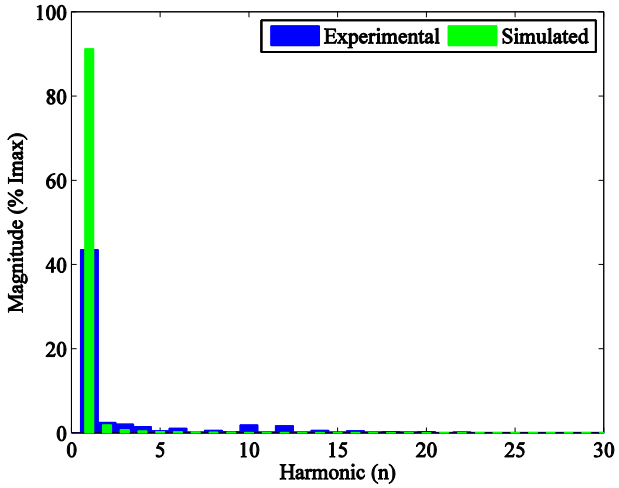

Fig. 12. DFT of the current injected into the electric grid simulated and experimental, inverter B.

The harmonic behavior for the current injected into the electric grid, simulated with classical PI controller in blue and the experimental in green, implementing the inverter C is shown in Fig. 13.

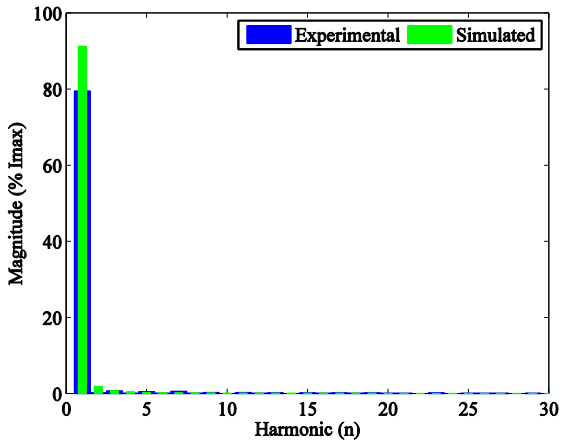

Fig. 13. DFT of the current injected into the electric grid simulated and experimental, inverter C.

The harmonic behavior for the output phase current at the inverter and for the phase current injected into the electric grid, simulated with classical PI controller are shown in Fig. 14.

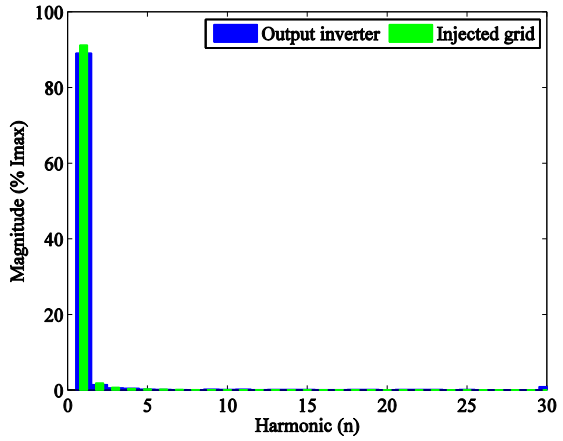

Fig. 14. Classical PI controller, DFT of the output current at the inverter and current injected into the electric grid, simulated.

The harmonic behavior for the output phase current at the inverter, and for the phase current injected into the electric grid, simulated with fuzzy PI controller, are shown in Fig. 15.

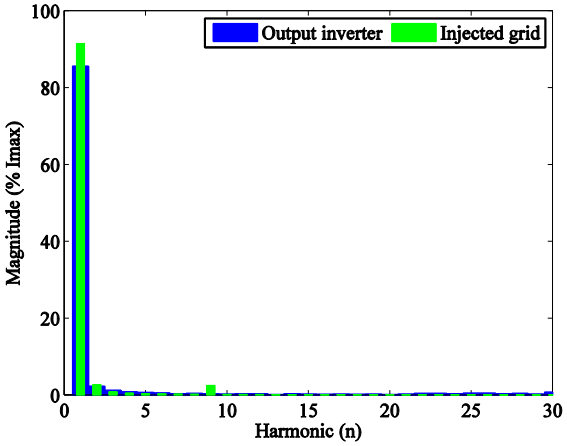

Fig. 15. Fuzzy PI controller, DFT of the output current at the inverter and current injected into the electric grid, simulated.

The harmonic behavior for the phase current injected into the electric grid, simulated with classical PI controller and fuzzy PI controller, are shown in Fig. 16.

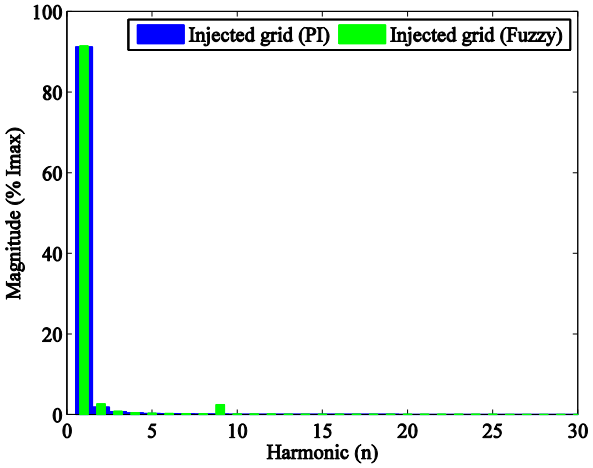

Fig. 16. Classical and fuzzy PI controllers, DFT of the current injected into the electric grid, simulated.

Ideal wave, comparison between the harmonic in percentage of the fundamental component for the current experimental and the simulated results with classical or fuzzy PI controllers, are shown in Table 7.

Table 7. Ideal wave, harmonic in percentage of the fundamental component for the current experimental and simulated

Harmonic (n)	Experimental			Simulated			
	Inverter			Classical PI controller		Fuzzy PI controller	
	A (%)	B (%)	C (%)	Output current at the inverter (%)	Current injected into the grid (%)	Output current at the inverter (%)	Current injected into the grid (%)
1	80.7	79.5	43.5	84.1	91.2	85.6	91.5
2	0.4	0.2	2.5	1.9	1.5	2.3	2.7
3	2.7	0.7	2.1	2.5	0.7	1.2	0.9
4	0.2	0.1	1.5	1.0	0.4	0.9	0.5
5	0.6	0.5	0.5	0.6	0.2	0.7	0.4
6	0.1	0.1	1.1	0.4	0.3	0.6	0.3
7	0.5	0.6	0.2	0.3	0.2	0.4	0.3
8	0.1	0.1	0.6	0.4	0.1	0.5	0.2
9	0.6	0.3	0.3	0.5	0.2	0.4	2.5

10	0.1	0.1	1.9	0.3	0.1	0.3	0.2
11	0.1	0.3	0.6	0.4	0.2	0.3	0.2

The observation of the Fig. 14, Fig. 15 and Fig. 16 is in favor of concluding that the current injected into the grid for the PV system with fuzzy PI controller presents a content of 2nd and 9th harmonic greater than the PV system with classical PI controller.

4.3 Case study 3 — No-ideal Sinusoidal Grid Voltage Waveform

This case study assesses the simulation results for an independent voltage source 230 V at 50 Hz with harmonic contents: 4% of second, 5% of third, 3% of fifth, 3% of seventh and 2% of ninth harmonic components. The current injected into the electric grid, simulated with classical PI controller in green, experimental in blue, implementing the inverter A are shown in Fig. 17.

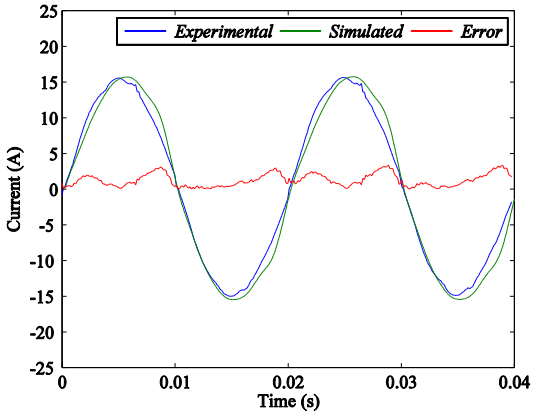

Fig. 17. Current injected into the electric grid simulated (no ideal) and experimental for the inverter A.

Fig. 17 also shows in red the absolute error between the two currents. The equivalent figure but for the current injected into the electric grid simulated with classical PI controller and experimental results implementing the inverter B are shown in Fig. 18.

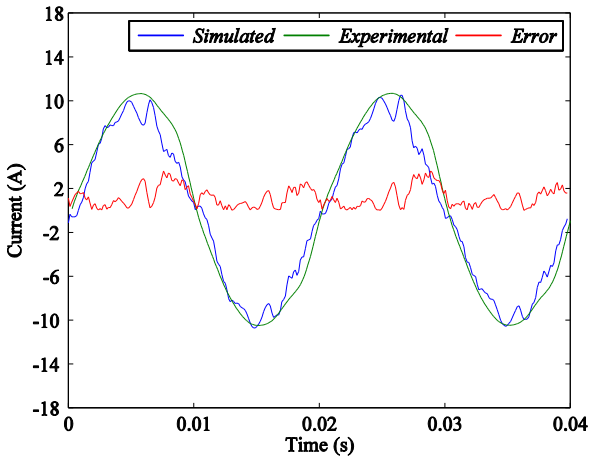

Fig. 18. Current injected into the electric grid simulated (no ideal) and experimental for the inverter B.

The equivalent figure but for the current injected into the electric grid simulated with classical PI controller and experimental results implementing the inverter B are shown in Fig. 19.

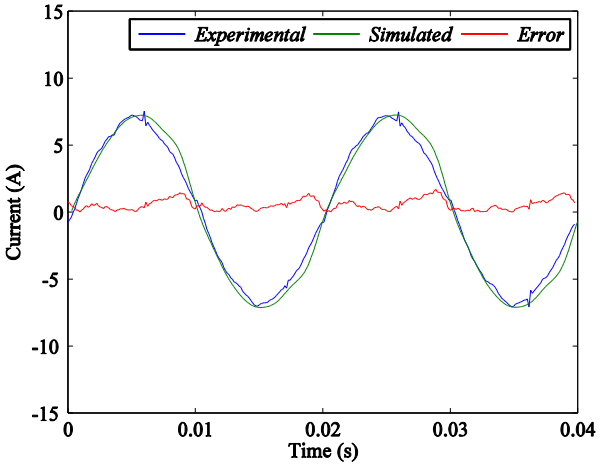

Fig. 19. Current injected into the electric grid simulated (no ideal) and experimental for the inverter C.

The harmonic behavior given by the DFT for the current injected into the electric grid, simulated with classical PI controller in blue and the experimental in green, implementing the inverter A are shown in Fig. 20.

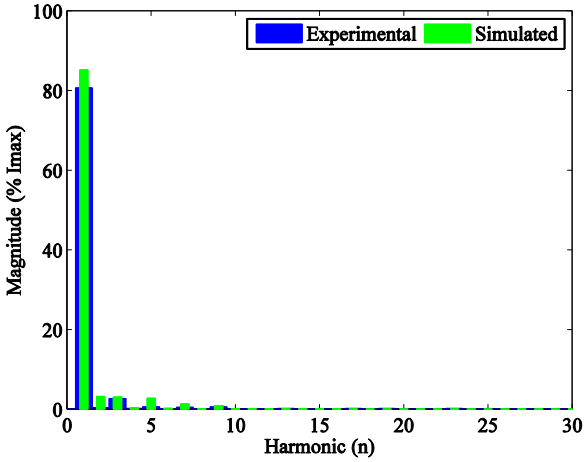

Fig. 20. DFT of the current injected into the electric grid simulated and experimental, inverter A.

The harmonic behavior for the current injected into the electric grid simulated with classical PI controller and the experimental implementing the inverter B is shown in Fig. 21.

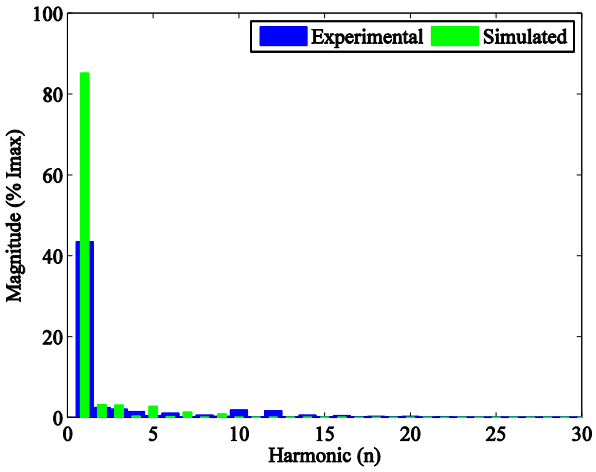

Fig. 21. DFT of the current injected into the electric grid simulated and experimental, inverter B.

The harmonic behavior for the current injected into the electric grid simulated with classical PI controller and the experimental implementing the inverter C is shown in Fig. 22.

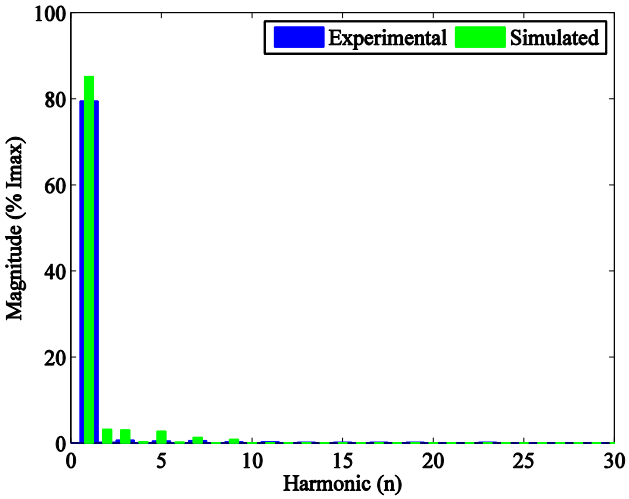

Fig. 22. DFT of the current injected into the electric grid simulated and experimental, inverter C.

The harmonic behavior for the output phase current at the inverter and for the phase current injected into the electric grid simulated with classical PI controller are shown in Fig. 23.

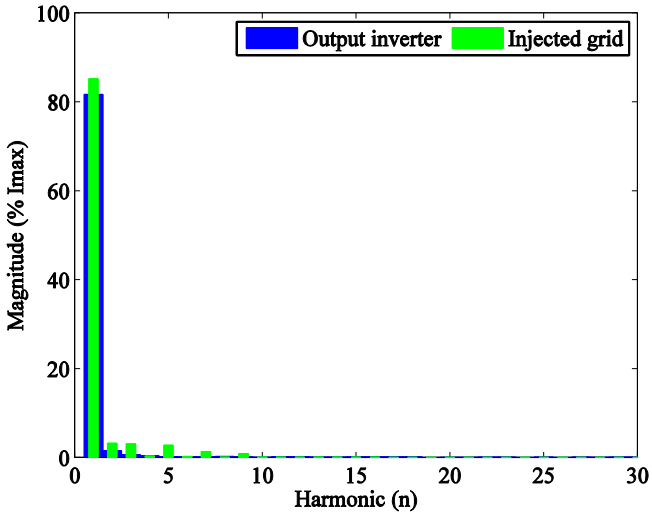

Fig. 23. Classical PI controller, DFT of the output current at the inverter and current injected into the electric grid, simulated.

The harmonic behavior for the output phase current at the inverter and for the phase current injected into the electric grid simulated with fuzzy PI controller are shown in Fig. 24.

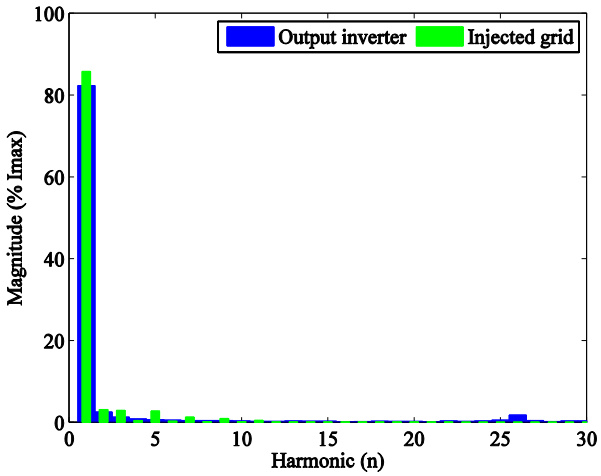

Fig. 24. Fuzzy PI controller, DFT of the output current at the inverter and current injected into the electric grid, simulated.

The harmonic behavior for the phase current injected into the electric grid simulated with classical PI controller and fuzzy PI controller are shown in Fig. 25.

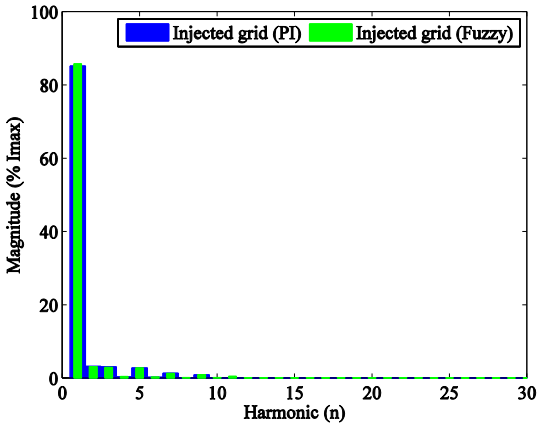

Fig. 25. Classical and fuzzy PI controllers, DFT of the current injected into the electric grid, simulated.

The observation of the Fig. 23, Fig. 24 and Fig. 25 is in favor of concluding that the current injected into the grid for the PV system with fuzzy PI controller presents a content of 2nd, 3rd, 5th, 7th and 9th harmonic similar than the PV system with classical PI controller.
No-ideal voltage wave comparison between the harmonic in percentage of the fundamental component of the current the experimental and of the simulated results with classical or fuzzy PI controllers is shown in Table 8.

Table 8. No-ideal wave, harmonic in percentage of the fundamental component for the current experimental and simulated

Harmonic (n)	Experimental			Simulated			
	Inverter			Classical PI controller		Fuzzy PI controller	
	A (%)	B (%)	C (%)	Output current at the inverter (%)	Current injected into the grid (%)	Output current at the inverter (%)	Current injected into the grid (%)
1	80.7	79.5	43.5	81.7	85.2	82.3	85.8
2	0.4	0.2	2.5	1.54	3.25	2.52	3.12
3	2.7	0.7	2.1	0.69	3.09	1.3	2.93
4	0.2	0.1	1.5	0.41	0.36	0.9	0.46
5	0.6	0.5	0.5	0.21	2.75	0.7	2.79
6	0.1	0.1	1.1	0.17	0.27	0.5	0.32
7	0.5	0.6	0.2	0.19	1.35	0.5	1.3
8	0.1	0.1	0.6	0.25	0.12	0.5	0.17
9	0.6	0.3	0.3	0.18	0.89	0.5	0.93
10	0.1	0.1	1.9	0.04	0.09	0.4	0.15
11	0.1	0.3	0.6	0.22	0.09	0.3	0.5

The harmonic content given by the DFT for the current injected into the grid with the ideal sinusoidal voltage grid waveform shows that the dominant harmonics are the 2nd and 3rd order ones. The harmonics of higher orders, basically odd ones, were also recorded but their magnitudes are negligible. While, for the non-ideal sinusoidal voltage grid waveform the

dominant harmonics are the 2nd, 3rd, 4th, 5th, 7th and 9th order. The harmonics of higher orders, basically odd ones, are also negligible.
The harmonic content for the current injected into the grid for the inverter A and the inverter B the dominant harmonics are the 3rd, 5th, 7th, 9th and 11th order. The harmonics of higher orders, basically odd ones, are also recorded but their magnitude is negligible, which does not occur for the inverter C where the dominating harmonics are even and odd harmonics. The largest part relevant even harmonics are the 2nd, 4th, 6th, 8th and 10th. The harmonic for the current injected into the grid for the inverter A, B, C with the proposed PV system, having the DC-DC boost and the two-level inverter is due the PWM control strategy. The connection of the PV system in the electric grid causes in the current injected into the electric grid the presence of the 2nd, 3rd and 5th order harmonics. The current injected into the grid for the inverter A and B show good grid performance regarding the THD, i.e., the THD is lower than the 5% limit imposed by standards IEEE 519 and IEEE 1547, while the inverter C has a THD out of these standards. The high order harmonics of the output current are filtered out by the second order filter. A comparison between the THD with ideal and no-ideal wave for the current injected into the electric grid experimental and the simulated with classical or fuzzy PI controllers is shown in Table 9.

Table 9. The THD for the current injected into the grid experimental and simulated

	Experimental			Simulated			
	Inverter			Classical PI controller		Fuzzy PI controller	
	A	B	C	Ideal wave	Non-ideal wave	Ideal wave	Non-ideal wave
THD (%)	3.73	4.17	10.24	5.005	7.29	4.94	7.03

A comparison between the THD with ideal and no-ideal wave for the electric grid voltage experimental and the simulated with classical or fuzzy PI controllers is shown in Table 10. The simulated results for the controllers with ideal wave and no-ideal wave, Table 7 to Table 10, shown that the fuzzy PI controller presents a slightly better similar behavior to the classical PI controller.

Table 10. The THD for the grid voltage experimental and simulated

	Experimental			Simulated			
	Inverter			Classical PI controller		Fuzzy PI controller	
	A	B	C	Ideal wave	Non-ideal wave	Ideal wave	Non-ideal wave
THD (%)	0.83	0.88	0.90	0.24	7.39	0.281	6.81

The root mean square error (RMSE) with the classical PI controller of the current injected into the electric grid is shown in Table 11.

Table 11. Simulations root mean square error (RMSE), current injected into the grid

Method	Inverter A	Inverter B	Inverter C
Simulated ideal wave RMSE (A)	1.099	1.263	0.665
Simulated non-ideal wave RMSE (A)	1.549	1.489	0.678

RMSE Variation (%)	140.92	117.91	101.98

The voltage THD profile of the electric grid is not significantly affected by the PV system. The voltage THD for the inverters and the proposed PV system is lower than the limit imposed by standards IEEE 519, IEEE 1547 and EN50160. The harmonics are related to the power-electronic conversion system and the control.

5. Conclusions

The increased PV system penetration leads to new technical challenges implying research for more realistic physical models of distributed power generation systems. The paper presents an integrated model for PV systems allowing a more accurate dynamic of the PV system. The model includes a maximum power point tracking and converters topologies for the power-electronic: the DC-DC boost followed by the two-level converts. The control strategy is based on the use of classical PI controllers or fuzzy PI controllers, PWM by SVM associated with sliding mode control and power factor control is introduced at the output of the inverter. Although more complex, this integrated model is justified for more realistic results. The fuzzy PI controller presents a slightly better behavior in comparison with the classical PI controller in the case study.
A comparison between simulation of a PV system integrated model and experimental results obtained from three commercial inverters measured during their in-situ operation is in favor of this contribution as an integrated relevant modeling. The harmonic content computed by the DFT for the current injected into the grid for the three commercial inverters have an acceptable agreement with the experimental results. Also, in what regards the configuration of the PV system, THD is lower than the limit imposed by standards IEEE 519, IEEE 1547 and EN50160. Hence, the performance of the PV system configuration is revealed as a feasible practical implementation.

Acknowledgment

This work was partially supported by Fundação Ciência e Tecnologia, through IDMEC/LAETA, Instituto Superior Técnico, Universidade de Lisboa and by Universidade de Évora, Cátedra BES – Energias Renováveis. The authors would like to acknowledge partial support under the FCOMP-01-0124-FEDER-016080 project and would also like to extend their appreciation to Eng. Maria João Martins from LNEG for the contribution in the inverter data acquisition that led to the data used in the case studies.

References

Alami, A.H., 2014. Effects of evaporative cooling on efficiency of photovoltaic modules. Energy Conversion and Management 77, 668–679.
Almeida, R.G., Peças Lopes, J.A., 2007. Participation of doubly fed induction wind generators in system frequency regulation. IEEE Trans. Power Syst. 22 (3), 944–950.
Beltran, B., Ahmed-Ali, T., Benbouzid, M.E.H., 2008. Sliding mode power control of variable-speed wind energy conversion systems. IEEE Trans. Energy Convers. 23 (2), 551–558.

Blaabjerg, F., Chen, Z. Kjaer, S.B., 2004. Power electronics as efficient interface in dispersed power generation systems. IEEE Transactions Industrial Electronics 19 (5), 1184–1194.
Blaabjerg, F., Teodoresco, R., Liserre, M., Timbus, A.V., 2006. Overview of control and grid synchronization for distributed power generation systems. IEEE Trans. Ind. Electron 53 (5), 1398–1409.
Cucchiella, F., D'Adamo, I., 2013. Issue on supply chain of renewable energy. Energy Conversion and Management 76, 774–780.
Dersch, J., Geyer, M., Herrmann, U., Jones, S.A., Kelly, B., Kistner, R., Ortmanns, W., Pitz-Paal, R., Price, H., 2004. Trough integration into power plants—a study on the performance and economy of integrated solar combined cycle systems. Energy 29, 947–959.
Díaz-Dorado, E., Cidrás, J., Carrillo, C., 2014. Discrete I–V model for partially shaded PV-arrays. Solar Energy 103, 96–107.
Ding, K., Zhang, J., Bian, X., Xu, J., 2014. A simplified model for photovoltaic modules based on improved translation equations. Solar Energy 101, 40–52.
Du, Y., Lu, D.D.-C., James, G., Cornforth, D.J., 2013. Modelling and analysis of current harmonic distortion from grid connected PV inverters under different operating conditions. Solar Energy 94, 182–194.
Duffie, J., Beckman, W., 2006. Solar Engineering of Thermal Processes, 3rd Ed., John Wiley & Sons.
Dzimano, B.S.G., 2008. Modeling of photovoltaic systems. Master Thesis, Ohio State University, USA.
Edwin, F., Xiao, W., Khadkikar, V., 2012. Topology review of single phase grid-connected module integrated converters for PV applications. In: Proc. 38th IEEE Industrial Electronics Society Conf. – IECON 2012, Montreal, Canada, 821–827.
Erlich, I., Kretschmann, J., Fortmann, J., Mueller-Engelhardt, S., Wrede, H., 2007. Modelling of wind turbines based on doubly-fed induction generators for power system stability studies. IEEE Trans. Power Syst. 22 (3), 909–919.
Fartaria, T.O., Pereira, M.C., 2013. Simulation and computation of shadow losses of direct normal, diffuse solar radiation and albedo in a photovoltaic field with multiple 2-axis trackers using ray tracing methods. Solar Energy 91, 93–101.
Fialho, L., Melício, R., Mendes, V.M.F., Figueiredo, J., Collares-Pereira, M., 2014a. Amorphous solar modules simulation and experimental results: effect of shading, in: Camarinha-Matos, L.M., Barrento, N.S., Mendonça, R. (Eds.), Technological Innovation for Collective Awareness Systems. Springer, Heidelberg, pp. 315–323.
Fialho, L., Melício, R., Mendes, V.M.F., 2014b. PV system modeling by five parameters and in situ test. In: Proc. 22th International Symposium on Power Electronics, Electrical Drives, Automation and Motion – Speedam 2014, Ischia, Italy, 577–582.
Giacobbe, L., 2005. Validação de modelos matemáticos de componentes de sistemas fotovoltaicos. Master Thesis. Instituto Superior Técnico/DEEC, Portugal.
Hasanzadeh, A., Edrington, C.S., Bevis, T., 2012. Comprehensive study of power quality criteria generated by PV converters and their impacts on distribution transformers. In: Proc. 37th IEEE Industrial Electronics Society Conf. – IECON 2012, Montreal, Canada, 5820–5826.
Hassaine, L., Olias, E., Quintero, J., Salas, V., 2014. Overview of power inverter topologies and control structures for grid connected photovoltaic systems. Renewable and Sustainable Energy Reviews 30, 796–807.

IEC 60891, 2009. Procedures for temperature and irradiance corrections to measured I–V characteristics of crystalline silicon photovoltaic devices.
IEC 60904–3, 2008. Photovoltaic devices - Part 3: Measurement principles for terrestrial photovoltaic (PV) solar devices with reference spectral irradiance data.
Ismail, M.S., Moghavvemi, M., Mahlia, T.M.I., 2013. Design of an optimized photovoltaic and microturbine hybrid power system for a remote small community: case study of Palestine. Energy Conversion and Management 75, 271–281.
Isofoton SA. < http://www.isofoton.com>.
Jiang, J.A., Huang, T.L., Hsiao, Y.T., Chen, C.H., 2005. Maximum power tracking for photovoltaic power systems. Tamkang Journal of Science and Engineering 8 (2), 147–153.
Kaneka Solar Energy. <http://www.kaneka-solar.com>.
Kazem, H.A., Khatib, T., 2013. Techno-economical assessment of grid connected photovoltaic power systems productivity in Sohar, Oman. Sustainable Energy Technologies and Assessments 3, 61–65.
Khan, F., Baek, S-Ho., Park, Y., Kim, J.H., 2013. Extraction of diode parameters of silicon solar cells under high illumination conditions. Energy Conversion and Management 76, 421–429.
Khatib, T., Mohamed, A., Sopian, K., 2013. A review of photovoltaic systems size optimization techniques. Renewable and Sustainable Energy Reviews 22, 454–465.
Kjaer, S.B., Pedersen, J.K., Blaabjerg, F., 2002. Power inverter topologies for photovoltaic modules–a review. In: Proc. 37th IEEE Industry Applications Conf., Pittsburgh, USA,782–788.
Kjaer, S.B., Pedersen, J.K., Blaabjerg, F., 2005. A review of single-phase grid-connected inverters for photovoltaic modules. IEEE Transactions Industry Applications 41, 1292–1306.
Liu, Y.-H., Chen, J.-H, Huang, J.-W., 2014. Global maximum power point tracking algorithm for PV systems operating under partially shaded conditions using the segmentation search method. Solar Energy 103, 350–363.
Marion, B., 2002. A method for modeling the current-voltage curve of a PV module for outdoor conditions. Progress in Photovoltaics: Research and Applications 10 (3), 205–214.
Melício, R., Mendes, V.M.F., 2007. Simulation of Power Converters for Wind Energy Systems. Información Tecnológica 18, 25–34.
Moradi, M.H., Tousi, S.M.R., Nemati, M., Basir, N.S., Shalavi, N., 2013. A robust hybrid method for maximum power point tracking in photovoltaic systems. Solar Energy 94, 266-276.
Morales-Acevedo, A., 2006. Solar renewable energy news international conference (SREN-2005). Solar Energy 80, 627–628.
Patrao, I., Figueres, E., González-Espín, F., Garcerá, G., 2011. Transformerless topologies for grid-connected single-phase photovoltaic inverters. Renewable and Sustainable Energy Reviews 15, 3423–3431.
Peças Lopes, J., Hatziargyriou, N., Mutale, J., Djapic, P., Jenkins, N., 2007. Integrating distributed generation into electric power systems: a review of drivers, challenges and opportunities. Electric Power Systems Research 77, 1189–1203.
Photowatt. < http://www.photowatt.com>.
Raj, J.S.C.M., Jeyakumar, A.E., 2014. A two stage successive estimation based maximum power point tracking technique for photovoltaic modules. Solar Energy 103, 43–61.
Rampinelli, G.A., Krenzinger, A., Chenlo Romero, F., 2014. Mathematical models for efficiency of inverters used in grid connected photovoltaic systems. Renewable and Sustainable Energy Reviews 34, 578–587.

Rauschenbach, H.S., 1980. The Principles and Technology of Photovoltaic Energy Conversion, Solar Cell Array Design Handbook, Springer.
Razkov, T.M., Ferekides, C.S., Morel, D., Stefanakos, E., Ullal, H.S., Upadhyaya, H.M., 2011. Solar photovoltaic electricity: Current status and future prospects. Solar Energy 85, 1580–1608.
Rus-Casas, C., Aguilar, J.D., Rodrigo, P., Almonacid, F., Pérez-Higueras, P.J., 2014. Classification of methods for annual energy harvesting calculations of photovoltaic generators. Energy Conversion and Management 78, 527–536.
Salas, V., Alonso-Abella, M., Olías, E., Chenlo, F., Barrado, A., 2007. DC current injection into the network from PV inverters of <5 kW for low-voltage small grid-connected PV systems. Solar Energy Materials and Solar Cells 91, 801–806.
Schüco. <http://www.schueco.com>.
Sedra, A.S., Smith, K.C., 2006. Microelectronic Circuits, Oxford Univ. Press. London, UK.
Seixas, M., Melício, R., Victor, V.M.F., 2014. Fifth harmonic and sag impact on PMSG wind turbines with a balancing new strategy for capacitor voltages. Energy Conversion and Management 74, 721–730.
Silva, J., Pinto, S., 2007. Control methods for switching power converters, in: Rashid, M. H. (Eds.), Handbook of Power Electronics, Academic Press, New York, pp. 935–998.
Spertino, F., Leo, P.D., Cocina, V., 2014. Which are the constraints to the photovoltaic grid-parity in the main European markets?. Solar Energy 105, 390–400.
Spertino, F., Leo, P.D., Corona, F., Papandrea, F., 2012. Inverters for grid connection of photovoltaic systems and power quality: Case studies. In: Proc. 3rd IEEE International Symposium on Power Electronics for Distributed Generation Systems (PEDG), 564–569.
Tsang, K.M., Chan, W.L., 2014. Rapid islanding detection using multi-level inverter for grid-interactive PV system. Energy Conversion and Management 77, 278–286.
Tyukhov, I., 2010. Advanced solar energy and educational technology. Global Journal on Technology & Optimization 1, 2–9.
Velasco, D., Trujillo, C.L., Garcerá, G., Figueres, E., 2010. Review of anti-islanding techniques in distributed generators. Renewable and Sustainable Energy Reviews 14, 1608–1614.
Viveiros, C., Melício, R., Igreja, J.M., Mendes, V.M.F., 2014. Fuzzy, integer and fractional order control: application on a wind turbine benchmark model. In: Proc. 19th International Conference on Methods and Models in Automation and Robotics – Mmar 2014, Międzyzdroje, Poland, 252–257.
Viveiros, C., Melício, R., Igreja, J.M., Mendes, V.M.F., 2015. On wind turbine model predictive pitch control: an event-based simulation approach, in: Moreira, A.P., Matos, A., Veiga, G. (Eds), Lecture Notes in Electrical Engineering. Springer, Switzerland, pp. 91–100.
Zeng, Z., Yang, H., Zao, R., Cheng, C., 2013. Topologies and control strategies of multi-functional grid-connected inverters for power quality enhancement: a comprehensive review. Renewable and Sustainable Energy Reviews 24, 223–270.

2.5 Simulation of a-Si PV System Grid connected by Boost and Inverter

L. Fialho[1], R. Melício[1,2], V.M.F. Mendes[3], A. Estanqueiro[4]

In International Journal of Renewable Energy Research, Vol.5, No.2, pp. 443-451, 2015.
http://hdl.handle.net/10174/16472

Abstract

This paper is about a PV system connected to the electric grid by power electronic converters, using classical PI controller. The modelling for the converters emulates the association of a DC-DC boost with a two-level power inverter (TwLI) or three-level power inverter (ThLI) in order to follow the performance of a testing experimental system. Pulse width modulation (PWMo) by sliding mode control (SMCo) associated with space vector modulation (SVMo) is applied to the boost and the inverter. The PV system is described by the five parameters equivalent circuit. Parameter identification and simulation studies are performed for comparison with the testing experimental system.

Keywords: Photovoltaic energy, MPPT, modelling, power electronics, simulation, experimental results.

Nomenclature

DCB	DC-DC boost
DFT	Discrete Fourier Transform
EGr	Electric grid
EUn	European Union
GAMS	General algebraic modelling system
IGBT	Insulated-gate bipolar transistor
MPP	Maximum power point
MPPT	Maximum power point tracking
PEltr	Power electronics
PGSys	Power generation systems
PSSe	Power system sector
PV	Photovoltaic

[1] Universidade de Évora, Portugal
[2] IDMEC-LAETA, Instituto Superior Técnico, Universidade de Lisboa.
[3] Department of Electrical Engineering and Automation, Instituto Superior de Engenharia de Lisboa, Portugal.
[4] Laboratório Nacional de Energia e Geologia, Lisbon, Portugal.

PVsy	Photovoltaic system
PwCo	Power converters
PWMo	Pulse width modulation
RMS	Root mean square
RMSE	Root mean square error
SMCo	Sliding mode control
STC	Standard test conditions
SVMo	Space vector modulation
SwV	Switching variable
THD	Total harmonic distortion
ThLI	Three-level power inverter
TwLI	Two-level power inverter

1. Introduction

Electricity market restructuring offers more flexibility at both points of production and utilization [1]. Similarly, with the reform in the power system sector (PSSe), the progresses in distributed power generation systems (PGSys) generated new opportunities for the electric sector [2]. Distributed PGSys include, for example, photovoltaic power, wave power, wind power, small hydropower or geothermal power. A summary of the hardware for some distributed PGSys is given in [3] and a review of management and electric grid (EGr) integration for distributed PGSys is given in [4].

The growth of photovoltaic PGSys is significant in the current years. Even foreseen as able to compete with the fossil-fuelled thermal PGSys, particularly, taken into consideration the environmental safeguarding value [5,6]. Climate changes and the environmental policy are becoming progressively important for the PSSe as pollution regulations are stricter and client perception of environmental effects is greater than ever. Nowadays, deceleration of greenhouse is acknowledged to be possible only if CO2 anthropogenic emissions are reduced [7]. The European Commission committed European Union (EUn) to become an economy energy-efficient with low-carbon emissions, endorsing the climate and energy package with plans to generate a new Energy Policy for the EUn. The proposals are intended for: reducing the anthropogenic emissions by 20% by 2020 and 50% until 2050; and increasing the quota of EUn energy consumption from renewable energies. In the future, solar energy is expected to be a significant part of the European Energy Policy.

Also, the European Commission considers that smart grids marks a new advance towards: a more active consumer role, improved integration of renewable energies into the EGr, increasing energetic efficiency with a significant impact on reducing the anthropogenic emissions, job creation and technological development in the EUn. In Portugal, the renewable energy reached a total installed capacity of 11 446 MW in September 2014, of which photovoltaic generation capacity is responsible for 346 MW.

A PV system (PVsy) converts the solar energy into electricity using solar cells. These cells may be assembled into panels and arrays. A PV array can be comprised by several panels connected in parallel or series in order to create larger systems with or without tracking systems, used to meet higher values of conversion during sunny days due to the diverse perpendicular positions to collect the irradiation coming from the sun [8].
Power electronics (PEltr) were developed for the adaptation of sustainable energy sources to the EGr [8,9]. These PEltr converters, e.g. inverters, allow operating the PVsy and tuning power extraction. The inverter is in employment by two reasons. First, serves as an interface between the low DC voltage at the PVsy output and the EGr typical AC voltage. Second, allows tracking the Maximum Power Point (MPP), i.e., the processing has to incorporate this functionality to avoid the fact that the power delivered from the modules is sensitive to the point of operation [7,10]. For instance, a tracking process based on $\partial P/\partial V$ feedback is in use on PVsy s to adjust the converters IGBT's to achieve the MPP energy conversion [8].
This paper is about a silicon amorphous PVsy implemented with a DC-DC boost and an inverter, considering two options: two-level or three-level topologies. Section 2 models the PV array, the DC-DC boost (DCB), the TwLI and ThLI. Section 3 model the control strategy for the PVsy based on the use of classical PI controller and having PWMo by SVMo associated with SMCo for controlling the converter. Section 4 presents a case study concerned with an assessment by simulation and comparison with experimental results of an amorphous technology PVsy linked to the EGr by a commercial converter based on the use of classical PI controller. Finally, conclusions are in Section 5.

2. Modelling

The modelling for the PVsy is a combination of an equivalent electric circuit for the PV module with the models for the boost converter and for the unavoidable interface necessary to inject the PV energy into the EGr. This unavoidability is due to the fact that the EGr is an alternate current one and the PV energy is a source of continuous current. Two configurations for the PVsy are modelled characterized by the PEltr converter used in the interface with the EGr: a TwLI and a ThLI. The configuration for the PVsy integrated into the EGr by a TwLI is shown in Fig. 1.

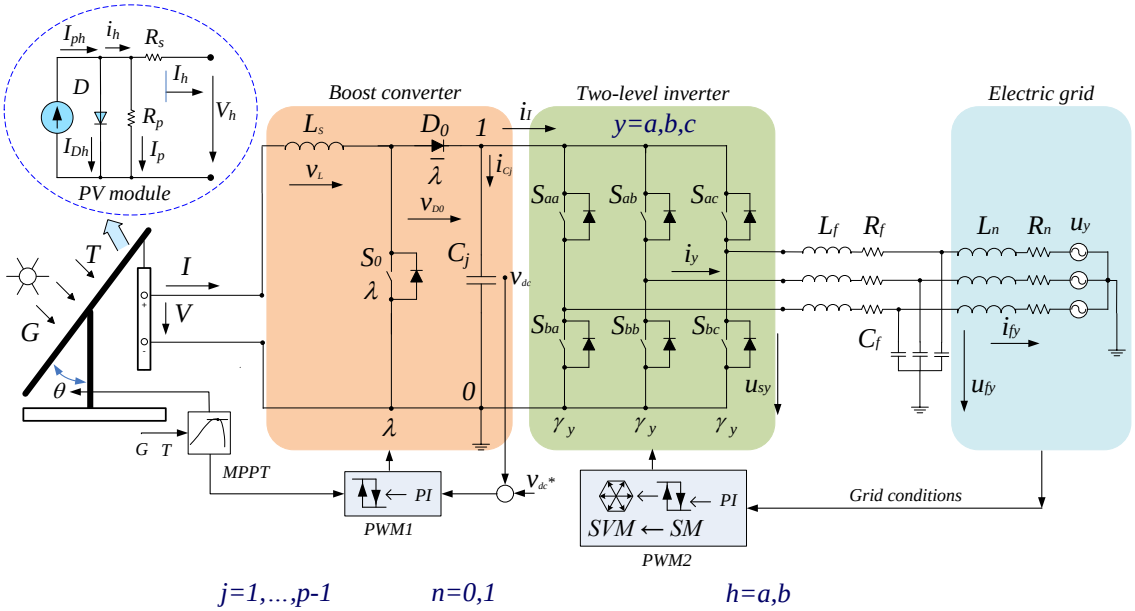

Figure 1. PV system integrated into the grid by a TwLI.

The PVsy linked to the EGr by a ThLI is shown Fig. 2.

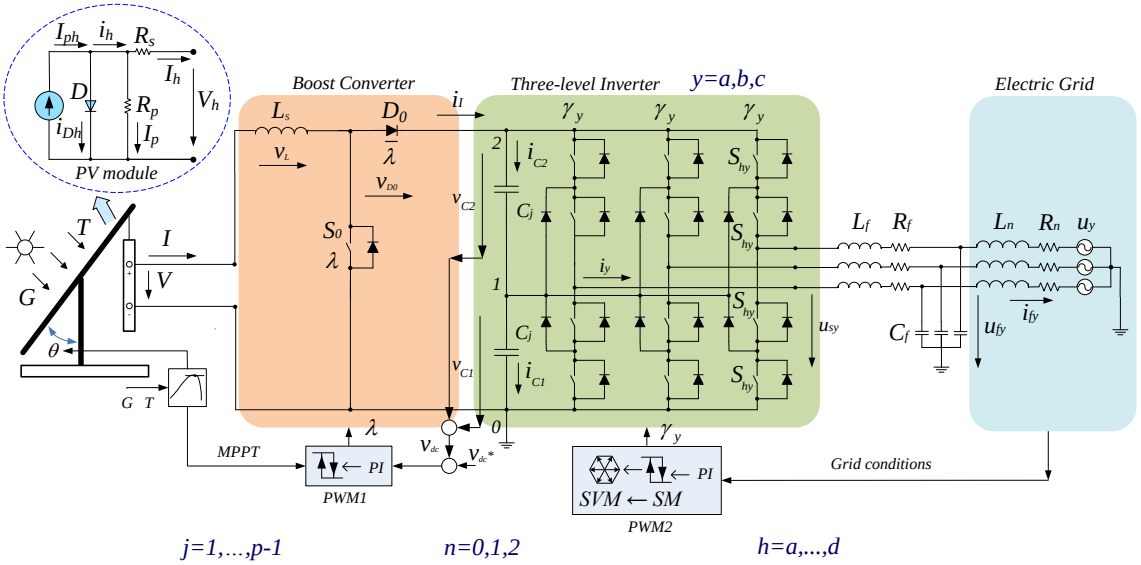

Figure 2. PV system connected to the grid by ThLI.

2.1 PV Module

The solar cells are considered to be subjected to the same G solar irradiance and T temperature of the semiconductor. Hence, the equivalent circuit of a cell is also the one for any association of cells with convenient parameters transformation. The PV module equivalent circuit is shown in Fig. 3.

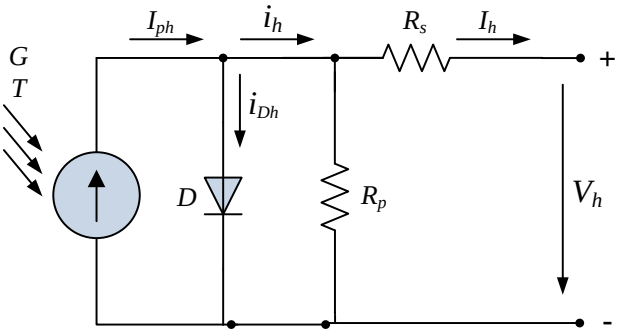

Figure 3. Equivalent circuit for a PV module.

The current i_h is given by:

$$i_h \equiv I_h + (V_h + R_s I_h) / R_p \tag{1}$$

where h is an index linked with operation conditions: $h = oc$, open circuit; $h = sc$, short circuit; and $h = mx$, MPP conditions. The diode *D* current i_{Dh} [11] is given by:

$$i_{Dh} \equiv I_0 \, e_h \tag{2}$$

where I_0 is the diode reverse bias current and e_h is defined [11] by:

$$\ln (e_h + 1) \equiv \gamma (V_h + R_s I_h) \tag{3}$$

where γ is given by $\gamma \equiv 1/mV_T$, m is the ideality factor, V_T is the junction thermal voltage given by the Boltzmann constant *K* times T divided by the electron charge.
Also, the current i_h is given by:

$$i_h \equiv I_S - i_{Dh} \tag{4}$$

A matrix formulation of (4) combining the conditions at open circuit, short circuit and MPP conditions [11] can be given by:

$$\begin{bmatrix} 1 & -e_{oc} & -1 \\ 1 & -e_{sc} & 0 \\ 1 & -e_{mx} & 0 \end{bmatrix} \begin{bmatrix} I_s \\ I_0 \\ i_{oc} \end{bmatrix} = \begin{bmatrix} 0 \\ i_{sc} \\ i_{mx} \end{bmatrix} \tag{5}$$

The MPP of a PVsy depends on *G* and *T*, at the MPP conditions the conversion is attained at the highest efficiency, implying the satisfaction of the relation given by:

$$-\left.\frac{dI}{dV}\right|_{mx} = \frac{I_{mx}}{V_{mx}} \tag{6}$$

Also, at MPP conditions holds the equality [11] given by:

$$\gamma V_{oc} i_{mx}^{sc} (I_{mx} - \delta)(e_{mx} + 1) - \delta i_{oc} e_{sc}^{mx} = 0 \quad (7)$$

where δ is defined [11] by:

$$\delta = \frac{\gamma V_{oc} i_{mx}^{sc} (e_{mx} + 1)}{\gamma V_{oc} i_{mx}^{sc} (e_{mx} + 1) + i_{oc} e_{sc}^{mx}} I_{mx} \quad (8)$$

and δ has to satisfy the relation [11] given by:

$$0 < \delta < I_{mx} \quad (9)$$

At open circuit conditions i_{oc} must satisfy the relation [11] given by:

$$\frac{V_{oc}}{2V_{mx}} (i_{mx} - I_{mx}) < i_{oc} < i_{mx} \frac{V_{oc}}{2V_{mx}} \quad (10)$$

The ideality factor m for a cell is assumed to between 2/3 and 2. An ideality factor of 2/3 is due to the Auger recombination: a type of recombination between an electron and a hole in a band-to-band transition giving energy to another electron or hole. While an ideality factor of 2 is due to band to band high level injection or depletion region recombination [11]. Hence, the boundaries for γ [11] are given by:

$$\frac{1}{2V_T} \leq \gamma \leq \frac{3}{2V_T} \quad (11)$$

The five parameters R_p, R_s, γ, I_{ph}, I_0 define the mathematical model for the PV cell equivalent circuit with a single-diode, shunt and series resistances. The General Algebraic Modeling System (GAMS) is used to code a mathematical programming problem for finding these parameters and the free solver COUENNE-Convex Over and Under Envelopes for Nonlinear Estimation for global solution of nonlinear programs is a convenient option due to involvedness on the formulation of the problem. The input data is at STC and is given by the producer of the PV module as technical data.
An I-V characteristic curve associated with the equivalent circuit of five parameters [11] obeys the relation given by:

$$I = I_{ph} - I_0 (e^{\gamma (V + IR_S)} - 1) - (V + IR_S) / R_p \quad (22)$$

Relation (12) cannot be explicit solved in order to the variables, i.e., in order to I or to V. Hence, numeric methods are normal employed to draw I-V characteristics curves. In this paper, (12) is coded in Matlab/Simulink for assessing the I-V characteristic curves using the iterative method of Newton-Raphson.

2.2 MPPT Algorithm

The criterion for MPPT is to follow the condition given by $\partial P / \partial V = 0$, i.e., if the condition is met, then the algorithm has found the MPP point. But typically the algorithm iterates around that

condition until eventually converges. The iterations procedures are as follow: if $\partial P/\partial V = 0$, no change is made in the out voltage; if $\partial P/\partial V > 0$, an incremental adjustment is set in order to increase the out voltage, i.e., in the direction of the MPP; if $\partial P/\partial V < 0$, an adjustment is set in order to decrease the out voltage to be in the right tracking for the MPP [8]. The Flowchart for the MPPT algorithm used for the PVsy is shown in Fig. 4.

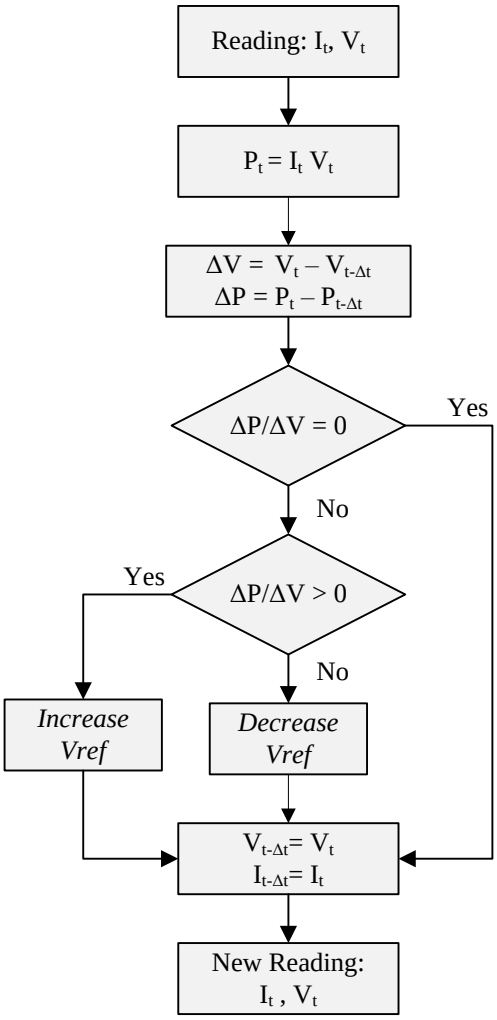

Figure 4. Flowchart for the MPPT algorithm.

2.3 DCB Converter

The configuration of the DCB converters is shown in Fig. 1 and Fig. 2. The DCB converter has one unidirectional commanded IGBT, S_0. The DCB converter is linked between the PV modules and a capacitor bank. This capacitor bank is then connected to a TwLI or a ThLI. The switching of the DCB converter is given by the switching variable (SwV) λ that identifies the state of the IGBT S_0 on the DCB converter and by the SwV $\bar{\lambda}$ used to identify the state of the diode D_0 of the boost. But to emulate the action of the boost converter these variables are not independent [12]. The two conditions to be satisfied by the switching variable of the DCB are given by:

$$\begin{cases} \lambda = 1 \text{ and } \bar{\lambda} = 0 \ (S_0 = 1 \text{ and } D_0 = 0) \\ \lambda = 0 \text{ and } \bar{\lambda} = 1 \ (S_0 = 0 \text{ and } D_0 = 1) \end{cases} \tag{13}$$

The current I is given by:

$$\frac{dI}{dt} = \frac{1}{L_s}[\mathrm{V} - \bar{\lambda}\ (\mathrm{V_{D0}} + V_{dc})\ ] \tag{14}$$

where $\mathrm{V_{D0}}$ is the diode forward voltage at direct current, V_{dc} is the capacitor voltage. The capacitor voltage V_{DC} is given by:

$$\frac{dv_{DC}}{dt} = \frac{1}{C}(\bar{\lambda}\ \mathrm{I} - i_I) \tag{15}$$

where i_I is the current injected into the inverter.

2.4 TwLI

The configuration of the TwLI is shown in Fig. 1. The inverter has $p = 2$ levels. The TwLI links a capacitor bank and a filter (second order filter). The filter is then linked to the EGr. A three-phase active symmetrical circuit models the EGr. This inverter is a DC-AC converter with 6 commanded IGBT's S_{hy}. The two IGBT's that are connected to the same phase represent a converter leg y. The switching function of a IGBT is given by the SwV γ_y, representing the IGBT h state in the leg y. The IGBT is identified by an index h, where $h \in \{a,b\}$. The inverter leg is identified by an index y, where $y \in \{a,b,c\}$. Each leg y of the converter is associated with a variable [13] n_y given by:

$$n_y = \begin{cases} 1, & (S_{ay} = 1 \text{ and } S_{by} = 0) \\ 0, & (S_{ay} = 0 \text{ and } S_{by} = 1) \end{cases} \quad y \in \{a, b, c\} \tag{16}$$

A restriction is imposed for each leg y [13]. The restriction is given by:

$$\sum_{i=1}^{2} S_{hy} = 1 \quad h \in \{a,b\} \quad y \in \{a, b, c\} \tag{17}$$

The current injected at the inverter i_I is given by:

$$i_I = \sum_{y=a}^{c} n_y i_y \quad n \in \{1, 0\} \quad y \in \{a, b, c\} \tag{18}$$

The inverter output voltage is given by:

$$u_{sy} = \frac{1}{3}(2n_y - \sum_{\substack{j=a \\ j \neq y}}^{c} n_j)\, v_{dc} \quad n \in \{0, 1\} \quad y \in \{a, b, c\} \tag{19}$$

The state equation of the voltage v_{dc} is given by:

$$\frac{dv_{dc}}{dt} = \sum_{j=1}^{p-1} \frac{1}{C_j} i_{cj} \quad j \in \{1, ..., p-1\} \quad n \in \{0, 1\} \tag{20}$$

More detailed information about this modelling is in [13].

2.5 ThLI

The ThLI configuration is shown in Fig. 2. This inverter has $p = 3$ levels. The inverter is a DC-AC converter with 12 IGBT's S_{hy}. The four IGBT's that are connected to the same phase represent a converter leg y. The switching voltage level variable n_y, where $0 \le n_y \le (p-1)$, identifies the IGBT h state, with $h \in \{a, b, c, d\}$. The index y with $y \in \{a, b, c\}$ identifies a leg. For the SwV of the voltage level on the leg y at each level [14] there are three valid conditions given by:

$$n_y = \begin{cases} 2, & (S_{ay} \text{ and } S_{by}) = 1 \quad \text{and} \quad (S_{cy} \text{ or } S_{dy}) = 0 \\ 1, & (S_{by} \text{ and } S_{cy}) = 1 \quad \text{and} \quad (S_{ay} \text{ or } S_{dy}) = 0 \\ 0, & (S_{cy} \text{ and } S_{dy}) = 1 \quad \text{and} \quad (S_{ay} \text{ or } S_{by}) = 0 \end{cases} \quad y \in \{a, b, c\} \tag{21}$$

The switching voltage level variable n_y is also used to identify the vector (level-1) in the calculation of the converter output voltage u_{sy}. The inverter output voltage u_{sy} in function of v_{dc} [14] is given by:

$$u_{sy} = \frac{1}{6}(2n_y - \sum_{\substack{j=a \\ j \neq y}}^{c} n_j)\, v_{dc} \quad n \in \{0, 1, 2\} \quad y \in \{a, b, c\} \tag{22}$$

For each capacity bank, the current [14] is given by:

$$i_{cj} = i_I - \sum_{y=a}^{c} \delta_{ny} i_y \quad j \in \{1, \ldots, p-1\} \quad y \in \{a, b, c\} \tag{23}$$

where the auxiliary variable δ_{ny} [14] is given by:

$$\delta_{ny} = \begin{cases} 0 & j > n_y \\ 1 & j \le n_y \end{cases} \quad j \in \{1, \ldots, p-1\} \quad n \in \{0, 1, 2\} \tag{24}$$

The state equation of the voltage v_{dc} [14] is given by:

$$\frac{dv_{dc}}{dt} = \sum_{j=1}^{p-1} \frac{1}{C_j} i_{cj} \quad j \in \{1, \ldots, p-1\} \tag{25}$$

More detailed information about this modelling is in [14].

2.6 Electric Grid

The EGr is modelled by a triphasic active symmetrical independent voltage source linked to an inductor and resistance emulating the short circuit impedance of the EGr. This model is shown in Fig. 1 and Fig. 2. The EGr injected phase current i_{fk} is given by:

$$\frac{di_{fy}}{dt} = \frac{1}{L_n}(u_{fy} - R_n i_{fy} - u_y) \quad y \in \{a, b, c\} \tag{26}$$

Where u_{fy} is the value for the independent voltage source, R_n and L_n are respectively the resistive part and the inductive part of the short-circuit impedance where the PV array is connected.

3. Control strategy

PI controllers implement the controller strategy considered in the simulation for the operation of the PVsy with two-level or three-level inverter in order to follow the references. Power converters (PwCo) are mutable structures due to the transistors on/off states and the PWMo by SVMo associated with SMCo is used to control the converter. The SMCo strategy is an option known by the advantage of having smart features, e.g., considerable robustness to parametric unreliability due to partial shading or EGr disturbances [11,13,14]. The aim of the SMCo is to change the system structure allowing the system to slide along a defined sliding surface. The control strategy of the PVsy with DCB and two-level or three-level power converter topologies using classical PI controllers has the diagram in box PWM1 and in box PWM2 shown in Fig. 1 or in Fig. 2. The convenient vector selection to ensure the converters stability, after the hysteresis comparator processing in the blocks of the SMCo and SVMo are given in [11,13,14]. The output space vectors in the $\alpha\beta$ plane for level *0* and level *1* for the TwLI [12,13] are shown in Fig. 5.

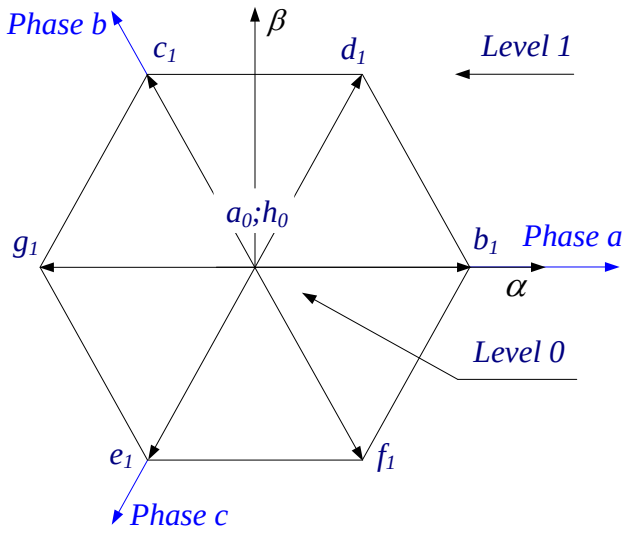

Figure 5. TwLI, output space vectors.

The output space vectors for level *0*, level *1* and level *2* for the ThLI [13,14] are shown in Fig. 6.

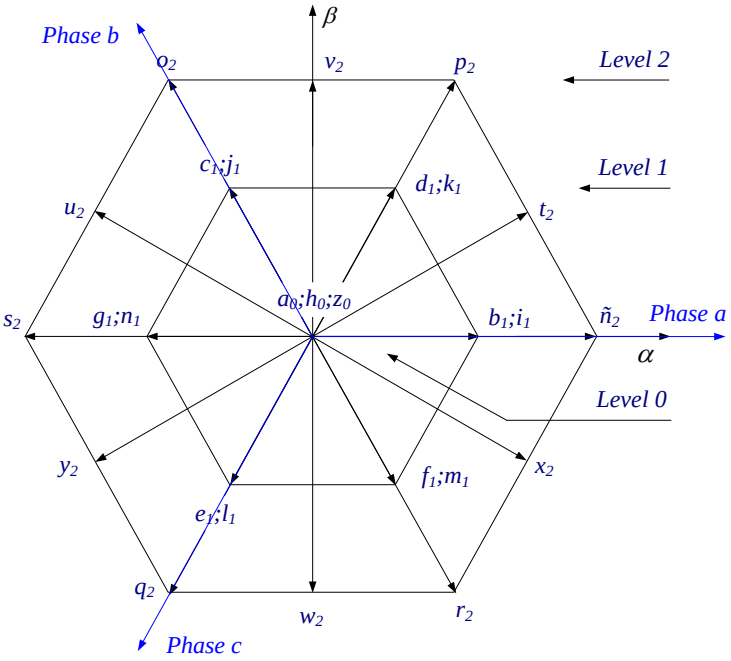

Figure 6. ThLI, output space vectors.

The SMCo is of particular interest in switching power inverters, with their variable structure, guaranteeing the correct choice of the space vectors. Changing the system structure allows the system sliding along a defined sliding surface $A(e_{\alpha\beta},t)$. There are current IGBT's physical restrictions, i.e., they cannot operate at infinite frequency. Likewise, a switching frequency with a finite value will have an error between his control value and the reference value $e_{\alpha\beta}$. The system sliding along the surface $A(e_{\alpha\beta},t)$ is guaranteed if the trajectory satisfied the following condition [13,14] given by:

$$A(e_{\alpha\beta},t)\frac{dA(e_{\alpha\beta},t)}{dt}<0 \tag{27}$$

The selection to ensure stability on the TwLI [13] is shown in Table 1.

Table 1. Output vectors selection for the TwLI

$\delta_\beta \setminus \delta_\alpha$	-1	0	1
-1	e_1	e_1;f_1	f_1
0	g_1	a_0;h_0	b_1
1	c_1	c_1;d_1	d_1

The selection to guarantee stability on the ThLI [14] is shown in Table 2.

Table 2. Output vectors selection for the ThLI

$\delta_\beta \setminus \delta_\alpha$	-2	-1	0	1	2
-2	p_2	p_2	w_2	o_2	o_2
-1	f_1	f_1;d_1;k_1	d_1;k_1;m1;y2	m_1;y_2;u_2	u_2
0	ñ2	b_1;g_1	a_0;h_0;z_0	i_1;n_1	s_2
1	x_2	c_1;x_2;t_2	c_1;e_1;l_1;t_2	e_1;l_1;j_1	j_1
2	r_2	r_2	v_2	q_2	q_2

4. Case study

The models for the PVsy using the five parameters cell equivalent circuit, the DCB, respectively the TwLI or the ThLI topologies shown in Fig. 1 or Fig. 2, the MPPT algorithm, and the control strategy are programmed in Matlab/Simulink to carry out the simulations for the case study. The measuring of the voltage and the current harmonic content at the inverter output is carried out with the experimental system by appropriated instrumentation and for the results obtained by the simulation with the discrete Fourier transform (DFT). The DTF is given by:

$$Y(k) = \sum_{n=0}^{N-1} e^{-j2\pi\, k\, n/N}\; y(n) \quad \text{for} \quad k = 0,\ldots, N-1 \tag{28}$$

where $y(n)$ is the output signal, $Y(k)$ is a complex number representing the phase and amplitude of the several sinusoidal components of $y(n)$. Also, the total harmonic distortion (THD) is given by:

$$\text{THD}\ (\%) = 100\, \frac{\sqrt{\sum_{H=2}^{50} Y_H^2}}{Y_F} \tag{29}$$

where Y_F is the root mean square (RMS) value of the fundamental component and Y_H is the RMS value for the harmonic H. The simulation is carried out for a silicon amorphous PV module situated in LNEG, with the coordinates 38°46'18.50' N, 9°10'38.50' W. The STC data for the amorphous silicon PV module Kaneka KA 58 [15] is shown in Table 3.

Table 3. Data for Kaneka KA58 solar module at STC

Technology	V_{MP}^*	I_{MP}^*	V_{oc}^*	I_{sc}^*
Amorphous	63 V	0.92 A	85 V	1.12 A

The switching frequency for IGBTs is 5 kHz. The experimental system is located in LNEG, Lisbon, Portugal. The PVsy's are connected via the electrical switchboard to the EGr of 230/400 V at 50 Hz EGr by the commercial inverter based on the use of classical PI controller, with a nominal AC power of 3.3 kW. The experimental PVsy's description and configurations are shown in Table 4.

Table 4. Experimental PV systems

Parameter	PV system
Module capacity	60 Wp
Manufacturer/model	Kaneka GEA 60
Technology	a-Si
Installed capacity	3.0 kWp
String configuration	5 modules×10 strings
Inverter	SolarStocc PS4000HV

Inverter rated capacity	3.3 kW

The irradiation and ambient temperature test data for the experimental systems is shown in Table 5.

Table 5. Irradiance and ambient temperature

Irradiance	800 W/m^2
Ambient temperature	13 °C
Date, hour	08/02/2012, 12:11

The simulation results are compared with experimental observation carried out using the amorphous PV technology. The simulated, green, and experimental, blue, curves for I-V; the absolute error, red, and MPP at STC conditions are shown in Fig. 7.

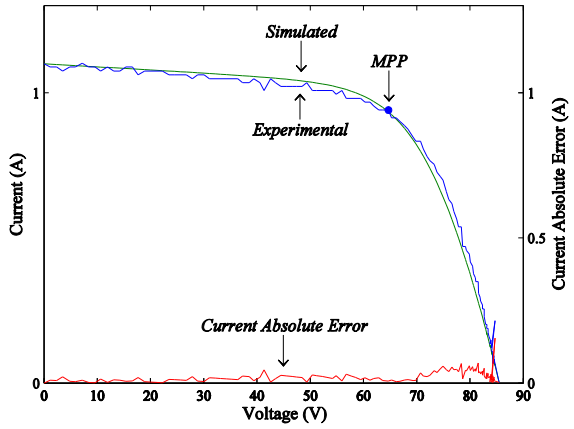

Figure 7. I-V curves simulated and experimental.

The simulated, green, and experimental, blue, curves for P-V; the absolute error, red, and MPP at STC conditions are shown in Fig. 8.

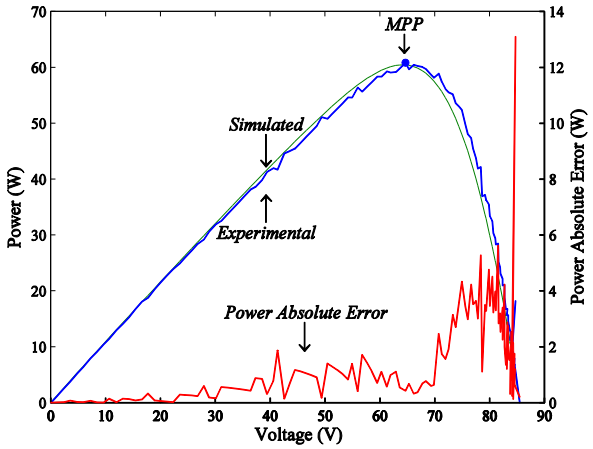

Figure 8. P-V curves simulated and experimental.

Both Fig. 7 and Fig. 8 favor the agreement of the identified parameters for the equivalent circuit with the performance data of the real PV module. Particularly, in the region of normal

operation, i.e., the neighborhood of the MPP, the relative error is low and the agreement is convenient for practical purposes. Hence, the MPP is important for the PVsy because maximizes the power output for a given set of conditions and therefore maximize the efficiency [16]. The current injected into the EGr, simulated, green, experimental, blue, and the absolute error on the current are shown in Fig. 9.

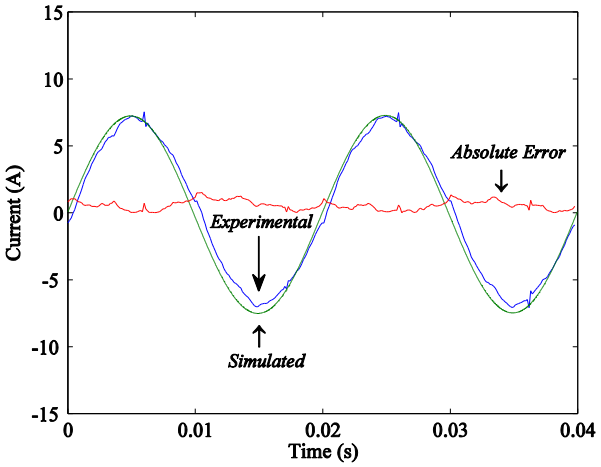

Figure 9. Electric grid current injected.

The simulations root mean square error (RMSE) for the I-V characteristic curve, P-V curve and current injection for the EGr -connected system is shown in Table 6.

Table 6. Simulations root mean square error (RMSE)

Simulation	I-V Curve	P-V Curve	Current injected into the grid
RMSE	0.0293 A	2.2328 W	0.6656 A

Both RMSE are a small relative value of the respective rated values, showing that the modelling is appropriated for describing the PVsy connected to the EGr by the commercial inverter.
For the EGr -connected system, the harmonic behaviour for the current injection, experimental data in blue and simulated with two-level or three-level inverters in green, are shown in Fig. 10a and Fig. 10b.

a) **b)**

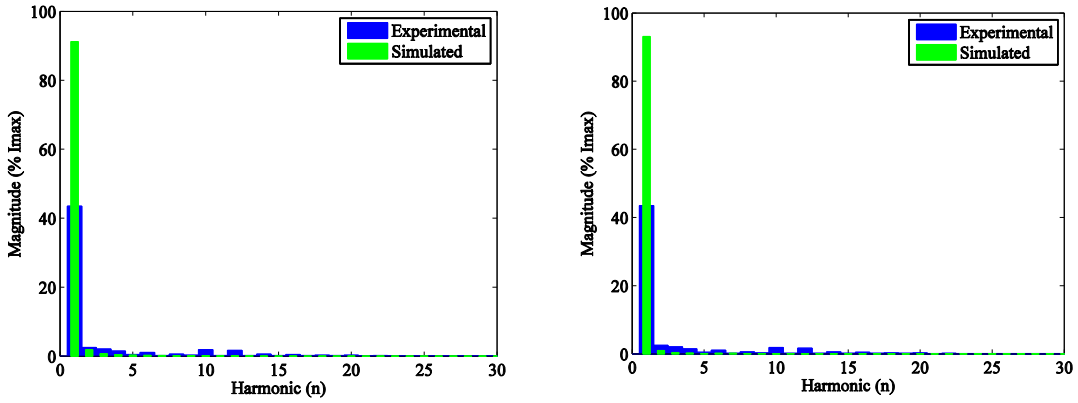

Figure 10. DFT of the current injection experimental and simulated with **a)** TwLI; **b)** ThLI.

Figure 10 allows concluding that: the PVsy with ThLI performs better than the one with the TwLI; the percentage of the fundamental harmonic calculated by the DFT for the simulated current injection has very favourable results, about 93%. The comparison between the harmonic percentage of the fundamental component for the current injection for the experimental and the simulated results with TwLI or ThLI are shown in Table 7.

Table 7. Experimental and simulated current harmonics

Harmonic (n)	Experimental (%)	Two-level (%)	Three-level (%)
1	79.5	91.2	93.1
2	0.2	1.5	1.0
3	0.7	0.7	0.4
4	0.1	0.4	0.25
5	0.5	0.2	0.1
6	0.1	0.3	0.2
7	0.6	0.2	0.2
8	0.1	0.1	0.1
9	0.3	0.2	0.1
10	0.1	0.1	0.1
11	0.3	0.2	0.1

The fundamental component percentage calculated with DFT for the simulated current injection into the EGr with ThLI is 93.1%, with TwLI is 91.2% and for the experimental current injection data is 79.5%. Those differences between the respective percentages are believed to happen in part due to the fact that the EGr is not a perfect ideal source of voltage. Additionally, the observation of Table 7 is in favour that the current injection for the PVsy with TwLI or ThLI based in classical PI control presents a content of high order harmonics relatively low due to the second order filter.
The comparison between the THD for the current experimental and simulated results with two-level or three-level inverters are shown in Table 8.

Table 8. Experimental and simulated current harmonics

Experimental (%)	Two-level (%)	Three-level (%)
4.17	5.005	2.41

The current injection THD is about 2.4 % for the PVsy with ThLI. Hence, the system has an adequate performance in what regards the fact that the current output THD is lower than the 5% limit required by the IEEE-519 standard.

5. Conclusions

Simulation studies on PV systems are essential to assist the engineers in what regards extracting the maximum energy, anticipating performance and deciding convenient measures to avoid malfunctions. A PV system modelling with DCB and TwLI or ThLI topology is proposed using the equivalent five parameter for PV modules; and DCB with two-level or three-level power inverter topology modelling, assuming a control strategy by PI controllers and PWMo by SVMo associated with SMCo. The PV system with ThLI presents a better behaviour in

comparison with the system with TwLI. The data comparison between simulation of a PV system integrated models and experimental results during the in situ operation is in favour of this contribution as an integrated relevant modelling.
The application of this modelling to a case study on a amorphous silicon solar module Kaneka KA 58 with a commercial inverter and a convenient filtering allows to anticipate a THD for the output current lower than the 5% limit required by the IEEE-519 standard, for the PV system with DCB and two-level or three-level power inverter topologies. Although disregarding in the simulations the fact that the EGr is not a perfect source of energy, the experimental results show a tolerable concordance with the simulated ones.

References

1. A. Poullikas, "A comparative assessment of net metering and feed in tariff schemes for residential PV systems", *Sust. Energy Technologies and Assessments*, vol. 3, pp. 1–8, 2013. http://www.sciencedirect.com/science/article/pii/S2213138813000313
2. J. Peças Lopes, N. Hatziargyriou, J. Mutale, P. Djapic, and N. Jenkins, "Integrating distributed generation into electric power systems: a review of drivers, challenges and opportunities", *Electric Power Systems Research*, vol. 77, pp. 1189–1203, 2007. http://www.sciencedirect.com/science/article/pii/S0378779606001908
3. F. Blaabjerg, Z. Chen, and S.B. Kjaer, "Power electronics as efficient interface in dispersed power generation systems", *IEEE Transactions Industrial Electronics*, vol. 19, pp. 1184–1194, 2007. http://ieeexplore.ieee.org/xpls/abs_all.jsp%3Farnumber%3D1331479
4. F. Blaabjerg, R. Teodoresco, M. Liserre, and A.V. Timbus, "Overview of control and grid synchronization for distributed power generation systems", *IEEE Transactions Industrial Electronics*, vol. 53, pp. 1398–1409, 2006. http://ieeexplore.ieee.org/xpls/abs_all.jsp?arnumber=1705631
5. T. Salmi, M. Bouzguenda, A. Gastli, and A. Masmoudi, "MATLAB/Simulink based modelling of solar photovoltaic cell", *International Journal of Renewable Energy Research*, vol. 2, pp. 213–218, 2012. http://www.ijrer.org/index.php/ijrer/article/view/157
6. H.A. Kazem, and T. Khatib, "Techno–economical assessment of grid connected photovoltaic power systems productivity in Sohar, Oman", *Sust. Energy Tech. and Assessments*, vol. 3, pp. 61–65, 2013. http://www.sciencedirect.com/science/article/pii/S2213138813000465
7. V. Fernão Pires, J.F. Martins, D. Foito, and C. Hão, "A grid connected photovoltaic system with a multilevel inverter and a Le-Blanc transformer", *International Journal of Renewable Energy Research*, vol. 2, pp. 84–91, 2012. http://www.ijrer.org/index.php/ijrer/article/view/131
8. R.J. Pereira, R. Melício, V.M.F. Mendes, and A. Joyce", Effect of shading on series solar modules: simulation and experimental results", *Procedia Technology*, vol. 17, pp. 295–302, 2014. http://www.sciencedirect.com/science/article/pii/S2212017314004940

9. E. Koutroulis, and F. Blaabjerg, "Methods for the optimal design of grid-connected PV inverters", *International Journal Renewable Energy Research*, vol. 1, pp. 54–64, 2011. http://ieeexplore.ieee.org/xpls/abs_all.jsp?arnumber=6020238
10. Y. Yang, and F.P. Zhao, "Adaptive perturb and observe MPPT technique for grid-connected photovoltaic inverters", *Procedia Engineering*, vol. 23, pp. 468–473, 2011. http://www.sciencedirect.com/science/article/pii/S1877705811053756
11. L. Fialho, R. Melício, V.M.F. Mendes, S. Viana, C. Rodrigues, A. Estanqueiro, "A simulation of integrated photovoltaic conversion into electric grid", *Solar Energy*, vol. 110, pp. 578–594, 2014. http://www.sciencedirect.com/science/article/pii/S0038092X14004812
12. L. Fialho, R. Melício, V.M.F. Mendes, L. Rodrigues, S. Viana, and A. Estanqueiro, "Simulation of a-Si PV System Linked to the Grid by DC-DC Boost and Two-level Converter", *16th International Power Electronics and Motion Control Conference and Exposition – PEMC 2014*, Antalya, Turkey, pp. 21–24, September 2014. http://ieeexplore.ieee.org/xpl/articleDetails.jsp?arnumber=6980627%2F069806
13. R. Melício, and V.M.F. Mendes, "Simulation of power converters for wind energy systems", *Información Tecnológica*, vol. 18, pp. 25–34, July–August 2007. http://dx.doi.org/10.4067/S0718-07642007000400005
14. M. Seixas, R. Melício, and V.M.F. Mendes, "Fifth harmonic and sag impact on PMSG wind turbines with a balancing new strategy for capacitor voltages", *Energy Conversion and Management*, vol. 79, pp. 721–730, March 2014. http://www.sciencedirect.com/science/article/pii/S0196890414000338
15. Kaneka Photovoltaic Products Inform. http://www.pv.kaneka.co.jp
16. D. Hohm and M. Ropp, "Comparative Study of Maximum Power Point Tracking Algorithms", *Energy Progress in Photovoltaics: Research and Applications*, vol. 11, pp. 47–62, 2003. http://onlinelibrary.wiley.com/doi/10.1002/pip.459

2.6 Simulation of a-Si PV System Linked to the Grid by DC Boost and Three-Level Inverter under Cloud Scope

L. Fialho[1], R. Melício[1,2], V.M.F. Mendes[3], M. Collares-Pereira[1]

In the Proceedings of the Doctoral Conference on Computing, Electrical and Industrial Systems, DoCEIS 2015, Technological Innovation for Cloud-based Engineering Systems, Vol. 450, pp. 423-430, 2015.
https://doi.org/10.1007/978-3-319-16766-4_45

Abstract
This paper is about a PV system linked to the electric grid through power converters under cloud scope. The PV system is modeled by the five parameters equivalent circuit and a MPPT procedure is integrated into the modeling. The modeling for the converters models the association of a DC-DC boost with a three-level inverter. PI controllers are used with PWM by sliding mode control associated with space vector modulation controlling the booster and the inverter. A case study addresses a simulation to assess the performance of a PV system linked to the electric grid. Conclusions regarding the integration of the PV system into the electric grid are presented.

Keywords: PV system, DC-DC boost, three-level inverter, simulation.

1 Introduction

The increment on the use of scarce fossil-fuel sources, the society wariness about the anthropogenic gas emissions and the increasing energy demand have strongly impelled the development of the use of renewable energy sources during the last decades [1]. For instance, the growth of the annual market regarding exploitation of solar energy is an evidentiary fact during the last decade. Particularly, a growing expansion is to be expected over the coming decade in what regards the deployment of photovoltaic (PV) systems.
The European Commission has launched a line of attack for the Europe to become a highly energy-efficient and a low-carbon economy with a set of proposals to create a new Energy Policy for Europe, reducing the anthropogenic gas emissions by 20% by 2020 and 50% until 2050, raising the overall share of conversion from renewable energy sources. Solar energy exploitation is expected to be significant on the European Energy Policy. Also, European Commission points out a future significant advance towards a more active role of the consumer by the implementation of the concept of smart grid (SG), improving integration into the grid for renewable energy sources and increasing energy efficiency. An advance thought to have a significant impact on mitigation of anthropogenic gas emissions, job and technology development [2].
A PV system directly converts solar energy into electric energy. The main device of a PV system is the solar cell. Solar cells are grouped to form PV arrays. An array is either a panel or a set of

[1] Universidade de Évora, 7002-554 Évora, Portugal
[2] IDMEC/LAETA, Instituto Superior Técnico, Universidade de Lisboa, Lisbon, Portugal
[3] Instituto Superior de Engenharia de Lisboa, R. Conselheiro Emídio Navarro, 1950-062 Lisbon, Portugal

panels connected in series or parallel to form large PV systems. Simulation of PV systems is vital to assist in exporting energy, anticipating bad performances and deciding convenient measures to avoid malfunctions and my significant benefit in real-time application from cloud-based solutions.
Power electronic converters have been developed for assisting in the integration of renewable energy conversion into the electric grid. Historically, low power PV systems use single-phase inverters, but in three-phase grid linking the use of only one single-phase inverter produces unwanted imbalance between the phase currents due to the injection of energy into only one phase of the grid. As reported in [3] a maximum power of 4.6 kW with 10 % of tolerance is possible to link to only one phase of a three-phase grid. Three single-phase inverters are needed for linking power greater than 5 kW to ensure a convenient balanced energy distribution between the phases.

2 Relationship to cloud-based solutions

A Cloud-based solution is significant support for launching a line of attack for a future highly energy-efficient management of energy conversion and usage. As the global energy demand increases with the growing world population, alternative sources of energy turn out to be attractive for exploitation in what regards a sustainable society's development. Within this attractive exploitation, the renewable energy from PV systems exploitation is considered one promising and reliable energy source for distributed generation (DG). DG and the increase usage of electric energy, for instances, the expected significant usage of electrical vehicles, will drive upcoming concerns on nowadays electrical grid about the ability to encompass with the future. So, a hatching thought about the electric grid is needed and the SG conception is on the way. A SG will benefit from cloud-based solutions allowing data interchange between end users and producers for transparency on energy consumption and on energy conversion of other forms of energy into electric energy. A Cloud-based solution allows the wanted consumer commitment in the management within the SG scope. The SG will be a source of information able to interact with other kinds of data, not only monitoring the flow of electric energy, but also an entire set of environments, leading to a foreseen increase data to be processed by SG management systems. So, the SG architecture has to be implemented with ensured security and reliability. A layered framework is one option gathering information about the SG components offering an awareness of the behavior, enabling people or machines to act accordingly over a services platform. The engineered software framework can be transposed to a Cloud architecture system, taking advantages of the existing internet cloud services to process with reduced operational costs the data storage and data transfer in real-time with reduced operational costs. For instance, as depicted in Fig. 1 for the PV system in study in this paper. This framework facilitates the integration of sensors and actuators with bidirectional data exchange [4], [5], [6], allowing real-time simulations speeding up the integration PV system energy into Smart Grid.

3 Modeling

The solar cell is modeled by the five parameter equivalent circuit: a photo electric current controlled source giving I_s, a shunt single-diode D draining the current i_{Dj}, a shunt resistance R_p draining the leakage current I_p, a series resistances R_s delivering the output current I_j of the cell having the output voltage V_j. As a normal assumption, assume that the cells associated

within the module are equally subjected to the same irradiance and the junctions are at the same temperature, then the equivalent circuit for the PV module is same of the cell, but with a suitable numerical transformation in the values for the parameters. The PV system under study is formed by a PV module, a DC-DC boost and a three-level power inverter linking the system to an electric grid. The PV system is shown in Fig. 1.

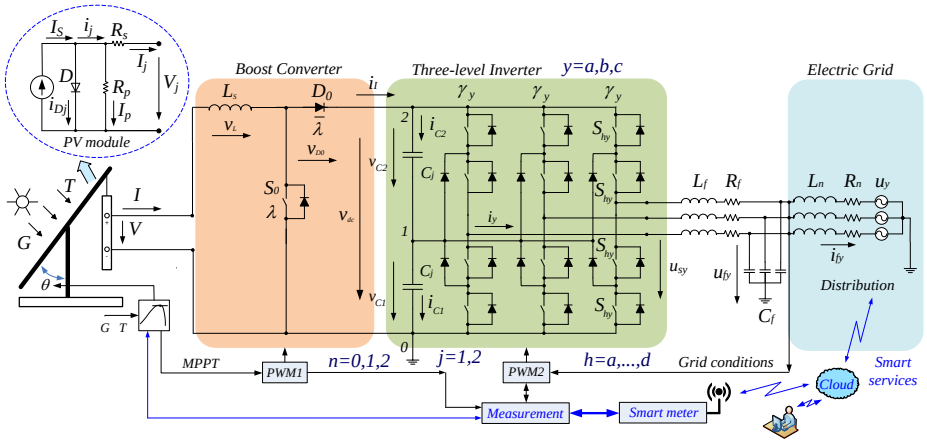

Fig. 1. PV system linked to the electric grid through power converters.

In Fig. 1, G is the solar irradiance, T is the cell p-n junction temperature in [K] and the current i_j [2] is given by:

$$i_j \equiv I_j + (V_j + R_s I_j)/R_p \tag{1}$$

where j is a condition index: $j = oc$ identifies open circuit condition; $j = sc$, short circuit condition, $j = mx$, maximum power point (MPP) condition. From (1), finding R_s at short circuit and at MPP conditions, holds the equations [2] given by:

$$V_{oc}\frac{i_{mx} - I_{mx}}{I_{mx}} - \frac{V_{mx} i_{oc}}{I_{mx}} - V_{oc}\frac{i_{sc} - I_{sc}}{I_{sc}} = 0 \tag{2}$$

The MPP of a PV system depends on G and T, at the MPP the conversion is at the highest efficiency and satisfies the relation [2] given by:

$$\gamma R_p i_{mx}^{sc}(V_{mx} - R_s I_{mx})(e_{mx} + 1) + V_{mx} - I_{mx}(R_s + R_p)e_{sc}^{mx} = 0 \tag{3}$$

The input parameters for the MPPT algorithm are the values of the voltage and the current of the PV system. The condition to be satisfied is given by $\partial P/\partial V = 0$, i.e., if the condition is met, then the algorithm has found the MPP point. But typically in practice the algorithm iterates around that condition until eventually converges. The iteration procedures are as follows; if $\partial P/\partial V > 0$, an incremental adjustment is set in order to increase the out voltage, i.e., in the direction of the MPP; if $\partial P/\partial V < 0$, an adjustment is set in order to decrease the out voltage in the direction of the MPP [7].

The General Algebraic Modeling System (GAMS) is used to code a mathematical programming problem to identify the five parameters for the equivalent circuit of the PV system, using data information from the tests of open circuit, short circuit, maximum power point (MPP)

conditions. The free solver COUENNE–Convex Over and Under Envelopes for Nonlinear Estimation for global optimization is used as a convenient option, due to the involvedness on the problem of identification of parameters [2].

The DC-DC boost converter has one unidirectional commanded IGBT, S_0. This converter is linked between the PV module and capacity banks, which in turn is linked to a three-level inverter. The modeling for the DC-DC boost converter is given by the switching variable λ used to identify the state of S_0 and the switching variable $\bar{\lambda}$ used to identify the state of the diode D_0. These variables have to satisfy the switching condition [8] given by:

$$\begin{cases} \lambda = 1 \text{ and } \bar{\lambda} = 0 \ (S_0 = 1 \text{ and } D_0 = 0) \\ \lambda = 0 \text{ and } \bar{\lambda} = 1 \ (S_0 = 0 \text{ and } D_0 = 1) \end{cases} \tag{4}$$

The module current I is modeled by the state equation given by:

$$dI/dt = 1/L_s \left[\mathrm{V} - \bar{\lambda} \ (v_{D0} + v_{dc}) \right] \tag{5}$$

where v_{D0} is the diode forward voltage at direct current and v_{dc} is the voltage at the capacity banks.

The three-level inverter is linked between capacity banks and a second order filter, which in turn is linked to the electric grid, modeled by a three-phase active symmetrical circuit. The DC-AC inverter is a three-level inverter, having twelve unidirectional commanded IGBT identified by S_{hy}, used as an inverter. The groups of four IGBT's linked to the same phase constitute the leg y of the inverter with $y \in \{a,b,c\}$ [9]. The converter has $p = 3$ levels. For the balance control strategy, the switching voltage level variable n_y which ranges from 0 to $(p-1)$ is used to identify the state of the IGBT h in the leg y of the inverter establishing the switching function of each IGBT. The index h with $h \in \{a,b,c,d\}$ identifies the IGBT. The three conditions to be satisfied for the switching voltage level variable of a leg y, at each level [9], are given by:

$$n_y = \begin{cases} 2, & (S_{ay} \text{ and } S_{by}) = 1 \quad \text{and} \quad (S_{cy} \text{ or } S_{dy}) = 0 \\ 1, & (S_{by} \text{ and } S_{cy}) = 1 \quad \text{and} \quad (S_{ay} \text{ or } S_{dy}) = 0 \\ 0, & (S_{cy} \text{ and } S_{dy}) = 1 \quad \text{and} \quad (S_{ay} \text{ or } S_{by}) = 0 \end{cases} \qquad y \in \{a,b,c\} \tag{6}$$

The inverter output voltage u_{sy} in function of v_{dc} [9] is given by:

$$u_{sy} = \frac{1}{6}(2n_y - \sum_{\substack{j=a \\ j \neq y}}^{c} n_j)\, v_{dc} \quad y \in \{a,b,c\}; \ n \in \{0,1,2\} \tag{7}$$

The voltage at the capacity banks v_{dc} appearing in (5) is a function of the electric charge stored or discharged from the capacitors by the action of the control of the converters. Hence, the state equation for this voltage is a function of the currents each capacitor i_{cj} [9] and is given by:

$$\frac{dv_{dc}}{dt} = \sum_{j=1}^{p-1} \frac{1}{C_j} i_{cj} \quad j \in \{1, \ldots, p-1\} \tag{8}$$

The current i_{cj} [9] is given by:

$$i_{cj} = i_I - \sum_{y=a}^{c} \delta_{ny}\, i_y \quad j \in \{1, \ldots, p-1\} \tag{9}$$

where the auxiliary variable δ_{ny} [9] is given by:

$$\delta_{ny} = \begin{cases} 0 & j > n_y \\ 1 & j \le n_y \end{cases} \quad n \in \{0, 1, 2\}; \quad j \in \{1, \ldots, p-1\} \tag{10}$$

The electric grid is modeled by an equivalent three-phase active symmetrical circuit, having a resistance and an inductance in series. Hence, for the electric current injected into the electric grid the state equation is given by:

$$\frac{di_{fy}}{dt} = \frac{1}{L_n}(u_{fy} - R_n\, i_{fy} - u_y) \tag{11}$$

where L_n and R_n are the electrical grid inductance and resistance, respectively, u_{fy} is the voltage at the filter, u_y is the voltage at the electric grid.

4 Control Method

The three-level inverter is a variable structure due to on/off switching states of the IGBT's. PI control and PWM by space vector modulation associated with sliding mode is used for controlling the inverter with the output vectors levels 0, 1 and 2 in the $\alpha\beta$ plane [9] shown in Fig. 2.

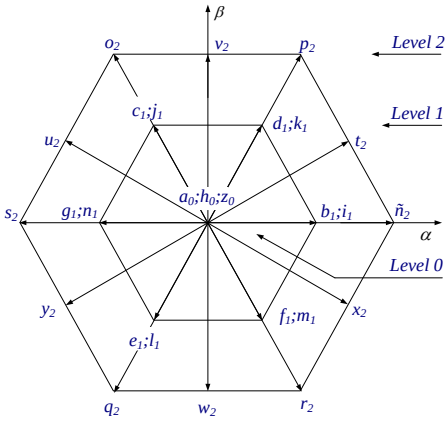

Fig. 2. Output space vectors for modeling of the three-level inverter.

The sliding mode control strategy is an option known by the advantage of having attractive considerable robustness to parametric uncertainties [9] due to partial shading or electric grid disturbances. Sliding mode control is particularly attractive in systems with variable structure, such as inverters, ensuring the choice of space vectors. The aim is to let the system slide along a predefined sliding surface $A(e_{\alpha\beta}, t)$ by changing the system structure. All transistors have a physical limitation due to the switch of finite frequency. So, an error exists between the control and the reference $e_{\alpha\beta}$ values. The sliding along the surface $A(e_{\alpha\beta}, t)$ is ensured by a state trajectory near the surfaces satisfying the condition [9] given by:

$$A(e_{\alpha\beta}, t)\frac{dA(e_{\alpha\beta}, t)}{dt} < 0 \tag{12}$$

The control for the MPPT is a simple adjustments over the DC-DC boost converter in order to follow the condition given by $\partial P/\partial V = 0$.

5 Case Study

The mathematical modeling for the solar cell with single-diode, shunt and series resistances, for the MPPT algorithm and for the PV system with the DC-DC boost and the three-level topology is implemented in Matlab/Simulink. This case study presents a simulation concerned with the data measured [11] from PV a-Si solar modules Kaneka KA58 provided in [10]. The irradiation is 800 W/m^2, module temperature is 13 °C and nominal AC power is 6 kW. The data for the a-Si solar module Kaneka KA58 at STC [12] are shown in Table 1. Table 2 shows the data results for the PV modelling simulation.

Table 1. Data for the Kaneka KA58 solar module at STC

Technology	V_m^*	I_m^*	V_{oc}^*	I_{sc}^*	β_{oc}	α_{sc}
Amorphous	63 V	0.92 A	85 V	1.12 A	-206 mV/ °C	1.3 mA/ °C

The current injected into the grid is shown in Fig. 3.

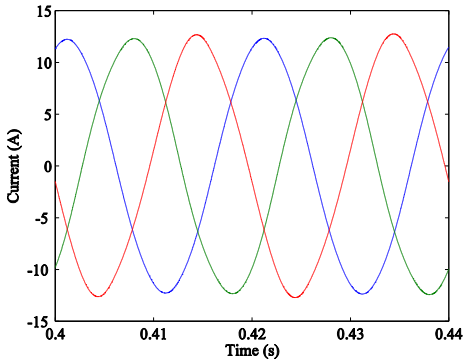

Fig. 3. Current injected into the electric grid.

The total harmonic distortion (THD) given by the DFT for the current injected into the electric grid is shown in Fig. 4.

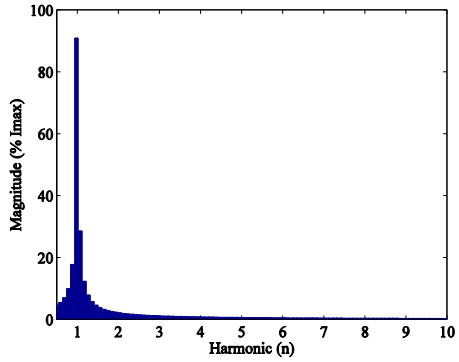

Fig. 4. Harmonics and interharmonics for the current injected into the electric grid.

Fig. 4 allows concluding that the percentage of the fundamental harmonic component calculated by the DFT for the current injected into the grid has a very favorable result, about 93 %. Additionally, the observation of Fig. 4 is in favor that the current injected into the electric grid for the PV system with classical PI control presents a content of interharmonics relatively

low and the higher order harmonics of the output current are filtered out by the second order filter.

Table 2. Data results for the Kaneka KA58 solar module

Parameter	R_s	R_p	m	I_{PV}	I_0
Kaneka KA58	6.28 Ω	976.02 Ω	243.08	1.11 A	1.18×10^{-6} A

The THD of the current injected into the electric grid has a very favorable result, about 2.4 %. Hence, the PV system with DC-DC boost and three-level power inverter topology has an adequate performance in what regards the fact that the THD of the output current is being lower than 5% limit imposed by IEEE-519 standard.

5 Conclusions

Simulation studies of PV systems are essential to assist engineers not only in the design phase, but also in real-time operation where cloud-base solutions may allow enough computer resources for a better management in what regards extracting of energy, anticipating performance and deciding convenient measures to avoid malfunctions. The increased integration of PV system into the electric grids leads to technical challenges implying research for more realistic physical models able of giving a better understanding of what concerns the eventually disturbance caused by PV systems, allowing to circumvent loss of energy quality and undesirable instability problems.

The paper proposes an integrated model for PV systems linked to the electric grid through power converters. The integrated model allows a more accurate description of the dynamic of the system. The model includes a maximum power point tracking and power-electronic modeling for the power converters: DC-DC boost converter and the three-level convert linked to the electric grid. The control strategy used in the simulation is based on the use of classical PI controllers, PWM by SVM associated with sliding mode control and power factor control is introduced at the output of the inverter. Although more complex, this integrated model is justified for more realistic results. The application of this modeling to a case study on a-Si solar modules Kaneka KA 58 with a convenient filtering allows to anticipate that the THD for the output current is lower than the 5% limit imposed by IEEE-519 standard for this PV system with DC-DC boost and three-level power inverter topology.

Acknowledgments.

This work was partially supported by Fundação para a Ciência e a Tecnologia, through IDMEC/LAETA, Instituto Superior Técnico, University of Lisbon and by Universidade of Évora.

References

1. López, M.E.A., Mantiñan, F.J.G., Molina, M.G. Implementation of Wireless Remote Monitoring and Control of Solar Photovoltaic (PV) System. In: 6th IEEE/PES Transmission and distribution: Latin America conference and exposition, pp. 1–6 (2012)

2. Fialho, L., Melício, R., Mendes, V.M.F. PV System Modeling by Five Parameters and in Situ Test. In: 22th SPEEDAM, pp. 577–582 (2014)
3. Rampinelli, G.A., Krenzinger, A., Chenlo Romero, F. Mathematical Models for Efficiency of Inverters Used in Grid Connected Photovoltaic Systems. Renewable and Sustainable Energy Reviews, 34, pp. 578–587 (2014)
4. Batista, N.C., Melício, R., Mendes, V.M.F. Layered Smart Grid Architecture Approach and Field Tests by ZigBee Technology. Energy Conversion and Management, 79, pp. 721–730 (2014)
5. Papageorgas, P., Piromalis, D., Antonakoglou, K., Vokas, G., Tseles, D., and Arvanitis, K.G. Smart Solar Panels: In-situ monitoring of photovoltaic panels based on wired and wireless sensor networks. Energy Procedia, 36, pp. 535–545 (2013)
6. Ayodele, T.R., Jimoh, A.A., Munda, J.L, Agee, J.T. Challenges of Grid Integration of Wind Power on Power System Grid Integrity: a Review. International Journal of Renewable Energy Research, 2, pp. 618–626 (2012)
7. Raj, J.S.C.M., Jeyakumar, A.E. A Two Stage Successive Estimation Based Maximum Power Point Tracking Technique for Photovoltaic Modules. Solar Energy, 103, pp. 43–61 (2014)
8. Fialho, L., Melício, R., Mendes, V.M.F., Rodrigues, L., Viana, S., Estanqueiro, A. Simulation of a-Si PV System Linked to the Grid by DC-DC Boost and Two-Level Converter. In: 16th PEMC, pp. 934–938 (2014)
9. Seixas, M., Melício, R., Mendes, V.M.F. Fifth Harmonic and Sag Impact with a Balancing New Strategy for Capacitor Voltages. Energy Conversion and Management, 79, pp. 721–730 (2014)
10. Giacobbe, L. Validação de Modelos Matemáticos de Componentes de Sistemas Fotovoltaicos. Master Thesis (in Portuguese), DEEC/IST (2005)
11. IEC 60904-1: Photovoltaic devices - Part 1: Measurement of photovoltaic (PV) current-voltage characteristics (2006).
12. Kaneka Photovoltaic Products Information, http://www.pv.kaneka.co.jp

CHAPTER 3. Commissioning, installation and characterization of the UEvora microgrids

3.1 Introduction

Chapter 3 presents the key tasks done on the experimental phase of this thesis, essential for the development and deployment of the main UEvora research infrastructures on BIPV microgrids with electrochemical energy storage. Experimental research work is usually very time consuming and the case of the UEvora microgrids added a new layer of complexity due to the necessity to design, build and commission the microgrids. Starting from a blank slate, this chapter represents long hours of: diagnosing and solving hidden technical issues; discussing operational methods and good practices; asking quotes, checking the available market, selecting and ordering equipment and materials; designing and installing electrical switchboards and monitoring equipment; dealing with diverse providers and manufacturers from multiple countries; programming and debugging; organizing the needed official documents for the internal university services or external entities, etc. but also making mistakes and learning, gathering extensive experience and "tightening every single screw" on the microgrids. This backstage, and sometimes hidden, work load is one of the motives for this chapter. Furthermore, the project context and operation principles for the ESSs are presented and explained, providing the reader with additional technical specifications of the microgrids.

3.2 Framework of the UEvora microgrids with energy storage

In 2012 the Renewable Energies Chair decided to start an R&D activity on the topic of the interface between PV systems and different applications, including BIPV and the very important topic of electricity storage. Possessing appropriate infrastructures – microgrids – for this effect became a major concern, resolved through the participation in the 7th framework and H2020 programs.

This installation, commissioning and initial tests of the UEvora microgrids started under the framework of the European Project PVCROPS[1] (PhotoVoltaic Cost r€duction, Reliability, Operational performance, Prediction and Simulation) [1]. The project began on November 2012 and had 36 months duration (Grant agreement nº 308468) under the general coordination of UPM (Universidad Politecnica de Madrid. The total EU contribution for the project was 3.798 million euros for 12 partners and PV CROPS addressed 3 key objectives of the call topic:

[1] PVCROPS project partners list:
Universidad Politécnica de Madrid (UPM - Spain); Universidad Publica de Navarra (UPNA - Spain); Universidade de Évora (UEvora – Portugal); Central Laboratory of Solar Energy & New Energy Sources of the Bulgarian Academy of Sciences (CLSENES – Bulgary); Dublin Institute of Technology (DIT - Ireland); Office National de l'Electricité (ONE - Morroco); ACCIONA ENERGIA S.A. (Spain); INGETEAM Power Technology SA (Spain); RTONE SARL (France); SUNSWITCH SA (Belgium); Renewable Energy Dynamics Technology LTD (REDT - Ireland); Association pour la Promotion des Energies Renouvelables - APERE ASBL (APERE - Belgium).

1) Improvement of performance, reliability and lifetime

2) Cost reduction of PV systems

3) Better integration of PV into grid

Among the UEvora tasks and project milestones were:

- The integration of two different technologies of batteries to increase the functionalities of BIPV systems (vanadium redox flow and lithium-ion batteries);
- The development of hardware and software to manage the energy flows, and to optimize control strategies;
- The development of control strategies for the adaptation to the new scenarios of self-consumption in BIPV.

The microgrids were conceived as demonstrators of the project, to rehearse and validate EMS developed in other PVCROPS tasks, in a real, full scale testing facility. This way, any designed simulation and assumptions made were tested taking into account real equipment operation and conditions (temperature, PV radiation, humidity, etc.). Also, feedback about real systems characterization parameters was provided to further improve simulations and EMS design.

An array of sensors, wattmeters and communication equipments was installed in order to guarantee high precision and fully independent measurements of the system components (inverters, batteries, etc.) and their real-time performance. These sensors and multifunction wattmeters were chosen to allow a fast measurement and data logging, improving the accuracy and runtime of the control system.

Instead of a common PLC a computer was chosen for overall control and datalogging due to lower cost, easier reparations and maintenance, and flexibility to run different software languages as LabVIEW, Python, Arduino (C/C++), etc.

Two innovative types of electrochemical energy storage technologies were chosen to integrate and rehearse within the microgrids: a Vanadium Redox Flow Battery (VRFB) and an Li-Ion Battery (LIB). The installation of these infrastructures coupled with smart energy management strategies were designed to test PV integration as part of the secondary regulation of the grid.

The successful and safe market introduction of these energy systems depended on a thorough and rigorous process of commissioning and testing. Commissioning and testing were critical for risk reduction. These microgrids can thus be put to test in a controlled environment before being part of our society common resources. These operational and live field tests provided the expertise in early project phases and delivered capability to disseminate good practices and results.

3.3 The Vanadium Redox Flow Battery

The vanadium redox battery uses vanadium ions in different oxidation states to store chemical potential energy. It is a flow battery technology and exploits the vanadium ability to exist in a solution form in four different oxidation states, using this property to design a battery with just one electroactive element, instead of two.

The positive and negative sides (tanks) of a VRFB are separated by a proton exchange membrane. This membrane selectively allows the exchange of protons. The electrodes are usually carbon based and the electrolyte is generally a solution of vanadium pentoxide (V_2O_5) solved with sulfuric acid (H_2SO_4).

Unlike other present-day battery types, the VRFB can complete up to 10.000 deep cycles without any appreciable loss of capacity or efficiency [2]. This is equivalent to up to 25 years of energy storage, matching the life of a PV or Wind system. After this lifetime, the vanadium electrolyte in the battery can be reused in a new system. This battery technology is emission free, non-flammable, non-explosive, and contains no heavy metals. The battery can be discharged down to 0% (100% DOD) and charged up to 100% without degradation or any side-effects. It has no self-discharge when shutdown and the limited self-discharge characteristics of VRFBs make them useful in applications where the batteries must be stored for long periods of time with little maintenance while maintaining a ready state.

The system has an estimated full cycle efficiency of up to 80%. The VRFB requires only minimal annual maintenance checks and can be monitored remotely, ideal for remote locations.

An important advantage of the VRFB is the capability to obtain the real State-of-Charge (SOC) at any moment independently of the charge/discharge state of the battery. This is achieved with a parallel circulation of a small flow of electrolyte from the tanks through a reference cell. With other technologies such as Lithium-Ion, Lead Acid or NiCd/NiMH only a theoretically estimated SOC can be obtained when the battery is charging/discharging.

Another important advantage over other storage technologies is the uncoupling of power and capacity. Flow batteries offer power as function of the number of installed stacks and capacity as function of the tanks electrolyte volume. This feature allows truly customized products for the desired solution and easily scalable to almost unlimited power or capacity, independently in terms of available power/capacity. This technology can have quick response times and do not needs to perform the "equalisation" charging process (charging to ensure that all cells have an equal voltage/charge).

During charging, an applied voltage causes vanadium ions to each lose an electron on the positive side ($VO^{2+} + H_2O \rightarrow VO_2^+ + 2H^+ + e^-$). The freed electrons flow through the outside electric circuit to the negative side, where they are stored ($V^{3+} + e^- \rightarrow V^{2+}$). During the discharge, stored electrons are released, flowing back through the outside circuit to the positive side, originating the reverse redox reactions.

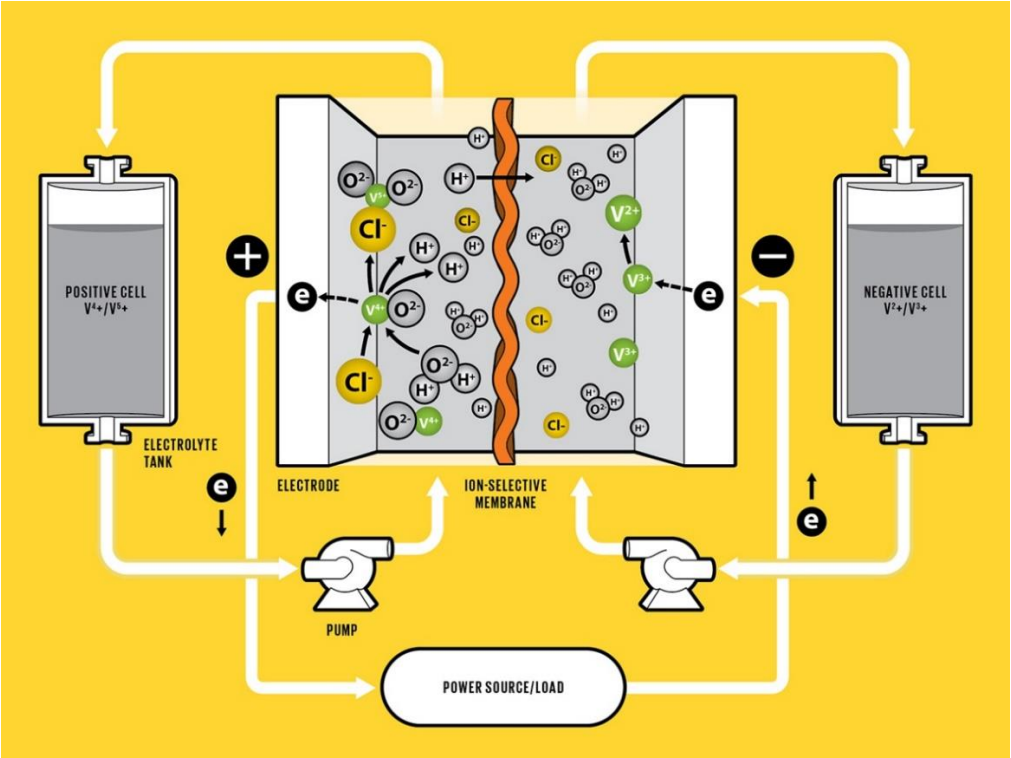

Figure 4: Vanadium Redox Flow Battery operating mode [3]

It is possible to recharge the system simply by replacing the depleted electrolyte if no power source is available to charge it and in case of accidental mixing of the tanks the battery suffers no permanent damage, and in that case, it just needs to be recharged again. Current commercial vanadium redox batteries achieve an energy density of about 25 Wh/L of electrolyte and 20 Wh/Kg of specific energy [4]. The VRFB specific energy is quite low compared to other energy storage technologies (for instance lead–acid: 33–42 Wh/kg [5])

The low energy density and the circulation of a liquid electrolyte makes this technology suitable for stationary energy storage applications but presents difficulties of use on a smaller scale or greater mobility applications. There is also the need to have auxiliary consumption services as the pumps or control system.

Nevertheless, the VRFB presents itself today as a promising technology to perform important energy storage tasks with high reliability and extended lifetime.

3.4 The Lithium-Ion Battery

The Lithium Ion battery technology is a rechargeable battery type in which lithium ions (Li^+) move from the anode to the cathode during discharge and back when charging. Li-Ion batteries are the most popular types of rechargeable ESS for portable electronics. The specific energy range for the lithium-based batteries is 200 Wh/Kg up to 600 Wh/Kg [6], depending on the battery technology (anode-cathode).

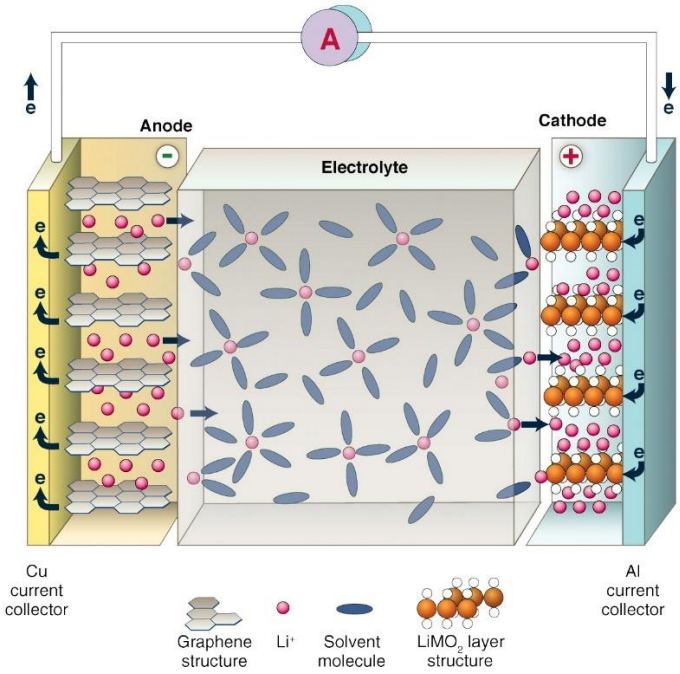

Figure 5: Schematic model of a lithium-ion battery [7]

LIB is typically a low maintenance ESS with self-discharge lower than other technologies, for instance, nickel-cadmium, and also with a longer lifetime.

Despite this it has several drawbacks. It is fragile and requires monitoring by a built-in protection circuit. This circuit protects the cells from over or under discharge and it also monitors the cells temperature to prevent extreme temperatures. The maximum number of cycles, that is, the lifetime, is also limited due to the aging process. There is a slow capacity deterioration, noticeable after one year [8]. Higher rate cycling and higher temperatures cause more rapid capacity loss. Furthermore, in LIB technologies power and capacity are coupled, preventing the design of storage systems perfectly suited for each application.

The safety issues [9] of the lithium-ion batteries are mainly caused by the failure of individual components (cathode, anode, electrolytes or current collector) and the whole system of battery in some extreme conditions, including overcharge, thermal runaway, dendritic lithium growth (internal short-circuits), current-collector dissolution, gas generation and so on. Overcharge can lead to thermal runaway and ultimately to fire or explosion of the batteries.

Multiple cell batteries need to be equalized over time, as single cells tend to have different voltage levels. Series connected lithium cells pose a more complex problem: each cell in the string must be monitored and controlled. The highest voltage cell in the series limits the top available capacity and the lowest voltage cell limits the lower SOC point available to operate.

LIBs evolution is being enhanced by automotive industry so that, in the last few years, this type of battery is showing up as the main commercial product to BIPV installations. Due to space restricted applications and its superior energy density, combined with better round-trip

efficiencies, integration with smart products and falling costs, this technology is currently a promising ESS for the future, despite its disadvantages.

3.5 Installation of the microgrids

The experimental infrastructures of the Renewable Energies Chair are in Polo da Mitra (Herdade da Mitra, Lat. 38.527613/ Long. -8.017783), therefore several sites were surveyed there to do the installation and integration in existing university buildings power use. The site requirements were easy accessibility to perform the installation, commissioning and O&M tasks, availability of a building electric grid and internet connections, enough space to install all the necessary equipments, roof/ground space to install the PV panels and capability to operate in a controlled environment (temperature, humidity and safety). The chosen sites were vacant and a wall enclosure on the VRFB site had to be built, as it was previously an open space to the outside (Figure 6).

The VRFB site was equipped with a “liquid-tight” spill-control tray system, capable of neutralizing a catastrophic spill of all the battery electrolyte. This spill containment system was built on to the floor and the surface was coated with an acid resistant paint, due to low pH nature of the vanadium solution electrolyte. Apart from this, the VRFB is equipped with several smaller containment trays and sensors, so it should be able to prevent any spill. Handling with acid solutions required also the installation of an emergency shower and eyewash. Both microgrids were also equipped with CO_2 fire extinguishers and personal protective equipment such as protective clothing, goggles and gloves. Air conditioning units were also fitted in both microgrids allowing air temperature and humidity control.

Figure 6: Selected site to install the VRFB Microgrid (Polo da Mitra)

Figure 7: Selected site to install the LIB Microgrid (Polo da Mitra)

The VRFB site had free rooftop space nearby, so the two PV strings were installed there. In the Li-Ion battery site, two strings of PV modules were installed on the ground close to the battery location.

The installation of both ESS was done by the Renewable Energies Chair team with the support of the personnel selected by the providers/partners for this effect: REDT energy storage [10] for the VRFB; CEGASA for the LIB, Ingeteam [11] for the inverters and all the partners within PVCROPS, testing their respective technologies. The inverter manufacturer had a previous work task to develop and install appropriate firmware for the operational specifications of the selected batteries. Some of the technical limits and alarms were programmed into the inverters firmware.

All the auxiliary systems, PV systems, inverters, electric grids and connections, communications, monitoring, datalogging, health and safety equipments were installed by the RE Chair team. All the installation systems comply with the appropriate codes, laws and regulations applicable in Portugal (e.g. RTIEBT - Regras Técnicas das Instalações Eléctricas de Baixa Tensão, Dec.-Lei nº153/2014, etc.).

3.6 Commissioning of the microgrids

3.6.1 VRFB microgrid

The VRFB microgrid was finally composed by a 6.74 kW_p rooftop PV system with two strings, one of monocrystalline PV panels with 3.24 kW_p and the other of polycrystalline silicon modules with 3.5 kW_p. The PV system is connected to a three-phase inverter (Ingeteam Sun 3Play) with two independent maximum power point tracking (MPPT) systems.

Figure 8: VRFB Microgrid rooftop PV system

The VRFB has a stack with 5 kW nominal power (10 kW peak power) and 60 kWh total capacity. This capacity is achieved with two tanks containing a total of 3600 L of electrolyte. The stack is composed by 40 cells in series, providing the total operational voltage range of 45V to 60V. This ESS is also connected to the three-phase grid by three inverters (one for each phase). The battery inverters are Ingeteam Ingecon EMS Home with 2.4 kW nominal power each. The microgrid configuration scheme is shown in Figure 9.

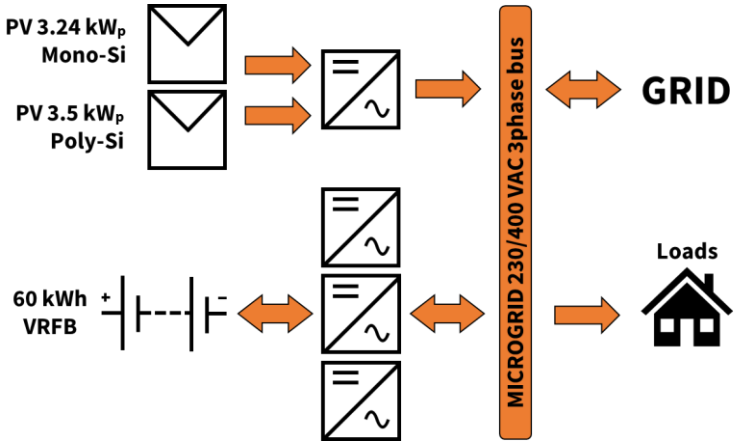

Figure 9: Simplified scheme of the VRFB microgrid (Orange arrows represent power flow)

Figure 10 shows the VRFB model installed, with two tanks with 2200 L capacity each and the 5 kW power stack in the middle. The top empty space in the electrolyte tanks is filled with a high purity (99.9999% pure) inert gas (Argon) in order to avoid electrolyte degradation through unwanted reactions with oxygen.

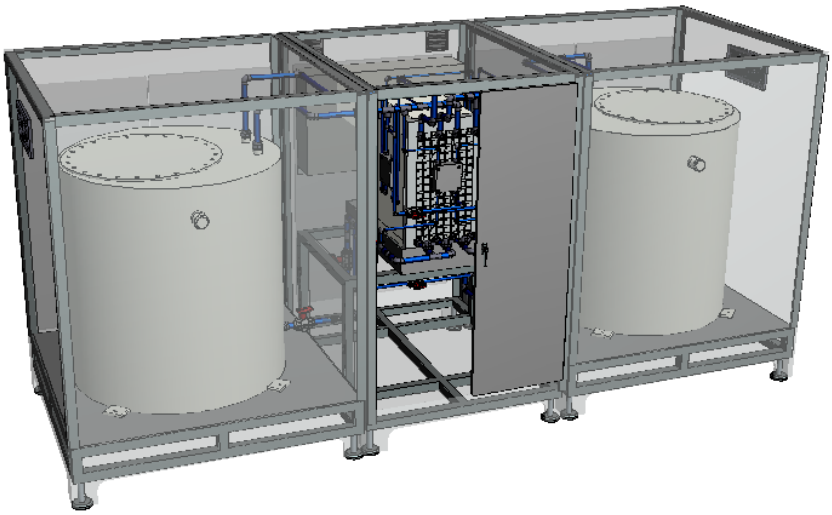

Figure 10: The selected VRFB model for the microgrid

A communications network was installed on site. The ethernet network with high data transfer rate is controlled by a local switch and is also connected to the university internal network and Internet. Additional communication with other devices was established via different communication protocols and/or wiring, as shown in the setup in Figure 11.

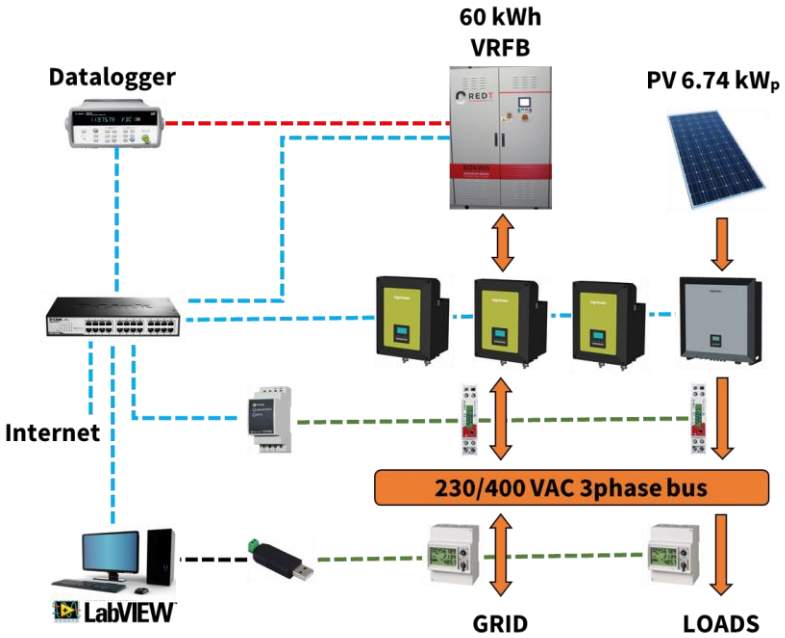

Figure 11. Simplified communication setup of the VRFB microgrid

Figure 11 connections legend: *Orange arrows – power; Blue dotted line – ethernet; Green dotted line – RS485; Black dotted line – USB and Red dotted line – low voltage measurement.*

Figure 12. VRFB at UEvora. On the left and right the electrolyte tanks are visible, in the middle, the control panel and behind it the stack (not visible).

The VRFB microgrid was installed as a three-phase system and the Li-Ion microgrid was installed as a single-phase system in order to test different type systems. By the same reasoning for the VRFB microgrid inverters were chosen with transformer and for the li-Ion microgrid without transformer. Whenever possible, different models were chosen to maximize operational experience and the research plus demonstrative aspects of these infrastructures.

The inverter model selected by Ingeteam (EMS Home 2.4) for the VRFB is of general use for other storage technologies and its firmware was previously adapted and updated for the technical specifications and limits of this application. Moreover, the selected model has its efficiency curve tuned for higher voltages, having an operational DC voltage range of 48 V - 330 V. Due to the VRFB low voltage range (45 V – 60 V) these inverters will be working near its lowest voltage limit and their efficiency is lower than normal. This also precludes deeper discharges of the VRFB (below 48 V, down to 45V), with leftover capacity available (although minimal) below this technical limit.

In case of a discharge below 48 VDC, the inverters are not able to turn on and charge again the battery has it does not have enough voltage. Then, it is necessary to use an external DC source to provide the inverters with enough voltage to turn on and start the charge process. It was defined a 48 V lower limit in the control system to prevent this.

The VRFB provides internal data such as DC voltage and current, reference cell voltage, operating temperatures, etc. It was found that despite the voltage readings of the reference cell were accurate enough for the end-user, they were not accurate enough for our precision control. The reference cell voltage provides an accurate, real-time and direct measurement of the battery SOC and a high precision data acquisition unit was installed to perform this task.

The VRFB microgrid currently comprises:

- PV generator, polycrystalline, 3.5 kW
- PV generator, monocrystalline, 3.24 kW
- 1x PV inverter, Ingeteam’s INGECON Sun 3Play 12.5 kW TL
- Vanadium Redox flow battery, REDT, 5 kW, 60 kWh

- 3x Battery inverter, Ingeteam's INGECON EMS Home 2.4 kW-
- 6x Single phase power analyser Circutor CVM-1D
- 1x RS485-TCP/IP adapter, Circutor TCP1RS+
- 1x USB-RS485 converter, Spectra
- 1x Data Acquisition Unit, Keysight 34972A
- 1x Three phase power analyser, Carlo Gavazzi EM24
- 1x Energy management controller unit, desktop PC + LabVIEW
- 1x Network router/switch
- 1x UPS, Eaton 9E, 15 kVA
- Electrical protections (MT Breakers, contactors, etc.)
- Wiring
- Auxiliary equipments (health and safety)

Figure 13: Inverters at the VRFB microgrid: PV inverter (gray), EMS Home bat. inverters (green)

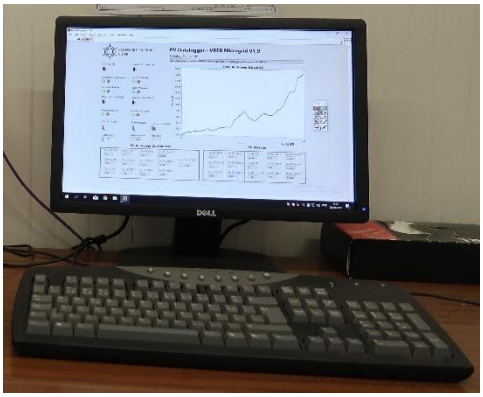

Figure 14: Microgrid PC control system

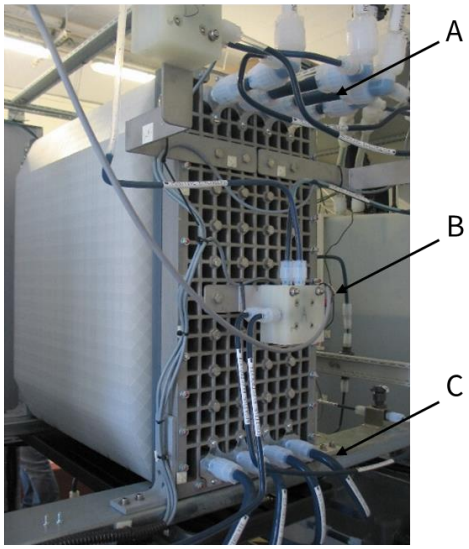

Figure 15. VRFB stack: outlet piping (A), reference cell (B) and inlet piping (C).

More detailed specifications and in-depth data about the VRFB Microgrid are available in the paper addressed in Chapter 4.

3.6.2 Lithium-Ion Battery microgrid

The LIB microgrid at the University of Évora is composed by a 3.3 kWp PV system (2 strings of amorphous silicon modules) and a 31.8 kWh lithium–ion battery connected to the electrical grid. Since the concept is to make these infrastructures available for other projects and users, in 2018, a 9.8 kWh lithium-ion battery was added to this microgrid. The current configuration scheme is shown in Figure 16.

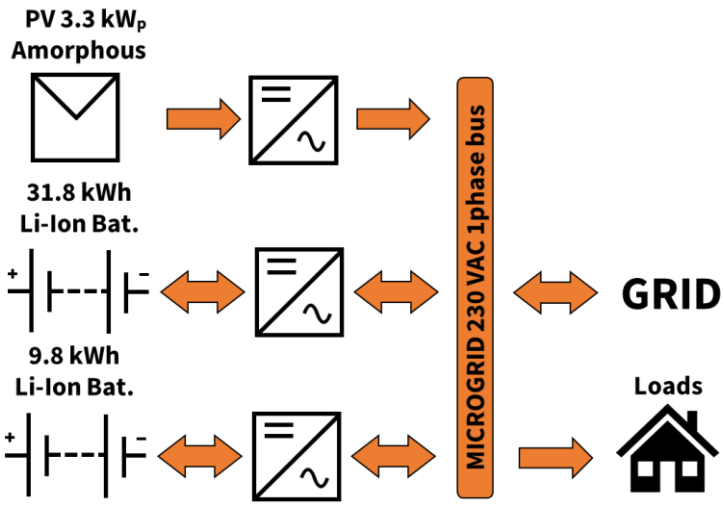

Figure 16: Simplified scheme of the Li-ion Bat. microgrid

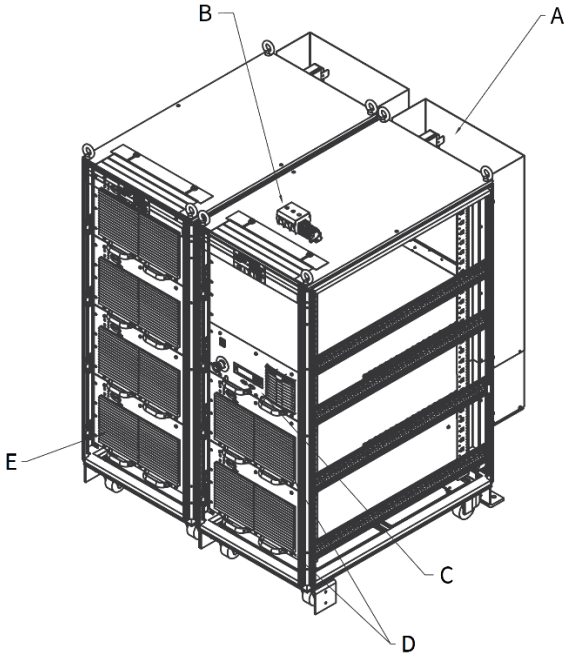

Figure 17: Cegasa LIB installed in the microgrid

Figure 17 legend: *A – Air exhaust; B – Grid and power supply connection; C – Control and Protection Module; D – Air intake; E – Energy module*.

The Cegasa battery is made by a 72s3p configuration (3 parallel subsets of 72 cells in series). The battery size is 1200 mm (width) by 1200 mm (depth) by 1700 mm (height) and has a total weight of 880 Kg. The following table presents its electrical specifications:

Table 1: Cegasa technical specifications for the LIB.

Electrical specification	Value (72s3p)
Nominal voltage	266.4 V
Maximum voltage	302.4 V
Minimum Voltage	194.4 V
Nominal discharge current at 1C	40 A
Maximum continuous discharge current	200 A
Nominal charge current at 0.2C	8 A
Maximum continuous charge current	120 A

This battery has three operation modes: Charge/discharge/standby mode; Balancing at rest and Set-up battery charge. The equalization of the cells is performed with the last two operating modes.

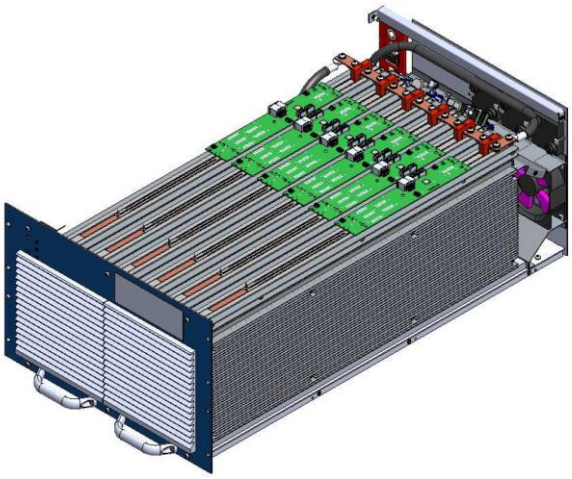

Figure 18: Energy Module (5.3 kWh). The installed battery is composed by six energy modules.

The *Balancing at rest* mode allows to equalize the battery cells at the current SOC. The battery control starts to discharge the cells with higher voltage level until all the cells have reached the lowest voltage cell value. The selective discharge is performed with small resistors on top of the energy modules, automatically controlled via relays.

The *Set-up battery charge* mode performs the equalization process simultaneously with a battery charge. At the end of this process the battery should be equalized and at 100% of SOC. The process begins with a charge up to the cells maximum voltage (4.05 V), performed simultaneously to a partial cell equalization. When maximum voltage is reached by the higher voltage cell a fine equalization process begins. After a pre-set tolerance is achieved regarding the cells voltage dispersion, the equalization stop and the battery is charged again. This process allows obtaining a fully charged battery in the end and a minimal cell voltage dispersion. Both factors combined translate into the maximum capacity of the system for the conditions under which it was carried out this process.

These equalization processes usually generate heat as the resistors dissipate the needed energy for each cell and the battery ventilation system should automatically be working along to minimize it.

The physical data communication set-up for this microgrid is shown in Figure 19.

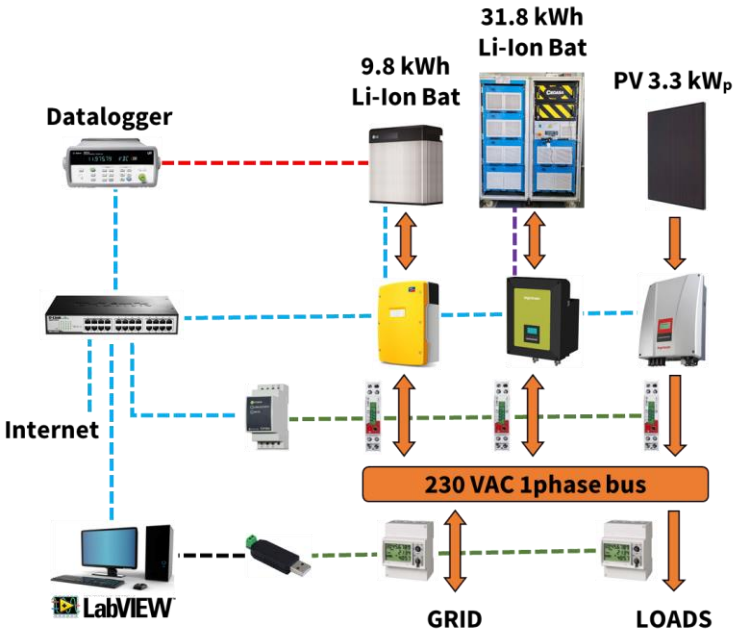

Figure 19. Communication set-up for the LIB Microgrid

Figure 19 connections legend: *Orange arrows – power; Blue dotted line – ethernet; Green dotted line – RS485; Black dotted line – USB; Purple dotted line – CANopen; and Red dotted line – voltage and temperature measurement.*

Figure 20. Li-ion batteries of the microgrid: Cegasa battery(left) and LG Resu10 battery (right)

Figure 21: Inverters at the LIB microgrid: PV inverter (left), EMS Home bat. inverter (center) and SMA bat. inverter (right)

Figure 22: Ground installed PV strings connected to the Li-ion bat. microgrid

In the installation and commissioning of the battery by Cegasa personnel, some problems were found regarding battery operation. These problems were addressed by the Cegasa team, before they left the site. Soon afterwards, as the UEvora team was performing initial tests, new problems were detected, and promptly reported (14th November 2014) to the manfacturer. Cegasa did several attempts to solve them but some malfunctions persisted until today. After the 9th July 2015, no further response or support was received from Cegasa to properly solve the pending problems.

In 2015 the Spanish Grupo Cegasa was declared insolvent with losses above 111 million euros in the previous four years. The lithium ion storage production unit was sold, and it is now operating as Cegasa Portable Energy, S.l., not providing any warranties or support over previous Li-Ion products.

The battery has several pending issues and was entering in shutdown at random times, interrupting the ongoing task without prior notice. After analysis by the UEvora team, it was found that one of the previous repairs by the Cegasa team had been poorly done. Various relays were then replaced by the UEvora team in the printed circuit boards of the cell management, which solved this problem. Despite all the effort by the UEvora team, it was decided to suspend the reparation attempts, given the seriousness and extent of the problems detected.

At the moment, this battery has the following detected and unsolved issues:

- During the cells equalization process the ventilation system do not work to cool the battery, bringing down the cabinet inside temperature. This is a safety hazard and causes sudden battery shutdown when reaching maximum safety temperature.
- The maximum temperature reading of the battery randomly switches to 126, value unrelated to the actual temperature.
- The battery maximum and minimum cell voltage readings exchange among themselves in random moments, which is a critical error and a safety risk.
- The SOC reading randomly shows a 2% reading, unrelated with the actual value. This poses another critical operation error.

In 2018, a new LIB was acquired and installed in the microgrid. The chosen battery system was a LG Chem RESU 10 LV (Figure 23) with 9.8 kWh capacity, 48V nominal operating voltage and with natural convection cooling [12]. It is an NMC Li-ion battery, it has a cathode combination of nickel-manganese-cobalt ($LiNiMnCoO_2$) and it was selected for its higher energy density and longer cycle life than the traditional lithium iron phosphate technology. The NMC Li-Ion batteries are currently used in electric vehicles and stationary ESS (e.g. Tesla). It is coupled with a new SMA inverter, the Sunny Island 4.4M with 3.3 kW power (5 kW, 3s) and a rated maximum efficiency of 95.5% [13]. This system is already fully operational and its initial characterization tests are ongoing. Future results regarding this battery will be part of another PhD thesis.

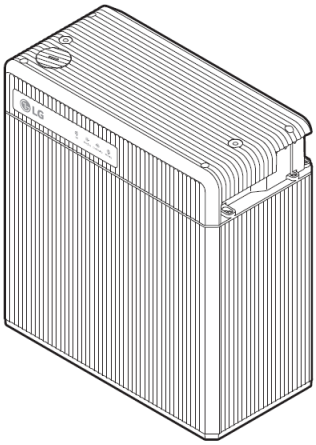

Figure 23: LG Resu10 Li-ion battery installed in the microgrid in 2018

The LIB microgrid currently comprises:

- PV generator, amorphous Si, 3.3 kW
- 1x PV inverter, Ingeteam's INGECON SUN Lite 5kW TL
- 1x Lithium-ion battery, CEGASA, 5 kW, 31.8 kWh
- 1x Battery inverter, Ingeteam's INGECON EMS Home 5 kW
- 1x Lithium-Ion battery, LG Resu10LV, 5 kW, 9.8 kWh
- 1x Battery inverter, SMA Sunny Island 4.4M, 3.3 kW
- 3x Single phase power analyser Circutor CVM-1D
- 1x RS485-TCP/IP adapter, Circutor TCP1RS+
- 1x USB-RS485 converter, Lindy

- 1x Data Acquisition Unit, Keysight 34972A
- 1x Three phase power analyser, Carlo Gavazzi EM24
- 1x Energy management controller unit, desktop PC + LabVIEW
- 1x Network router/switch
- 1x UPS, Eaton 9E, 15 kVA
- Electrical protections (MT Breakers, contactors, etc.)
- Wiring
- Auxiliary equipments (health and safety)

3.6.3 Software control and communication

To perform the control and datalogging tasks it was necessary to develop in-house software. This software was developed in LabVIEW due to the requirements regarding test, measurement, and control with rapid access to hardware and data. The developed software allows the interaction with virtually any kind of sensor or equipment, communicating (control commands, data, etc.) and enabled to work with any desired equipment setup within the microgrid. As general requirements for this software:

- Each program cycle should run with one second step (mandatory to implement successful EMS dealing with quick variations of PV power or loads);
- It should be able to use all the major communication protocols/ hardware (Modbus, RS485, USB, serial port, NI-VISA, etc.);
- It should be flexible enough to easily implement different EMS or algorithms;
- It should display clear and real-time data to the operator and allow to change control parameters during program execution;
- It should act as datalogger, saving program execution results and microgrid data;
- It should automatically impose technical or safety limits and display equipment alarms.

The software has been developed following a modular programming approach in LabVIEW.

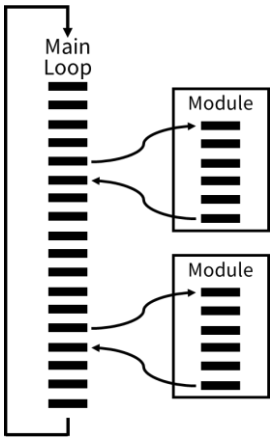

Figure 24: Modular programming

This modular programming allows for independent lower function modules development (sub programs), executing simpler tasks. These lower function modules are then

called from the main loop, as many times as required, in a timely manner. This principle produces a streamlined main loop, cleaner and easier to debug and modify. Furthermore, this programmatic approach enables the reuse of this lower function blocks in different main loops, speeding up the programming task of new algorithms or EMSs. For instance, sending a command to read the battery SOC and receiving the response constitutes a lower function block, and it is called from the main program and executed when necessary. There is no limit on how many subfunction blocks can be used and their hierarchy levels.

Following the previous approach, for each equipment in the microgrid a set of subfunctions is developed allowing interaction with it, sending and receiving commands, data, alarms, etc. After testing and debugging these simpler structures, ensuring their reliability, a set of specific functions is available for use.

In a second stage, the main loop is programmed, using subfunctions as needed, and it is tested and debugged. A runtime analysis is developed to safeguard the required full cycle time. Also, a stress analysis is conducted on the control software, to perform a safety analysis and identify critical faults.

The main cycle gathers the relevant data, uses it to make the necessary computations and sends the new commands to the inverters, according to the EMS defined at the time. Several functions deal with errors, unexpected results and redundant measurements. A different set of functions deal with security and safe operation of the equipment, implementing alarms and automatic safety actions. It was also implemented a logging function to register data for posterior analysis. A critical asset also carefully programmed: the Human-Machine Interface (HMI). This visual mode displays the current state of the EMS, with the relevant parameters and data from the whole system. Apart from displaying, it also enables entering changes in control parameters, execution runtime modification (delays), etc.

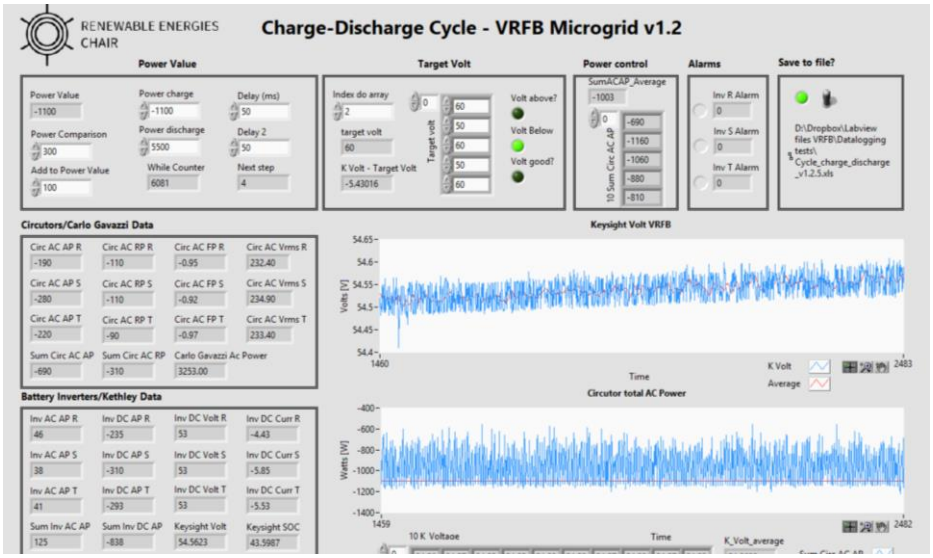

Figure 25. Display interface of the control software made in LabVIEW. VRFB full charge-discharge characterization cycles test showing.

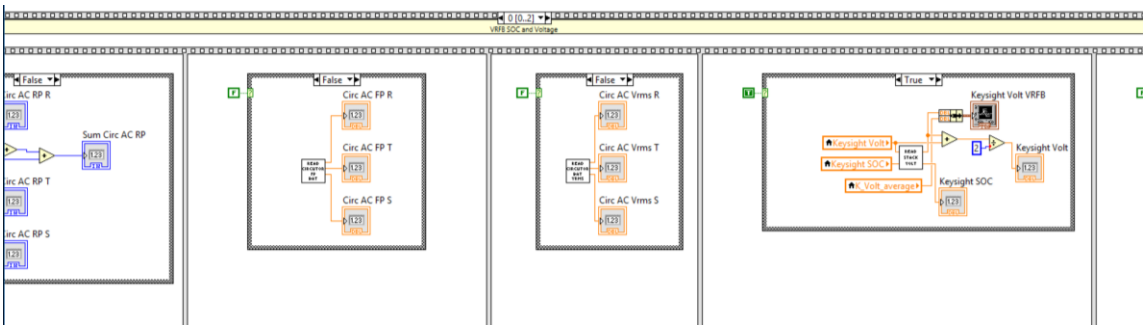

Figure 26: LabVIEW graphical programming interface: example of usage of subfunctions to read the power factor and RMS AC voltage with the multifunction wattmeters.

This software is still being used quite successfully to control the microgrids and it is updated in a continuous improvement process, increasing its efficiency and performance. An additional PV datalogger software was developed (Figure 27) for the microgrids to do continuous datalogging of the PV production, even if no rehearsal or test are ongoing on the infrastructure.

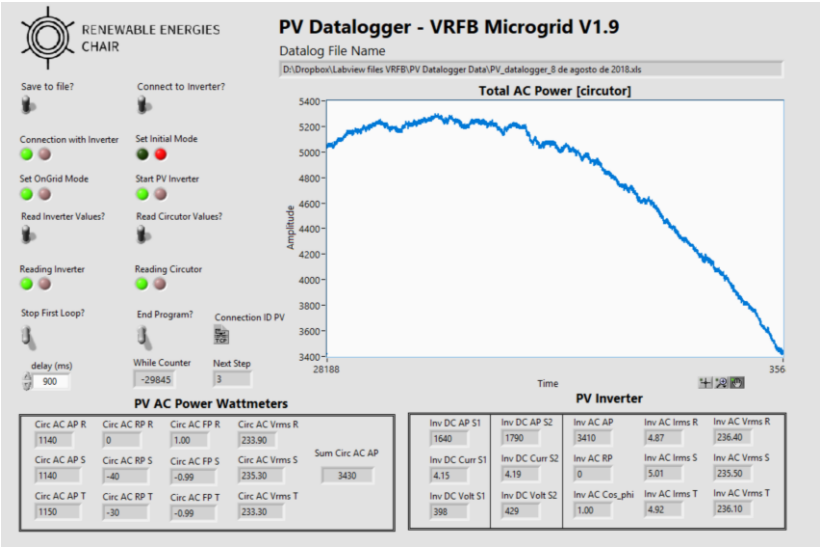

Figure 27: PV datalogger software of the VRFB microgrid (8th August 2018 PV production profile showing)

3.6.4 Implementation Outcomes

The implementation of these demonstrators led to the development and enhancement of different commercial products thanks to the continuous feedback from the UEvora researchers to the different manufacturers, mainly Ingeteam and REDT, and back. As a result, Ingeteam and REDT have been able to test on field and redesign their products, namely, the battery inverters, energy management systems and the VRFB. The continuous feedback from the different partners for the enhancement of their products have made this implementation somewhat long but has led to highly valuable results presented under this section.

Commercial VRFB is a novel technology still being developed by REDT. Since the installation and commissioning of the 5 kW/ 60 kWh system at the University of Évora, following

the results, the discussions, and learning from the demonstration and validation periods, REDT has been able to apply considerable improvements to their system design and functionality in preparation for volume production, sales and full commercialization of the VRFB.

This evolutionary process has led to the re-design for the next generations of VRFB system which are now in production, and incorporate the following:

- Revised internal component configuration with new format electrolyte tanks in order to achieve an overall reduction in system dimensions and volume.
- Re-designed, shorter pipework configuration and routing to save space, material cost and more efficient electrolyte flow. Re-designed piping fittings to avoid electrolyte drips.
- The sourcing and use of lower cost, variable speed pumps with more reliable performance with low pH fluids.
- Re-designed Argon gas pipework flow methodology and material to prevent leaks and improve efficiency.
- Adoption of an alternative system control PLC, allowing the removal of a number of electronic components, and provided further cost and space savings.
- A re-designed and re-engineered single module system with an overall footprint reduction of 30% enabling installation in smaller sites, easier installation and maneuverability.
- VRFB integrated with a weatherproof IP65 casing suitable for outdoor installation as well as indoor site locations.
- Planned overall 50% cost reduction to be achieved for volume production by the re-design and re-engineering process.
- Re-evaluation and re-statement of system and electrolyte performance with a claimed 17% improvement from 60 L/kWh to 50 L/kWh – higher energy density.

As for Ingeteam, it had to adapt the inverter for the VRFB, whose characteristics are different than usual ESSs. The battery inverter firmware prototype has been developed to control a two-way storage system, fully adapted to its technical specifications. Furthermore, during this project, the following re-design and re-engineering of state-of-the-art photovoltaic and battery inverters has been carried out:

- Software adaptation for accepting set-points and commands from an external controller.
- Software adaptation for operating VRFBs.
- Hardware adaptation for getting quick responses to set-points at the power's output.
- Integration and on field rehearsal of their new two MPPT PV inverter.
- Re-design of inverter enclosure for image improvement.
- Re-design of the display interface for better user experience.
- Cost reduction actions.

Also, Ingeteam has developed a EMS manager and EMS Manager tools. The innovative energy management controller (EMS Manager) solution for the domestic, commercial and industrial markets has been developed in PVCROPS to simplify the implementation of battery-based BIPV systems. The EMS Manager controls the energy generation from renewable sources, based on the power production data obtained from the power converters and on total loads consumption. It allows end users to implement management strategies based on the different devices connected to the system, making it possible to automatically control how and when to consume the energy self-generated. This product has been developed in part thanks to the permanent feedback between the UEvora team and Ingeteam.

3.7 Energy storage systems characterization tests

The ESSs initial characterization tests and Energy Management Strategy validation tests were performed in the already described microgrids. Due to the Cegasa LIB technical problems and the impossibility to perform any rehearsals with it, for the EMS validation a similar smaller capacity LIB [14] (also from Cegasa) was used but installed at the IES-UPM (Instituto Energia Solar of the Universidad Politécnica de Madrid). The used LIB is a similar model with smaller capacity (10.6 kWh – 2 energy modules) but using the same technology, identical battery management system and communication protocol. It is constituted by a 72s1p cell configuration, so the voltage operational limits are also identical to the UEvora LIB. Similarly, the same inverter model was used, so the control programming developed by UEvora was fully compatible with it and it was thus used. Some programming adaptation was needed to interface with different energy meters.

The first performed tests on the VRFB allowed to assess the control and experimental specifications of the demonstrators, for instance, roundtrip efficiency, i.e., the efficiency of a complete charge and discharge cycle of each battery.

The roundtrip efficiency is defined as the total energy discharged divided by the total energy charged. The attained results are presented in the poster intitled “Performance Characterization of a Vanadium Redox Flow Battery” (see annexes).

The tests yielded a DC roundtrip efficiency of 81.11% for the Vanadium Redox Flow Battery, and 95.18% for the Lithium-ion Battery [14]. These figures were used to program the design and were integrated in the EMS algorithms.

Other work done using the microgrids is presented in the next chapters.

References

[1] CORDIS, Community Research and Development Information Service (EU Commission), PVCROPS project [Online]. Available at https://cordis.europa.eu/project/rcn/105879_en.html (Accessed 3 August 2018).

[2] REDT Energy Storage, REDT 5-30 Specifications. [Online]. Available at http://www.camcocleanenergy.com/files/REDT%205-30%20-%20Specifications%20sheet.pdf (Accessed 3 August 2018).

[3] Z. G. Yang, Is this the ultimate grid battery?, IEEE Spectrum, vol. 54, pp. 36-41, November 2017.

[4] B. Li, J. Liu, Progress and directions in low-cost redox-flow batteries for large-scale energy storage, National Science Review, vol. 4, pp. 91–105, January 2017.

[5] PowerSonic rechargeable batteries, Sealed Lead-Acid Batteries Specifications [Online]. Available at http://www.power-sonic.com/ps_psg_series.php (Accessed 3 August 2018).

[6] T. Plack; R. Kloepsch.; S. Dühnen; M. Winter, Lithium ion, lithium metal, and alternative rechargeable battery technologies: The odyssey for high energy density, J. Solid State Electrochem, Vol. 21, pp. 1–26, 2017.

[7] Bruce Dunn, Haresh Kamath, Jean-Marie Tarascon, Electrical energy storage for the grid: A battery of choices, Science, Vol. 334, pp. 928-935, 2011.

[8] Scott B. Peterson, Jay Apt, J.F. Whitacre, Lithium-ion battery cell degradation resulting from realistic vehicle and vehicle-to-grid utilization, Journal of Power Sources, Vol. 195, pp. 2385-2392, 2010.

[9] Jianwu Wen, Yan Yu, and Chunhua Chen, A Review on Lithium-Ion Batteries Safety Issues: Existing Problems and Possible Solutions, Materials Express, Vol. 2, pp. 197-212, 2012.

[10] REDT Energy Storage, official website [Online]. Available at https://redtenergy.com (Accessed 4 August 2018).

[11] Ingeteam, official website [Online]. Available at https://www.ingeteam.com (Accessed 4 August 2018).

[12] LG Chem, RESU10 specifications sheet [Online]. Available at http://www.lgesspartner.com/front/normal/en/product/productInfo.dev (Accessed 4 August 2018).

[13] SMA, Sunny Island 3.0M/4.4M Datasheet [Online]. Available at https://www.sma.de/en/products/battery-inverters/sunny-island-30m-44m.html (Accessed 4 August 2018).

[14] A. Makibar, L. Narvarte Fernández, Characterization and Efficiency Test of a Li-ion Energy Storage System for PV Systems, European Photovoltaic Solar Energy Conference and Exhibition, pp. 1652 – 1658, 2015.

CHAPTER 4. Energy management strategies - implementation and rehearsal

4.1 Validation of the Energy Management Strategies

Two EMSs were tested in the microgrids: Self-Consumption Optimization and Constant Power Control. The self-consumption optimization strategy intends to maximize the self-consumption of the PV generated energy. The constant power control strategy aims at smoothing the power profile exchanged with the grid. It attenuates daily power fluctuations, meaning that surplus PV generation is stored during the day and used at night, hence partially maximizing self-consumption also. The constant power control will not be addressed in this thesis. It will be further developed and presented in a different thesis. The chosen test minimum period was one week, and it took place at the VRFB microgrid and the LIB microgrid at IES-UPM (Madrid), due to critical failures with the UEvora LIB, described in the previous chapter.

Further details about the VRFB microgrid tests and results are presented in the following paper.

4.2 Implementation and Validation of a Self-Consumption Maximization Energy Management Strategy in a Vanadium Redox Flow BIPV Demonstrator

Luis Fialho[1,2], Tomás Fartaria[1,2], Luis Narvarte[3] and Manuel Collares Pereira[1,2]

In Journal Energies, Vol. 9, pp 496, 2016.
http://dx.doi.org/10.3390/en9070496

Abstract

This paper presents the results of the implementation of a self-consumption maximization strategy tested in a real-scale Vanadium Redox Flow Battery (VRFB) (5 kW, 60 kWh) and Building Integrated Photovoltaics (BIPV) demonstrator (6.74 kWp). The tested energy management strategy aims to maximize the consumption of energy generated by a BIPV system through the usage of a battery. Whenever possible, the residual load is either stored in the battery to be used later or is supplied by the energy stored previously. The strategy was tested over seven days in a real-scale VRF battery to assess the validity of this battery to implement BIPV-focused energy management strategies. The results show that it was possible to obtain a self-consumption ratio of 100.0%, and that 75.6% of the energy consumed was provided by PV power. The VRFB was able to perform the strategy, although it was noticed that the available power (either to charge or discharge) varied with the state of charge.

[1] Renewable Energies Chair, Universidade de Évora, 7002-554 Évora, Portugal
[2] Instituto de Investigação e Formação Avançada (IIFA), Universidade de Évora, Palácio do Vimioso, Largo Marquês de Marialva, Apart. 94, 7002-554 Évora, Portugal
[3] Instituto de Energía Solar, Universidad Politécnica de Madrid, 28040 Madrid, Spain

Keywords

Vanadium redox flow battery; building integrated photovoltaics (BIPV); energy management strategy; self-consumption maximization; real-scale battery

Introduction

With the current increase of distributed renewable energies generators (such as rooftop photovoltaic power) in electrical grids, and more affordable energy storage systems (ESS), it is becoming much more viable to match individual demand for electricity with on-site photovoltaic (PV) production [1–3]. In the case of residential installations, the use of ESS for short-term management of supply—i.e., allowing the shift of PV energy to higher consumption periods (such as the evening peak or at night)—could increase self-consumed electricity from 30% to 70% [4–6].

To allow this increase, a battery must be integrated in the grid-connected PV system and an ad-hoc energy management strategy (EMS) must be implemented in a control unit that correctly manages the electricity flow between the PV generator, the battery, and the grid. In recent years, several EMSs focused on the maximization of the self-consumption of on-site-produced PV electricity have been presented [7–10], in which they assert that this strategy is useful and economically viable, even without feed-in-tariffs.

This EMS requires a reliable and efficient battery technology with a low power/energy ratio, such as the Vanadium Redox Flow Batteries (VRFB). This promising technology has as main advantages the decoupling of power and capacity, a very long lifetime (reported as above 10000 cycles, or 25 years of operation), very low maintenance, and deep discharge capability (almost 100.0%) [11]. Very few batteries of this kind exist in laboratories, especially at such a scale that allows real-life test conditions, so the investigation of these batteries is mostly done with simulations (and sometimes in small lab battery cells) [12,13]. In order to test the performance of this kind of EMS, a real-scale VRB demonstrator was built in the University of Évora, part of the FP7 PVCROPS European project [14]. This demonstrator consists of a PV generator of 6.74 kWp, a PV inverter of 10 kW, a battery inverter of 7.4 kW, and a VRFB of 60 kWh. The main objective of this paper is to present the results of the validation tests of the self-consumption energy management strategy mentioned above and to show its suitability for building integrated PV applications. Useful conclusions for the future operation of these kinds of systems are also discussed.

2. Real-Scale VRFB Demonstrator

The methodology used in this paper is based on the implementation of a real-scale demonstrator, installed at the University of Évora (Portugal). It consists of a rooftop mounted PV system (BIPV) and an electrical storage system (Vanadium Redox Flow battery), both connected to a building, which in turn is connected to the public electric grid (see Figure 1).

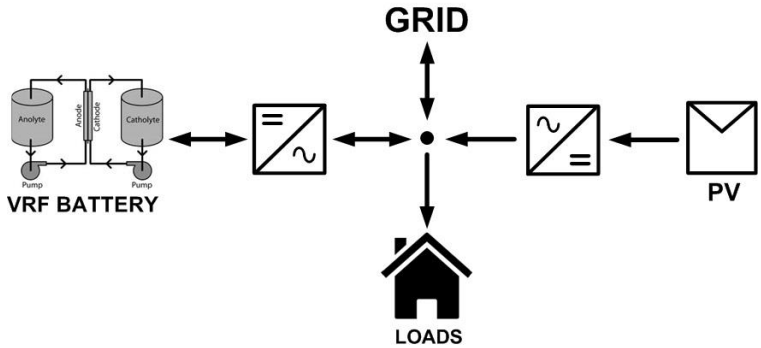

Figure 1. Demonstrator (photovoltaic (PV) plant and Vanadium Redox Flow battery (VRFB) with respective converters) simplified schematic. Inverters convert power from PV and battery (DC) to the grid (AC).

2.1. Equipment

The BIPV system is composed of two strings, a 3.24 kWp of monocrystalline PV panels and 3.5 kWp of polycrystalline cells, connected to a three-phase power inverter [15] with two independent maximum power point tracking (MPPT), connected to the building AC power grid. The energy storage is provided by a Vanadium Redox Flow Battery with 5 kW nominal power and 12 h storage [11], providing a total capacity of 60 kWh. The battery is also connected to the triphasic AC grid by three synchronized inverters (one per phase) [15]. Figure 2 shows the rooftop mounted PV system while Figure 3 shows the battery and four inverters (PV inverter in gray and the three battery inverters in green).
To operate the demonstrator, a control system was implemented using a PC with LabVIEW software to send and receive commands, and for overall system communication. This PC also acts as data logger to receive and store data. This PC receives data with parameter values from all the equipment (inverters, battery, and other sensors), runs the LabVIEW software with the EMS, and continuously ensures the operation safety. In addition, each equipment has its own safety measures and surveillance implemented.


Figure 2. Roof mounted PV system.

Figure 3. VRFB (right) and the inverters (left).

The main innovative feature of this demonstrator is the usage of a real-scale Vanadium Redox Flow Battery. Table 1 shows the main technical specifications of the VRFB installed in the demonstrator. Table 2 shows the three battery inverters specifications, and Table 3 shows the photovoltaic inverter manufacturer specifications.

In this battery, the electrolyte is stored in two tanks (for positive and negative species). The electrolyte is then pumped through the piping system to a stack of cells where the reduction–oxidation reaction occurs. The electron exchange takes place in cells (connected in series to constitute the stack) where a special ion membrane separates the two electrolytes and only permits H^+ and V^+ to pass.

The use of two tanks and a stack allows the decoupling of the battery power density (determined by the active area of the cells in the stack) from its energy density—i.e., the total energy that it can store (given by tank capacity and specific electrolyte energy density). This energy–power decoupling allows a battery to be tailored for many special cases, such as low power and large capacity (residential BIPV) or large power and lower capacity to mitigate power fluctuations (wind farms or PV plants). Another important feature of this battery technology is the absence of self-discharge, as there is no reaction outside the stack.

Table 2. VRFB technical specifications.

Specifications	**Value**
Manufacturer	REDT
Capacity	60 kWh (5 kW for 12 h)
Rated Power	5 kW
Maximum Operating Voltage	62 V
Minimum Operating Voltage	48 V
Electrical connection	Three-phase
Lifetime	+10,000 deep charge/discharge cycles
Full cycle (discharge/charge) Energy Efficiency	70%–80%

Table 3. Battery inverters technical specifications.

Specifications	Value
Manufacturer	Ingeteam
Model	EMS Home 2.4
DC Max Current	50 A
DC Operating Voltage Range	48 V–250 V
Rated AC Power	2.4 kW
Electrical connection	single-phase

Table 4. PV inverter technical specifications.

Specifications	Value
Manufacturer	Ingeteam
Model	3Play 12.5TL M
PV Power Range	12.9 kW–16.8 kW
DC Voltage Range MPPT1 and MPPT2	200 V–820 V
Rated Output AC Power	12.5 kW
Electrical connection	three-phase

Another distinct characteristic of this battery is the usage of vanadium as the main electrolyte element. The VRFB exploits the ability of vanadium to exist in four different oxidation states: from V^{2+} through V^{5+}, dissolved in sulfuric acid (H_2SO_4). It is used as the positive electrolyte (V^{5+}/V^{4+}) and as the negative electrolyte (V^{2+}/V^{3+}). The usage of only one element allows the restoration of the electrolyte by simply mixing both electrolytes (positive and negative) and then separating them again by recharging the battery. This process (electrochemical reversibility) makes the electrolyte virtually infinite and non-degradable. The only source of electrolyte degradation is the occurrence of a side reaction with elements in air. To avoid this unwanted reaction, the empty space in the electrolyte tanks is filled with a high purity inert gas (Argon).

As these batteries are mostly composed of plastic piping and tanks and as the electrolyte is isolated from air, its lifetime is longer than other technologies, reported as 10,000 cycles [11]). In addition, as previously referred to in the introduction, another important feature of this technology is that it allows very deep discharges (close to 100%), so the whole battery capacity can be used.

2.1.1. Determination of the State of Charge

The VRF battery installed in this demonstrator is equipped with a parallel electrolyte circuit that carries a small part of the electrolyte flow to just one external cell (called the reference cell) that is neither subjected to charge nor discharge. As this cell voltage is only affected by the real

electrolyte state, this cell voltage is the actual battery voltage in a rested state (not influenced by charge or discharge). In addition, the state of charge (SOC) is proportional to this voltage, so by knowing the reference cell voltage, one can obtain the real SOC.

The function relating SOC with reference cell voltage was obtained experimentally by the battery manufacturer. Figure 4 shows the SOC variation with the battery voltage (determined by the reference cell voltage multiplied by 40, as the stack is formed by 40 cells in series). In order to obtain the SOC value during the battery operation, this graphic was fit to Equation (1) so the SOC is computed using the reference cell voltage measurement. Equation (1) was defined as a piecewise function, computed as a numerical fit of the data within the operating ranges (from 41.8 V to 65.4 V), as no single function could be fitted properly. Each function was chosen as the one that yielded the best numerical fit for their respective ranges (R-Squared ≥ 0.99).

$$SOC(V) = \begin{cases} 0.0031V^4 - 0.5606V^3 + 37.848V^2 - 1136.7\text{V} + 12810, \text{ if } 41.8\text{V} < \text{V} \leq 52.4\text{V} \\ -0.1544V^3 + 25.961V^2 - 1443.4\text{V} + 26577, \text{ if } 52.4\text{V} < \text{V} \leq 58.8\text{V} \\ 0.0609V^3 - 11.88V^2 + 773.28\text{V} - 16694, \text{ if } 58.8\text{V} < \text{V} \leq 65.4\text{V} \end{cases} \quad (1)$$

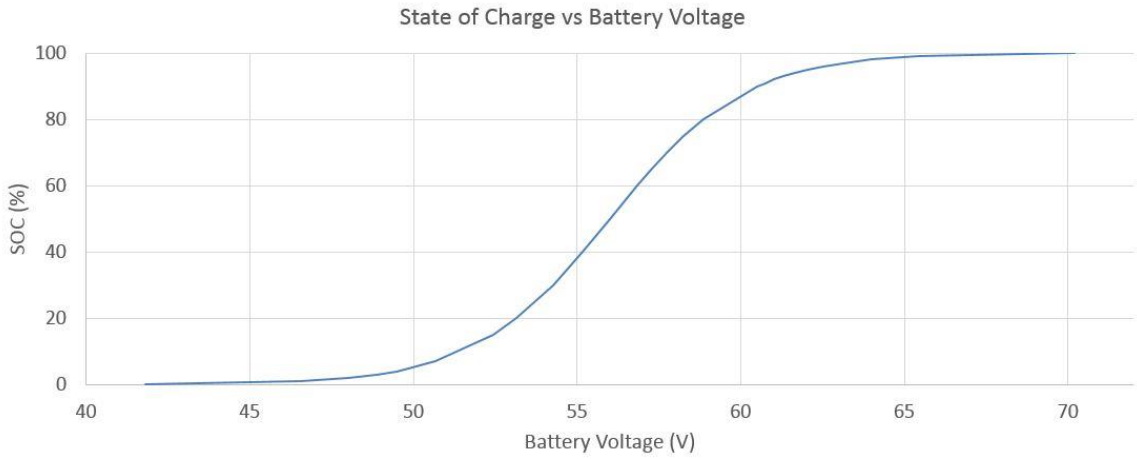

Figure 4. State of charge versus battery voltage. The battery voltage is determined by the voltage of the reference cell multiplied by 40, as the stack is formed by 40 cells in series.

2.2. Instrumentation and Data Acquisition

In order to properly implement an EMS, several parameters are measured, allowing the computation of useful variables that enable smooth system operation. Furthermore, to allow a more complete study of each piece of equipment, several additional measurements (other than critical variables already provided by the equipment) are necessary. Table 4 summarizes the monitored variables. For example, regarding the PV system, it is only necessary to know the AC Power given by the inverter. However, to evaluate the efficiency of the PV system or detect problems, more data is necessary (global radiation in the plane of the BIPV system, PV cells temperature, and wind speed). These measurements are made using a weather station on the roof consisting of a pyranometer, a temperature sensor, and an anemometer, as shown in Figure 5. These sensors are read and processed by a control electronics (arduino Leonardo

board), which in turn sends the data via a wireless zigbee network to another arduino connected to the main PC.

Figure 5. Pyranometer and anemometer installed on the roof.

The logged variables regarding the battery and inverters system are: DC power, AC power, battery voltage, current, and state of charge (SOC). Other useful variables are also read to ensure that the installation is healthy and operating within safe conditions (for example battery temperature, piping flow and pressure, electric grid parameters, and safe battery voltage range). The data is transmitted with Modbus protocol over TCP, via Ethernet. In order to obtain a more precise SOC value — it being a crucial parameter — an independent digital bench voltmeter was installed to the reference cell. This independent measurement allows a precision improvement from 0.7% (battery control measurement) to 0.1% (multimeter measurement) of the reference cell voltage. Furthermore, a three phase wattmeter (power analyzer) was installed to measure the power exchanged from the BIPV system and battery to the electric grid. In addition, three wattmeters were installed to obtain AC power measurements for each phase/ battery inverter.

Table 4. Monitored variables during the demonstrator operation. BIPV: Building Integrated Photovoltaics.

BIPV	PV inverter	Battery	Battery Inverter	Grid
Global Radiation	AC Voltage	Ref. Cell Voltage	AC Voltage	AC 3-phase Power
PV Cell temperature	AC Current	Temperature	AC Current	
DC Voltage	AC Power	DC Voltage	AC Power	
DC Current		DC Current		
DC Power		DC Power		

2.3. Electrical Loads

The loads used for the tests were simulated using the building to which the demonstrator is connected, as the consumption of all building loads is much larger than the power and capacity of the battery and PV system. The loads were simulated as being equally distributed by the three-phase electric grid. In this way, whenever a load is to be supplied, the power is sent to the building grid and that same power value is subtracted from the wattmeter measurement. This operation yields the power that would be exchanged with the grid if the loads were real and directly connected to the demonstrator. The load profile used is based on real 15 minute interval measurements made during a year of a real domestic installation [16]. This profile was then scaled according to the demonstrator specifications in order to provide a load profile level balanced to the system scale in what concerns battery usage and installed PV power. This method allows the loads to be of a suitable size relative to the real system specifications.

3. Self-Consumption Maximization Strategy

The strategy tested in the demonstrator was the self-consumption maximization strategy. The main objective of this EMS is to maximize the consumption of PV energy produced locally in the building, hence avoiding injecting energy to the electrical grid. This is achieved by giving priority to PV power and either storing the residual load (energy produced by PV system minus the energy consumed by loads) in an ESS or by taking energy stored previously. Thus, the only exceptional case in which there is an exchange of energy with the grid is when the battery can no longer absorb more energy or when the PV + battery system cannot provide enough energy to the required loads.

According to the regulation of certain countries (such as Spain, Germany, Portugal, South Africa, Puerto Rico, etc.), the feeding of PV power into the electrical grid is either forbidden or highly restricted, so it is necessary to take measures to avoid this situation [17–21]. Either the excess power should be curtailed—i.e., PV production is limited to a sub-optimal value to avoid producing more power than what is being consumed at the moment—or, ideally, the excess power would be either stored or used by some deferrable loads (for example, a water heater, washing machine, etc.) [16].

In countries where a feed-in tariff (FIT) is paid for renewable electrical energy, the use of a battery could help to maximize profit. It could ensure that no PV power is lost due to regulatory restrictions or technical problems (for example, a sudden power outage) and even delay the sale of energy to a time when it might be purchased at a higher value (such as during peak hours). In a stand-alone system or in one where no PV power is allowed to be sold to the electrical grid (or if the selling price is too low), the user can store the energy for later usage, lowering the necessity to buy electricity from the grid.

A flowchart of the self-consumption maximization strategy is presented in Figure 6. In the first step, the control system acquires data from PV production, loads consumption, and the battery state of charge (SOC). Then, it computes the difference between the loads consumption and PV production, referred to as residual load ($P_{residual}$). If the differential is positive, it means that current PV power is not enough to supply the loads. Hence, $P_{residual}$ is provided by the battery (if it has enough accumulated energy). If the battery cannot provide the total necessary power (due to a low SOC), the remainder has to be provided by the electric grid. The reverse happens when there is more PV power being generated than consumed in a given moment. In this case, the remainder should be stored in the battery. If the battery cannot absorb all of the excess

power (for instance, near maximum SOC), the remaining power must be fed to the grid (considering the case with no active loads management).

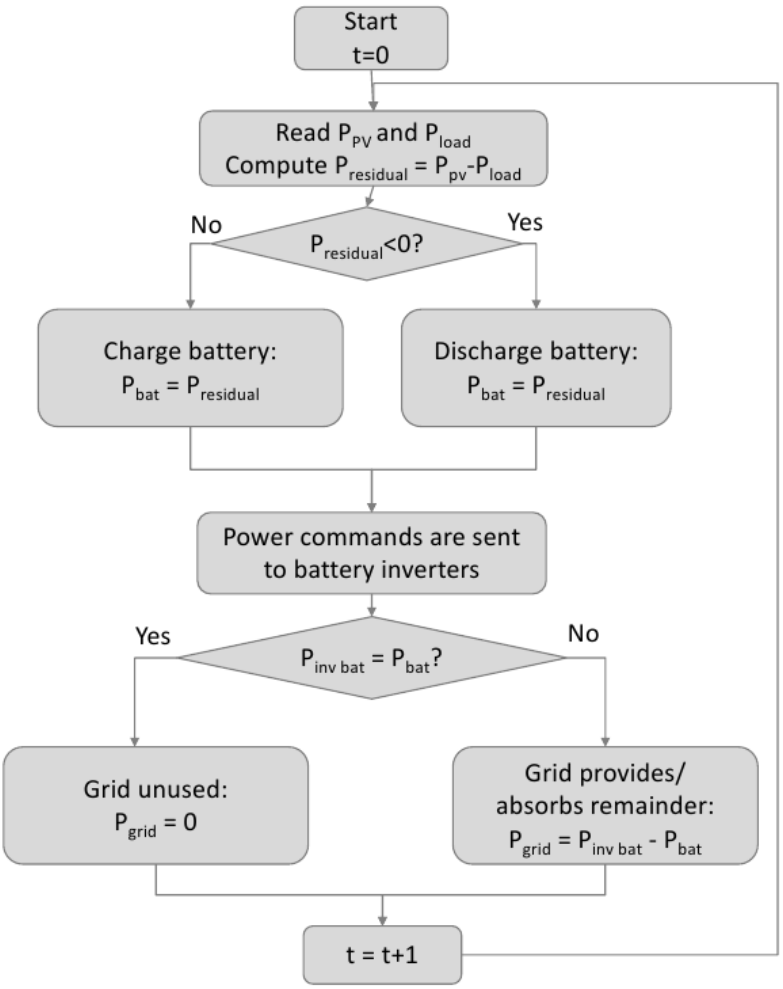

Figure 6. Flowchart of the self-consumption maximization strategy implemented in the demonstrator

This cycle should run at least every second to provide a quick response to any changes in PV production, consumption, or other situations (for example a blackout or a sudden problem in a piece of equipment). In this way, the grid is not largely affected by large fluctuations in PV production that could otherwise be fed to the electric grid with poor quality (high power variations in a short time).

With the proper implementation of this EMS, the benefits obtained should be: lower energy exchange with the public grid, higher self-consumed PV power, and a higher load supply with PV power (either directly or by the battery). In order to validate this EMS—tested in the real size VRFB demonstrator—the following merit factors were defined to quantify the obtained improvements: self-consumption ratio, maximum positive (from the grid), and negative (into the grid) peak grid power, respectively given by Equations (2) to (4).

$$\text{Self-consumption ratio} = \frac{\int_0^\infty \left(P_{PV}(t)+P_{grid}(t)\right)dt}{\int_0^\infty P_{loads}(t)\,dt} \quad (2)$$

Maximum Positive $P_{grid} = Max\{\overline{P_{grid\ 15min}}\}$ (3)

Maximum Negative $P_{grid} = Min\{\overline{P_{grid\ 15min}}\}$ (4)

and $\overline{P_{grid\ 15min}}$ is the average value for each 15 minute time interval, given by:

$$\overline{P_{grid\ 15min}} = \frac{1}{900}\sum_{0}^{900} P_{grid}(t) \quad (5)$$

where *t* is time in seconds.

4. Validation of the Self-Consumption Maximization Strategy in the VRFB Demonstrator

4.1. Testing Campaign

A testing campaign was carried out in the time frame of one week. It was considered a sensible duration for the EMS validation, representing a balance between a short-time test (one day) and a longer period—for instance, one month. Figure 7 shows fifteen minute averages of the main parameters (PV power, loads consumption, and power exchanged with the battery) recorded during the testing of the Self-Consumption Maximization strategy. Figure 8 shows the power exchanged with the battery and the power exchanged with the grid in the same time period.

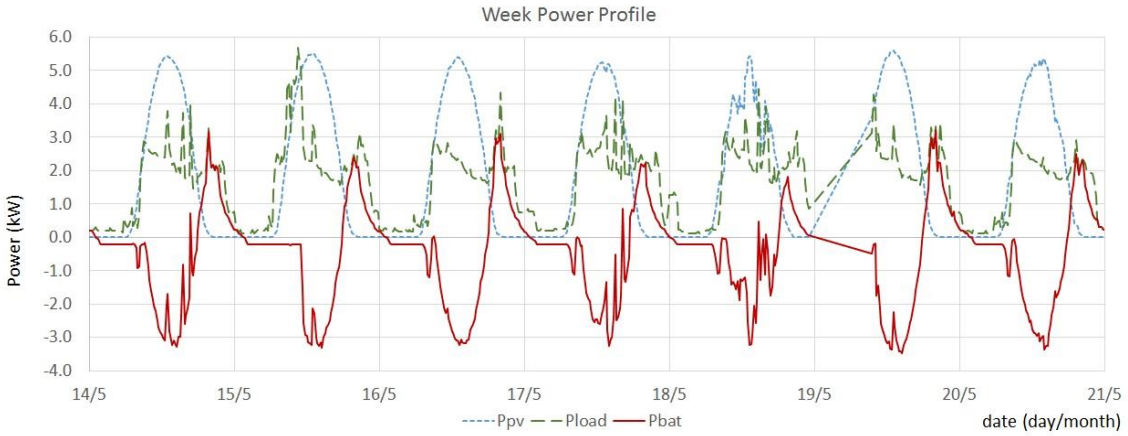

Figure 7. One week display of the PV, loads, and battery power profiles (P_{PV}, P_{load}, and P_{bat}, respectively).

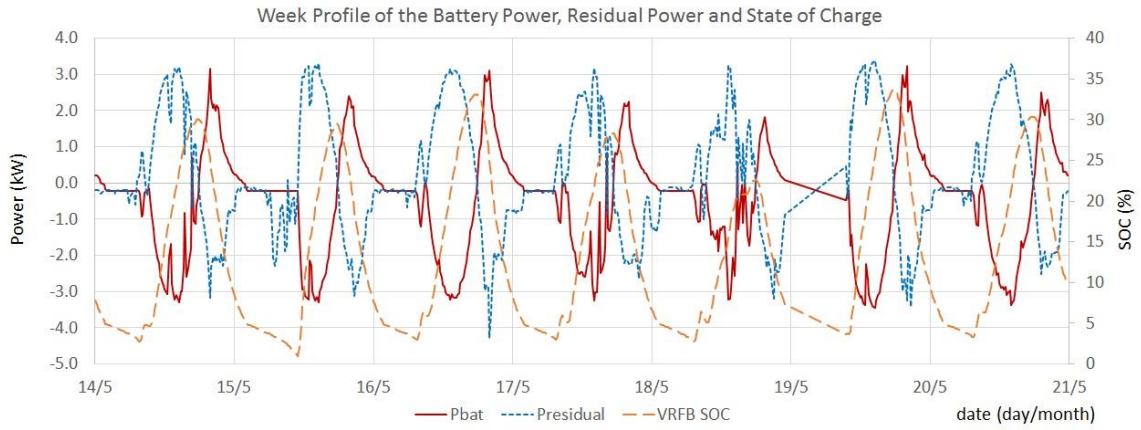

Figure 8. Variation of P_{bat}, $P_{residual}$, and state of charge (SOC), one week period.

Figure 9 shows the solar radiation on the PV plane (pyranometer) and PV cell temperature in the same time period.

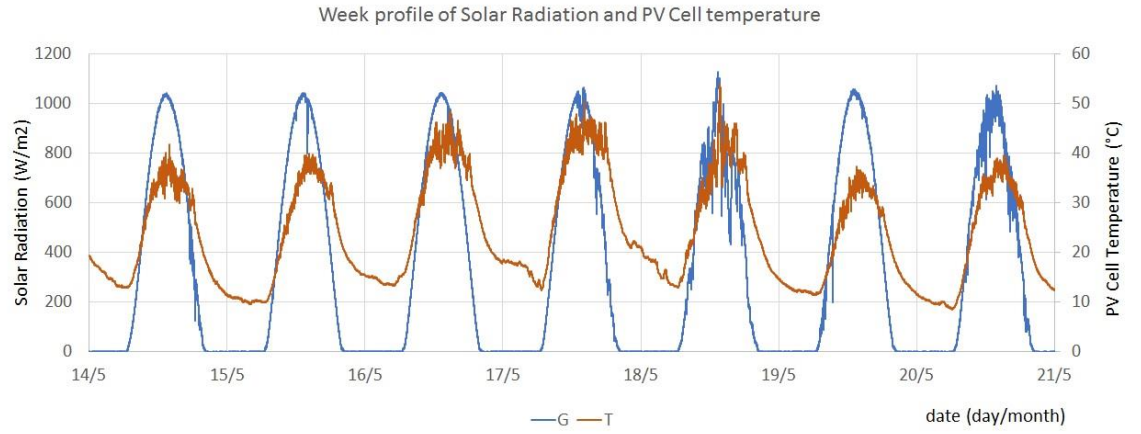

Figure 9. Week profile of Solar Radiation (PV plane) and PV Cell Temperature.

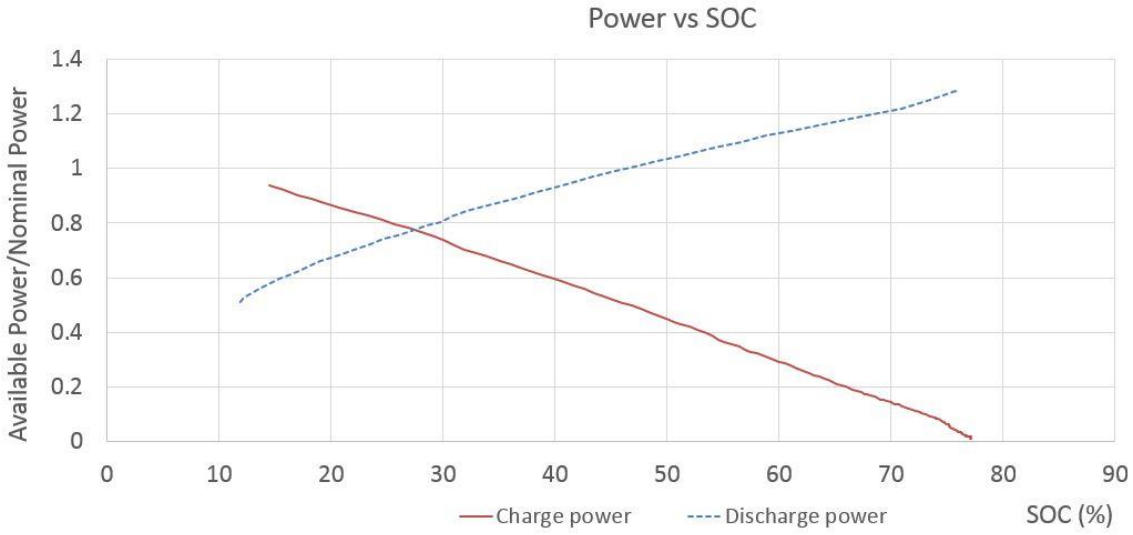

Figure 10. Variation of available discharge (blue) and charge (red) power, relative to the nominal power with the battery SOC.

From the graphics shown in Figures 7 and 9, the PV generation (blue dotted line in Figure 7) was mostly regular, with a clean radiation profile with only one day with significant variation (seen in Figure 9 on 18 May 2015). When the PV power is higher than the consumption, the remaining power (residual load positive) is stored in the battery (battery power is negative when charging). Usually, later in the day, when PV power is decreasing, the residual load (negative) is supplied by the battery.

However, when comparing Figure 7 with Figure 8, it can be seen that despite the energy stored in the battery being enough to supply the loads, the power that the battery could deliver was not enough. This is due to the ratio of power versus SOC not being constant throughout the major range of SOC. When the battery is partially discharged (lower SOC), the discharge power that it can provide is lower than the nominal power. The reverse situation occurs with the charge power when the battery is almost at full capacity (higher SOC), as shown in Figure 10.

Figures 11 and 12 show that, at the beginning, the residual load (blue line) began to be entirely supplied by the battery (red line). When the battery got below 5% of SOC (purple line), the loads had to be supplied by the grid, as below this value, the battery voltage gets close to the inverter minimum voltage range. To avoid this situation, a safety measure was implemented. In Figure 11, one can see that despite this safety measure, the battery SOC continued to fall, suggesting that the value used to charge the battery is not enough to overcome the consumption of the inverters and the battery internal losses.

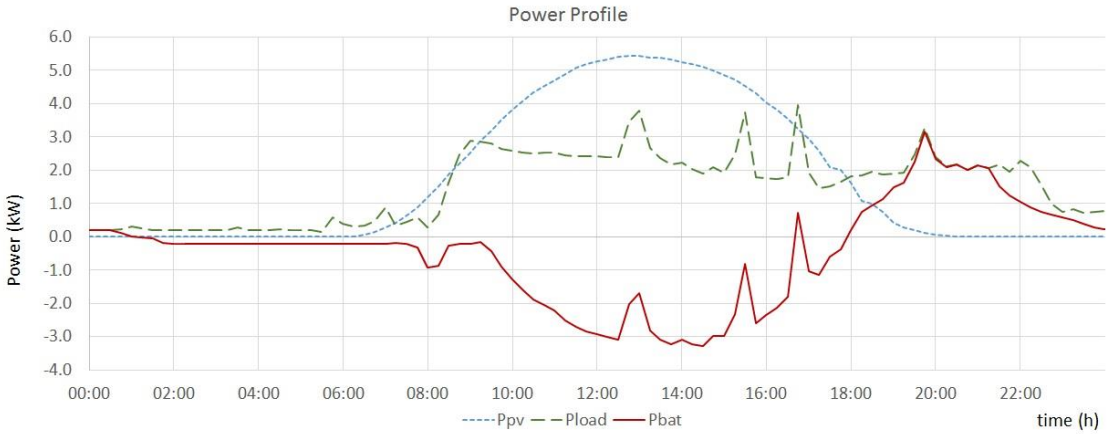

Figure 11. First day of the self-consumption maximization test.

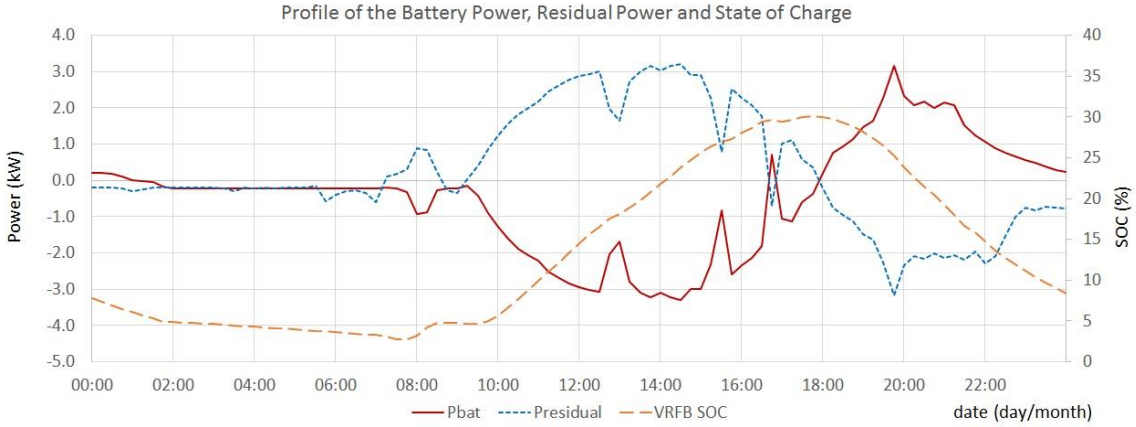

Figure 12. Display of the first day of the self-consumption maximization test.

When the PV power began to increase, the residual load also began to increase (positively), so the available power was used to charge the battery. At the end of the day, when PV power decreased, the previously stored energy was used to supply the loads. At the end of the day (after 21 h), some power had to come from the grid, as the battery could not entirely provide the necessary power to the evening load peak.

5. Results

To properly assess the validation and to quantify the self-consumption maximization performance, several merit factors were computed and compared with the case in which the demonstrator did not have an ESS.

Table 5 shows the comparison summary of the merit factors for the demonstrator with and without storage, evaluating the overall EMS performance for the testing period. Table 6 shows the merit factors computed for each day of the testing period.

In terms of total energy, the installation was able to self-consume 100.0% of the PV generation, and it was able to supply 75.6% of the total consumption. Hence, it was necessary to get 24.4% of the energy from the grid. The maximum peak power from the grid was 2.5 kW, without energy injection into the grid. Considering the demonstrator without storage, only 65.2% of the total energy generated by the PV system was self-consumed, and the peak power injected to the grid was 3.3 kW, while the peak power taken from the grid reached 4.2 kW.

To decrease the grid contribution, it is possible to increase the installed PV power or decrease the loads power consumption. In order to have a flexible demonstrator system, allowing the testing of different EMS that can require larger storage capacity, the total installed battery capacity ended up not being completely used in this test.

This occurrence hints at the opportunity to develop and implement strategies that can provide more benefits than an exclusively short-term or long-term EMS. The remaining unused battery capacity can be used as reserve power in case of an unforeseen blackout, to take advantage of electricity price fluctuations, to provide power to neighbour installations, or even to charge electric vehicles. Additionally, a higher available PV power could be stored in the battery for later use, decreasing the grid necessity. The extra capacity relative to the PV system size also raises the important question of how to optimize the battery capacity regarding PV generation and loads consumption.

Table 5. Comparison between the full demonstrator and a virtual one without storage.

Merit Factor	Storage	No Storage
Self-consumption ratio (%)	100.0	65.2
Maximum positive peak Pgrid (kW)	2.5	4.2
Maximum negative peak Pgrid (kW)	0.0	3.3

Table 6. Comparison between demonstrator results with and without storage.

Date		Self-Consumption Ratio (%)	Maximum Positive Peak P_{grid} (kW)	Maximum Negative Peak P_{grid} (kW)
14/05	storage	100.0	1.2	0.0

15/05	no storage	67.5	3.2	3.2
	storage	100.0	2.5	0.0
16/05	no storage	61.6	3.1	3.3
	storage	100.0	1.4	0.0
17/05	no storage	63.5	4.3	3.2
	storage	100.0	2.1	0.0
18/05	no storage	66.1	2.6	3.2
	storage	100.0	2.6	0.0
19/05	no storage	66.4	3.2	3.2
	storage	100.0	1.2	0.0
20/05	no storage	65.5	3.4	3.4
	storage	100.0	1.2	0.0
	no storage	66.9	2.5	3.3

This test yielded several useful results for the future operation of this technology demonstrators:

- The Vanadium Redox Flow technology has the ability to decouple power and capacity but the available power at extreme SOC varies. Figure 10 shows the variation of discharge (blue) and charge (red) power with the SOC. This fact also reveals the importance of analysing these systems as power sources/sinks and not only in terms of global energy.
- The system formed by the VFRB and inverters has achieved an overall average efficiency of 57.7% during the testing period. The efficiency is penalized by the battery operating voltage range being bellow the ideal voltage range of the inverters. The used inverters have a working voltage ranging from 48 V to 300 V, although their efficiency is higher at the top end of this range [15].
- The inverters consumption and battery internal losses are not entirely supplied during the safety procedure. Although the VRF battery is not damaged by an over-discharge, a voltage below the working range can turn the battery inverters off (the battery inverters are powered by the battery and require a minimum of 45 V), hence disturbing the normal operation of the installation.

6. Conclusions

The test results of the use of a VRFB as the storage system for the testing of a self-consumption maximization strategy, implemented in a real-size demonstrator, were presented. The results show that the VRFB is a suitable technology to be combined with BIPV systems.

Regarding the EMS testing, the strategy successfully maximized the consumption of locally-produced PV energy. Using the battery to store excess PV power (positive residual load), it was possible to completely avoid the injection of energy into the public electric grid—i.e., 100.0% self-consumption ratio. In addition, the total energy consumed by the loads was 75.6%, supplied by PV generation. A closer analysis of the system operation shows that an increase in PV power could further decrease the necessity of the electrical grid, as a large part of the battery capacity (approximately 65.0%) was unused.

The correct performance of the EMS is also shown by the reduction of power exchanged with the grid. The peak power from the grid was reduced in 59.0% in comparison with the case without energy storage. This means that the prosumer—apart from benefiting the whole

electrical system—not only reduces their electric bill due to the reduction of grid energy consumption, but also due to the reduction of the utility contracted power tariff.
This work also showed the relevance of the equipment operational limits (in this case, the battery inverters DC voltage range) to the EMS, and the non-negligible variation of available charge/discharge power with the battery SOC. In future developments of energy management strategies, all these operational limitations should be taken into account to ensure the proper and safe working mode of the whole system as planned.

Acknowledgments

The authors would like to acknowledge the support of this work, developed under the PVCROPS Project, which has received funding from the European Union's Seventh Framework Programme for research, technological development and demonstration under grant agreement n_308408.
This work was also supported by the Renewable Energies Chair of the University of Évora (PhD scholarship, author Luis Fialho) and by a PhD scholarship (author Tomás Fartaria) from FCT – Fundação para a Ciência e Tecnologia, Portugal, Grant number SFRH/BD/84396/2012.
The authors also would like to acknowledge the support of the European Commission OPENAIRE FP7 Post-Grant Open Access Pilot for supporting the publication of this work.

References

1. Richter, N. Is Rooftop Solar Finally Good Enough to Disrupt the Grid? 2015. Available online: https://hbr.org/2015/05/is-rooftop-solar-finally-good-enough-to-disrupt-the-grid (accessed on 11 April 2016).
2. Feldman, D.; Barbose, G.; Margolis, R.; James, T.; Weaver, S.; Darghouth, D.; Fu, R.; Davidson, C.; Booth, S.; Wiser, R. Photovoltaic System Pricing Trends: Historical, Recent, and Near-Term Projections. 2014. Available online: http://www.nrel.gov/docs/fy14osti/62558.pdf (accessed on 11 April 2016).
3. International Energy Agency (IEA). Global EV outlook: Understanding the electric vehicle landscape to 2020. 2013. Available online: http://www.iea.org/publications/globalevoutlook_2013.pdf (accessed on 11 April 2016).
4. Rickerson, W.; Couture, T.; Barbose, G.L.; Jacobs, D.; Parkinson, G.; Chessin, E.; Belden, A.; Wilson, H.; Barrett, H. Residential Prosumers-Drivers and Policy Options (Re-Prosumers). 2014. Available online: http://iea-retd.org/wp-content/uploads/2014/06/RE-PROSUMERS_IEA-RETD_2014.pdf (accessed on 11 April 2016).
5. Solar Power Europe. Global Market Outlook, For Solar Power 2015–2019. Available online: http://www. solarpowereurope.org/insights/global-market-outlook (accessed on 11 April 2016).
6. Vrettos, E.; Witzig, A.; Kurmann, R.; Koch, S.; Andersson, G. Maximizing local PV utilization using small-scale batteries and flexible thermal loads. 2013. Available online: http://www.eeh.ee.ethz.ch/uploads/tx_ethpublications/Vrettos_etal_2013.pdf (accessed on 11 April 2016).

7. Zaheeruddin; Manas, M. Renewable energy management through microgrid central controller design: An approach to integrate solar, wind and biomass with battery. Energy Rep. 2015, 1, 156–163.
8. Merei, G.; Moshövel, J.; Magnor, D.; Sauer, D.U. Optimization of self-consumption and techno-economic analysis of PV-battery systems in commercial applications. Appl. Energy 2016, 168, 171–178.
9. Lang,T.; Ammann, D.; Girod, B. Profitability in absence of subsidies: A techno-economic analysis of rooftop photovoltaic self-consumption in residential and commercial buildings. Renew. Energy. 2016, 87, 77–87.
10. Pascual, J.; Barricarte, J.; Sanchis, P.; Marroyoa, L. Energy management strategy for a renewable-based residential microgrid with generation and demand forecasting. Appl. Energy 2015, 158, 12–25.
11. Renewable Energies Dynamics Technology Ltd. PVCROPS case study. Available online: http://www.redtenergy.com/case-studies/energy-storage-80kwh (accessed on 11 April 2016).
12. Sum, E.; Rychcik, M.; Skyllas-kazacos, M. Investigation of the V(V)/V(IV) system for use in the positive half-cell of a redox battery. J. Power Sources 1985, 16, 85–95.
13. Rychcik, M.; Skyllas-Kazacos, M. Characteristics of a new all-vanadium redox flow battery. J. Power Sources 1988, 22, 59-67.
14. PVCROPS. Available online: http://www.pvcrops.eu (accessed on 11 April 2016).
15. Ingeteam. Available online: http://www.ingeteam.com (accessed on 11 April 2016).
16. Pascual, J.; Sanchis, P.; Marroyo, L. Implementation and Control of a Residential Electrothermal Microgrid Based on Renewable Energies, a Hybrid Storage System and Demand Side Management. Energies 2014, 7, 210–237.
17. Puerto Rico Electric Power Authority (PREPA). Minimum Technical Requirements for Photovoltaic Generation (PV) Projects. 2012. Available online: http://www.nrel.gov/docs/fy14osti/57089.pdf (accessed on 23 June 2016).
18. Red Electrica de España, Instalaciones conectadas a la red de transporte: requisitos mínimos de diseño, equipamiento, funcionamiento y seguridad y puesta en servicio. 2005. Available online: http://www.ree.es/sites/default/files/01_ACTIVIDADES/Documentos/ProcedimientosOperacion/PO_resol_11feb2005.pdf (accessed on 23 June 2016).
19. Republic of South Africa Grid Code Secretariat (NERSA), Grid connection code for renewable power plants (RPPs) connected to the electricity transmission system (TS) or the distribution system (DS) in South Africa. 2012. Available online: http://www.nersa.org.za/Admin/Document/Editor/file/Electricity/TechnicalStandards/South%20African%20Grid%20Code%20Requirements%20for%20Renewable%20Power%20Plants%20-%20Vesion%202%206.pdf (accessed on 23 June 2016).
20. Bundesverband der Energie (BDEW). Technical Guideline Generating Plants Connected to the Medium-Voltage Network: Guideline for generating plants connection to and parallel operation with the medium-voltage network. 2008. Available online: https://www.bdew.de/internet.nsf/id/A2A0475F2FAE8F44C12578300047C92F/protect\T1\textdollarfile/BDEW_RL_EA-am-MS-Netz_engl. pdf (accessed on 23 June 2016).

21. Ministério do Ambiente, Ordenamento do Território e Energia, Governo de Portugal, Decreto Lei n.º 153/2014. 2014. Available online: http://www.legislacao.org/primeira-serie/decreto-lei-no-153-2014-306472 (accessed on 23 June 2016).

Self-Consumption Optimization Strategy in the Lithium-Ion Battery

Figure 28 and Figure 29 show two representative days of testing this strategy in the LIB demonstrator. In the beginning of the day, as no PV power (blue line) is generated, the loads (orange line) are supplied by the stored energy of the battery (green line). When the PV power increases, the EMS control sends the command to the battery inverters (grey line) to take the excess power (PV-loads) and store it in the battery. When the battery reaches full capacity, it stops charging. This algorithm enables providing the needed power to the loads, even when the PV production is not enough or unavailable (nigh time) or with consumption power peaks. The battery is able to provide the necessary energy, reducing the necessity to buy/inject energy from the public electrical grid. This occurs at sunset with PV power gradually diminishing and power supplied from the battery increase completely matching the consumption needs.

As expected, battery available power (charge or discharge) depends on the actual SOC, i.e., operating near the upper/lower SOC limits the available charge/discharge power, respectively. This relation SOC - available battery power relation needs to be foreseen and programmed in any EMS. The effects of this can be seen on Figure 28 around the 13th and 37th hours, when the power command sent to the battery (P_{setBat}) is not fulfilled by the inverters/battery.

The sign convention used for power/energy in all microgrids, control algorithms, monitoring equipment, EMS, programming and data analysis is to consider positive the energy flowing towards the loads and negative in the reverse direction.

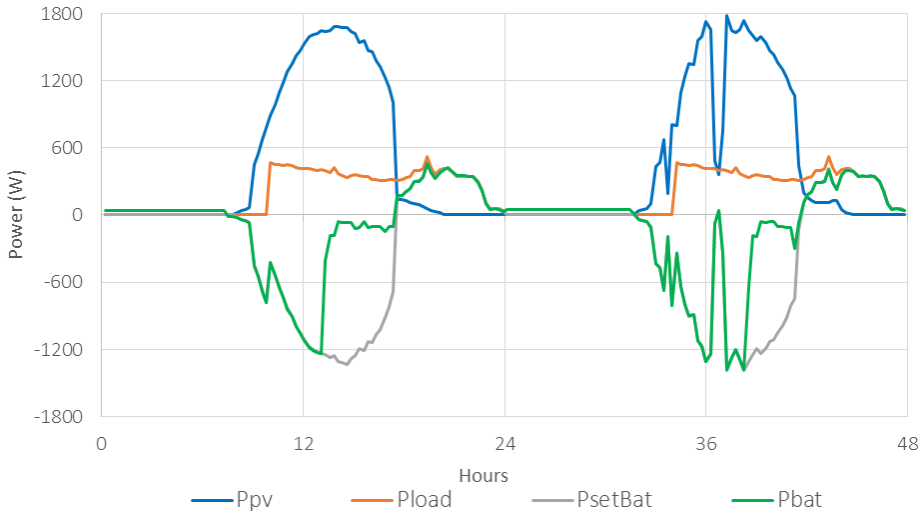

Figure 28: Graphic of a two-day period of the Self-Consumption Optimization strategy run in the LIB microgrid.

Figure 28 legend: *Blue line - PV power; Orange line - loads consumption; Grey line - power command sent to the battery inverters; and Green line – power exchanged with the battery inverters.*

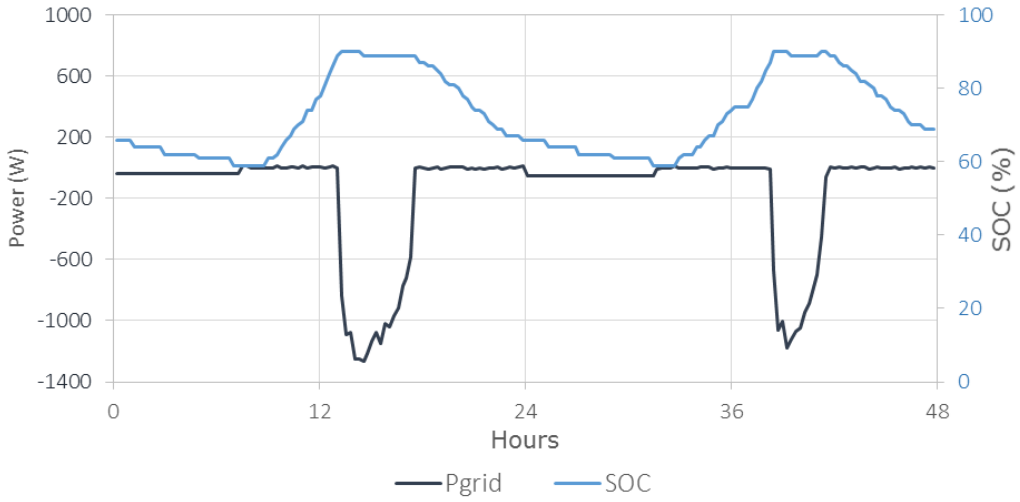

Figure 29: Graphic of a two-day period of the Self-Consumption Optimization strategy run in the LIB microgrid.

Figure 29 legend: *Grey line – power exchanged with the grid (negative stands for injection into grid and positive taken from the grid); and Blue line – battery SOC.*

The self-consumption optimization strategy was successfully tested in the LIB microgrid, since it is clear the very low power exchange from and to the grid. Very small differences occurred due to small mismatch between the power commands sent to the battery inverters and the actual power delivered, as some delay of the measuring equipment data acquisition. The EMS failed to comply when operating near the SOC limits, being impossible to absorb or inject at given moments. This limitation was identified, and it should be adequately solved with further development of the EMS algorithm, in order to take into account this additional technical constraint.

Apart from these periods, the power exchange with the grid was very low (below 100 W) in all the tests period. Figure 30 show a longer test period with the same EMS in the LIB microgrid.

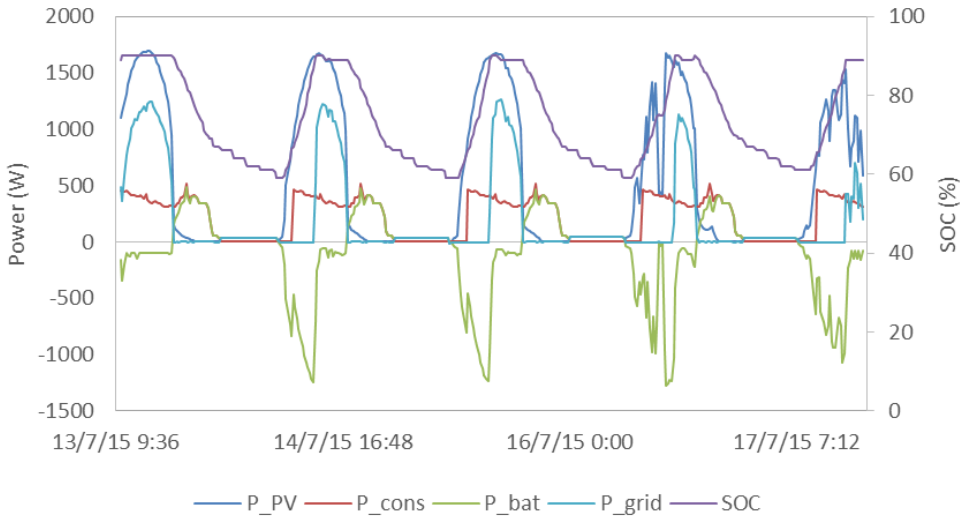

Figure 30. Self-consumption optimization results on the LIB microgrid.

This EMS was also validated in the VRFB microgrid and detailed results are presented in the following paper in this chapter.

Looking at the merit factors in the next table, it can be observed how, thanks to this strategy, little power is taken from the grid. As a result, also power fluctuations have been reduced. Due to the smaller battery capacity available at the IES-UPM microgrid, it was undersized in relation with load consumption needs and PV generation. Having a smaller capacity than the originally planned battery for these tests (UEvora Cegasa battery) it reached faster the upper SOC limit, forcing the injection of surplus PV energy into the grid, instead of storing it. In this case, the available battery operational limits partially impaired the EMS performance.

Table 5: Merit factors for both demonstrators performing the strategy. Absolute values, and reduction relative to the net power (%).

Merit factors	LIB	VRFB
Maximum Power from grid (P+)	0.011 kW (98 %)	2.506 kW (42 %)
Maximum Power to grid (P-)	1.266 kW (6 %)	0.049 kW (99 %)

Two microgrids have been implemented at the University of Évora for testing. Each microgrid is associated with a type of energy storage system. The energy management strategies developed were successfully tested and validated in real conditions. Some constraints were identified and will need to be addressed in future research to fine tune the implementation of EMS.

CHAPTER 5. Conclusions

5.1 Conclusions

Increasingly, the share of renewables in the upcoming years can lead to the necessary reduction of emissions and, combined with energy efficiency actions, the rise of global average temperature could and should be kept below 2°C, the widely recognised target to prevent catastrophic climate change.

The cost of solar technologies has been steadily declining, mainly due to the cumulative experience effects, improvements in technologies and economies of scale/production. The growth of photovoltaic systems present challenges to the research and development that should be addressed and properly solved.

The broad topic of this thesis was by itself a challenge, forcing the necessary focus and planning in specific topics, but also letting outcomes to be sometimes conducting the research for next step. There are still potential matters to address but the time and resources management imposed the selection of themes and results presented.

This chapter presents the overall conclusions as more in depth conclusions are found in the papers and posters of this thesis.

This thesis intended to address several challenges posed by the current state of the art regarding the simulation, modelling and validating of several elements of a modern PV system, such as the PV conversion (PV module), the power electronic converters, the energy storage and the system control and management. In order to understand the complete system, it was necessary to first understand the operation of single elements. Several models were presented allowing the accurate simulation of the PV conversion trough a PV module, modelling its I-V curve starting from limited data. These models' results are presented in the papers of Chapter 2. The initial model was further developed and also integrated with the modelling of the power electronic converters, firstly the two level and secondly the three-level converter, injecting into the grid. All these models were validated and presented the ability to replicate accurately real observations and results. The programming language used for the simulations was MATLAB, enabling easy and fast future updating and integration with other models with low implementation and computation cost.

In the framework of PVCROPS (a 7th FP project), two real-scale microgrids with ESS were designed, installed and used to answer several questions in this thesis. They provided real demonstrators and allowed the trial and rehearsal of energy management strategies, characterization of different ESSs and innovative equipments. These systems were implemented in collaboration with the companies that design and manufacture batteries, inverters and Energy Management Systems and has yield highly valuable feedback between partners and consequent important results. As expected due to innovative level of both ESSs several faults and technical issues have arose but were promptly overcome with very positive results and contributed to the evolution of commercial ready products.

The EMS proved to work in a simulation environment, and finally it has been proven that its output can be used to design and run real battery-based BIPV systems with successful outcomes. Some small constraints were detected but can be quickly solved in future work. The deployment of these two microgrids provided UEvora with a on field, fully prepared, experimental laboratory, enhancing the research already developed in these subjects and they are now truly unique infra-structures in Portugal.

Regarding the lithium-ion battery, a workaround was used, and the characterization and validation tests were carried out in a partner institution with a similar LIB. In any case, this unfortunate situation reflected the risky experience that can take place with a rapidly evolving global market with innovative and truly competitive products where manufacturers can fail and be replaced the next day.

The work developed also allowed the identification of research limitations and further research should be conducted on the referred topics, enabling richer and broader answers to the issues of this thesis. The formulation of key questions for future research is covered in the next chapter.

In conclusion the author expect that this thesis and the work presented will be helpful for those pursuing design, simulation and performance assessment of BIPV systems integrated with energy storage systems and the grid. The transition for a renewable energy powered world is inevitable. The introduction of diverse renewable energy sources for a flexible, reliable and resilient electric grid can be achieved with energy storage technologies and smart management, becoming the next renewable energy revolution.

CHAPTER 6. Future Research Lines

6.1 Future research lines

Throughout the work developed for this thesis many more questions emerged, pointing out to the need for new models, new experimental validation tests or even new alternative ideas, as well as innovative fields of research with great potential, yet to be developed. Many new ideas came up but were left in standby mainly due to time constraints. Further in-depth and more complete models will be developed and validated in future works. This PhD thesis was faced as starting point, not as a closed work, but rather the beginning of more and better research on the path to sustainability and application of solar energy systems.

As of 2018, solar power demand is growing and will grow very strong in Europe over the next few years [1]. In June 2018, the European Union agreed in raising its target for the amount of energy it consumes from renewable sources, the European energy ministers agreed a binding renewable energy target of 32% by 2030 [2]. This deal also includes a chapter, intitled by the European Parliament, as *The Renewable Self-Consumer Era*, where according to the provisional deal, member states must ensure that an EU consumer is entitled to become a renewable self-consumer. It will allow each EU consumer to generate renewable energy for their own consumption, store and sell excess production without any charge or fee on self-consumed energy.

Concerning self-consumption, solar energy it is now much cheaper than retail electricity in most European markets and will quickly continue to reduce its cost. This will be a driver to invest in onsite distributed power generation and, in developed European countries, end-users start to understand that it can be a smart investment even without feed-in tariffs or other subsidies.

Portugal also has seen in the end of 2017 the commissioning of its first commercial solar PV plant (Montes Novos, 4.1MWp) without feed-in tariffs or other subsidy programmes, and in 2018 the first big size PV plant (Ourika, 46MWp) selling energy to the grid at Iberian market prices [3].

Solar PV module prices are steadily decreasing and are predicted to decrease as far as 35% [4] in 2018 due to the Chinese government curtailing solar growth through new policies initiated in the 1st of June. China, being the world's largest solar market, will put the PV industry probably facing a global oversupply and a consequent further price drop.

With a similar downward trend, battery energy storage has a quickly falling cost. In the residential market, many consumers in some European countries prefer to have better control over their energy bill, combined with the benefits of digital and smart energy products. This leads to increasing sales of this solar plus storage technologies. In smaller European markets such as Portugal, this evolution is still further behind, but it is seen as inevitable.

Research and Development topics on battery energy storage have excellent future prospects and research needs to explore and solve pending issues in order to optimize and

improve their integration, control, efficiency, safety, cost, etc. It is necessary to do further technical and economic simulations of different self-consumption schemes considering different scenarios and frameworks. Different generation and storage technologies, demand side response, operating strategies, consumption patterns, electrical tariffs, etc., should be simulated and validated experimentally with the existing facilities, if possible. Innovative self-consumption schemes, as collective self-consumption, should also be simulated to evaluate the opportunities of electricity sharing among prosumers. Apart from this behind-the-meter strategies, different energy management strategies should be developed to seamlessly integrate in the grid the increasing renewable energy production, the new electric vehicles market, their charging stations or smart vehicle to grid (V2G) technologies. Hybrid storage technology (for instance: VRFB + Lithium Ion batteries) should also be subject of research, developing appropriate control strategies to take into account each technology strengths and weaknesses and achieve better results as far as overall efficiency, lifetime, cost, etc.

During the work of this thesis, the European PVCROPS project was completed, which gave rise to the installation of the first two microgrids with energy storage at the University of Évora. Other R&D projects had their kick-off, already with my active involvement from the initial application/idea stage up to the research/execution phase, for example:

MASLOWATEN (H2020) – focused on research, development and demonstration of systems for high power photovoltaic pumping or irrigation. [5]

GRECO (H2020) - boosting the photovoltaic research with open science tools, open data, open access and citizen science. [6]

AGERAR (Interreg POCTEP) – to promote energy efficiency and sustainability criteria in residential and commercial microgrids, increasing and improving the usage of energy storage and IT technologies. [7]

PEARLPV (CostAction) – to improve the energy performance and reliability of photovoltaic (PV) solar energy systems in Europe leading to lower costs of electricity produced by PV systems by a higher energy yield, a longer life time eventually beyond the guaranteed 20 years as specified by manufacturers, and a reduction in the perceived risk in investments in PV projects. [8]

Simultaneously, the Renewable Energies Chair experimental infrastructure is growing and being improved. A new lithium-ion battery ($LiNiMnCoO_2$) with 9.8kWh of capacity and its inverter were installed and integrated in the microgrid with the previous LIB. Further expansion of the infrastructure storage capabilities is also ongoing with the acquisition processes for different storage technologies such as a sodium nickel chloride battery (molten salt battery). Auxiliary equipments were also upgraded and each microgrid is now supported by a 15 kVA UPS, enabling full uninterrupted operation.

The monitoring hardware was also improved and a full electrical real time characterization (DC and AC) is now possible, fully integrated with the control and monitoring software (developed in-house). This LabVIEW software is constantly evolving, currently being able to control and data log all the equipments and monitoring hardware systems in the microgrids with remote real time control accessibility. New scientific and diagnostic tools are

now available such as a precision IV tracer, thermographic camera, multichannel dataloggers, an unmanned aerial vehicle (UAV-drone) for PV inspection and monitoring, electroluminescence equipment, etc. All this new and updated scientific tools will allow to pursue new research lines, perform rehearsals and fast prototyping with new collaboration work with other institutions and researchers.

An interesting field of research, with work already under way, is the research and development of precision low cost equipment with IoT (internet of things) capabilities for PV applications. The first version of a low-cost IV tracer is now operational and validated experimentally with high evolutive potential. It will allow permanent on field real-time IV tracing and, therefore, improved monitoring of PV plants, being part of a network of physical devices embedded with electronics, software, sensors, and connectivity enabling to connect and exchange data.

A recent research field has also emerged for solar energy systems: floating photovoltaic plants. It is still an application with little state-of-the-art experience and reduced installed capacity worldwide. It presents some clear advantages: installation where the land is a premium commodity or is not available, potentially fewer obstacles to block sunlight and potential higher energy generation efficiency due to the lower temperature underneath the panels. Additionally, the aquatic environment benefits due to the solar plant shading preventing water evaporation and probably limiting algae growth (eutrophication) and thus potentially improving water quality. This gave rise to the opportunity to design technical specifications, study and monitor in the near future floating PV plants in Portugal [9], deepening the knowledge and studying their real impacts and performance as well as an in-depth study of all the particular characteristics related to the commissioning and operation in an aquatic environment.

Another active research field it will take place with the GRECO project [6], following the research done within the MASLOWATEN project [5] and it is focused on the water-energy nexus, in particular in high power photovoltaic pumping. A large potential market [10] is estimated for this solution, lowering the energy costs and carbon footprint of the agriculture sector. Some milestones have already been achieved as cloud passing resilience trough advanced control algorithms or fully operational real scale demonstrators in the previous work but still presents a wide range of exciting potential research areas.

As for the PV modules field the challenges are as daunting as ever, but the opportunities are equally boundless. As the PV energy generation becomes mainstream and the global installed capacity increases, the aging of existing plants presents new challenges regarding on field repairs, quality control and recycling. The scaling up of a wide range of available PV technologies (silicon, CIGS, CdTe, GaAs, perovskites, etc.) present by itself a lifetime research topic on these issues.

Batteries are and will also evolve at high speed, both in energy density, safety and cost. Membrane technology for VRFB and LIB is evolving fast. Portugal is very well positioned in the present race, with new technology for flow batteries (FEUP)[11] and with the biggest European raw materials availability (Lithium)[12].

References

[1] SolarPower Europe (2018), Global Market Outlook for Solar Power 2018 – 2022.

[2] European Parliament, 14th June 2018, Press Release, [Online]. Available at http://www.europarl.europa.eu/news/en/press-room/20180614IPR05810/energy-new-target-of-32-from-renewables-by-2030-agreed-by-meps-and-ministers (Accessed 31 July 2018).

[3] MIBEL – Mercado Ibérico de Electricidade, [Online]. Available at http://www.mibel.com (Accessed 31 July 2018).

[4] Bloomberg New Energy Finance (2018), Chinese Burn Will Only Make the Solar Industry Stronger [Online]. Available at https://www.bloomberg.com/view/articles/2018-06-05/chinese-burn-only-makes-the-solar-industry-stronger (Accessed 31 July 2018).

[5] MASLOWATEN project, received funding from the European Union's 2020 Research and Innovation Programme under grant agreement n. 40771, [Online]. Available at http://maslowaten.eu (Accessed 31 July 2018).

[6] GRECO project, received funding from the European Union's 2020 Research and Innovation Programme under grant agreement n. 787289, [Online]. Available at https://www.greco-project.eu (Accessed 31 July 2018).

[7] AGERAR project, received funding from INTERREG Espana-Portugal Programme, European Fund for Regional Development under operation n. 0076_AGERAR_6_E, [Online]. Available at http://institucional.us.es/agerar/pt (Accessed 31 July 2018).

[8] PEARLPV Cost Action, CA 16235, which is supported by COST (European Cooperation in Science and Technology), a funding agency for innovation and research networks [Online]. Available at https://www.pearlpv-cost.eu (Accessed 31 July 2018).

[9] Jornal Económico, Alqueva: energia solar para poupar até 40%, [Online]. Available at http://www.jornaleconomico.sapo.pt/noticias/alqueva-energia-solar-para-poupar-ate-40-300160 (Accessed 1 August 2018).

[10] L. Narvarte, J. Fernández-Ramos, F. Martínez-Moreno, L.M. Carrasco, R.H. Almeida, I.B. Carrêlo, Solutions for adapting photovoltaics to large power irrigation systems for agriculture, Sustainable Energy Technologies and Assessments, Vol. 29, pp. 119-130, October 2018.

[11] Project SunStorage website, [Online]. Available at http://sunstorage.pt/project (Accessed 27 August 2018).

[12] Diário de Notícias, Portugal pode ser o primeiro produtor europeu de lítio, [Online]. Available at https://www.dn.pt/dinheiro/interior/portugal-pode-ser-o-primeiro-produtor-europeu-de-litio-9302108.html (Accessed 27 August 2018).

Annexes

Scientific posters presented at EUPVSEC 2015

Validation of a Energy Management Strategy for a BIPV System with a Lithium Ion Battery Demonstrator

Luis Fialho[1], Tomás Fartaria[1], Manuel Collares Pereira[1] , Aitor Makibar[2]
[1] ST Renewable Energies Chair, Universidade de Évora, Portugal
[2] Instituto de Energía Solar, Universidad Politécnica de Madrid, Spain

BIPV System Demonstrator

Lithium Ion Battery:

- 5kW nominal power
- 31.8kWh capacity
- 302.4 V Vmax / 194.4 V Vmin
- 5C (200A) max discharge
- 3C (120A) max charge

Battery Inverter: 5kW nominal power

PV installation: 3.224 kWp (a-Si)

PV inverter: 5kW nominal power

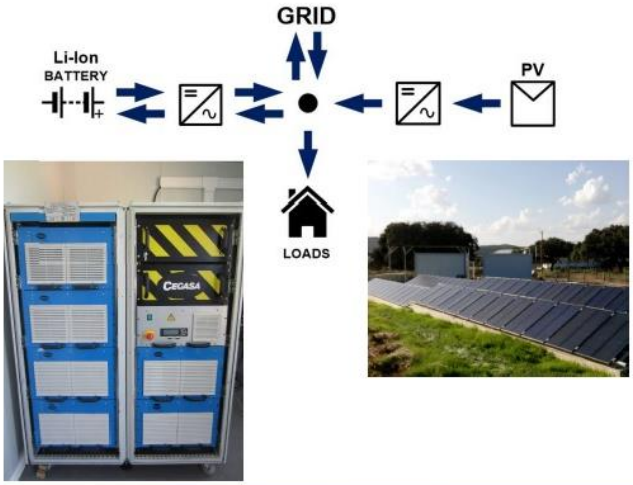

Self Consumption Optimization Strategy

General Objective:
Study of grid interface in rooftop PV systems with energy storage.
The specific objective for this energy strategy is to maximize the consumption of locally produced PV power, hence minimizing the injection of power into the electrical grid.

Implementation:

$P_{setBat} = P_{pv} - P_{load}$

$P_{grid} = P_{setBat} - P_{bat}$

Due to battery operational limits (voltage and SOC), a control to avoid overdischarge/charge was implemented.

Conclusions:
Within the battery operational SOC limits the strategy achieved a minimized peak power (50W) exchange with the grid.

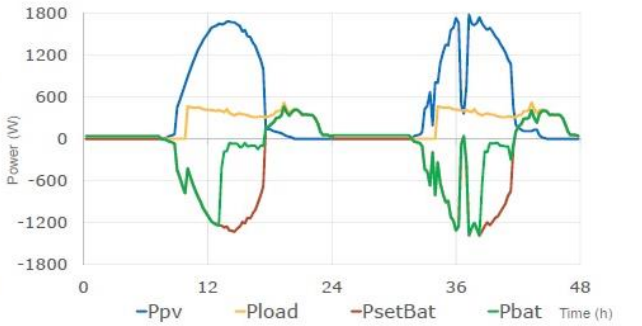

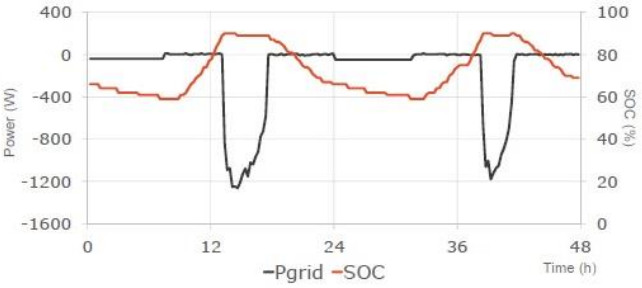

P_{setBat}	AC Power command to battery inverters
P_{pv}	PV AC power
P_{load}	Loads AC power consumption
P_{grid}	AC Power exchange with the grid
P_{bat}	Measured battery inverters AC power
SOC	Battery state of charge

For more information see also poster "Validation of a Energy Management Strategy for a BIPV System with a Vanadium Battery Demonstrator".

Validation of a Energy Management Strategy for a BIPV System with a Vanadium Battery Demonstrator

Luis Fialho[1], Tomás Fartaria[1], Manuel Collares Pereira[1]
[1] ST Renewable Energies Chair, Universidade de Évora, Portugal

BIPV System Demonstrator

Vanadium redox flow Battery:

- 5 kW nominal power
- 60 kWh capacity

Battery Inverters: 3x2.4 kW nominal power

PV installation: 6.74 kWp (m-Si and p-Si)

PV inverter: 12.5 kW nominal power (2 MPPT)

Three phase installation

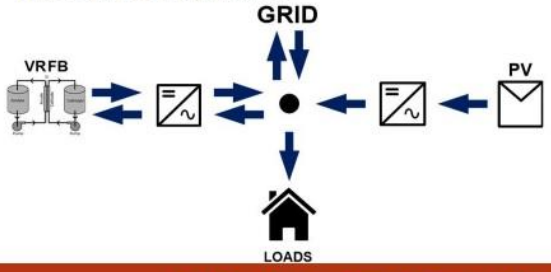

Self Consumption Optimization Strategy

General Objective:
Study of grid interface in rooftop PV systems with energy storage.
The specific objective for this energy strategy is to maximize the consumption of locally produced PV power, hence minimizing the injection of power into the electrical grid.

Implementation:

$P_{setBat} = P_{pv} - P_{load}$

$P_{grid} = P_{setBat} - P_{bat}$

Due to technical operational limits (voltage and SOC), a control to avoid overdischarge/charge was implemented.

Conclusions:
The strategy achieved a minimized peak power (1.4kW) exchange with the grid, even at lower SOC levels (SOC<30%).

P_{setBat}	AC Power command to battery inverter
P_{pv}	PV AC power
P_{load}	Loads AC power consumption
P_{grid}	AC Power exchange with the grid
P_{bat}	Measured battery inverter AC power
SOC	Battery state of charge

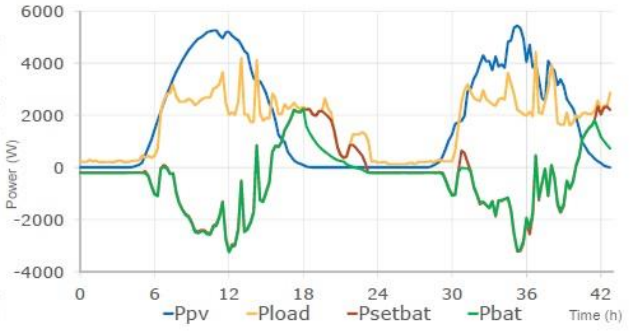

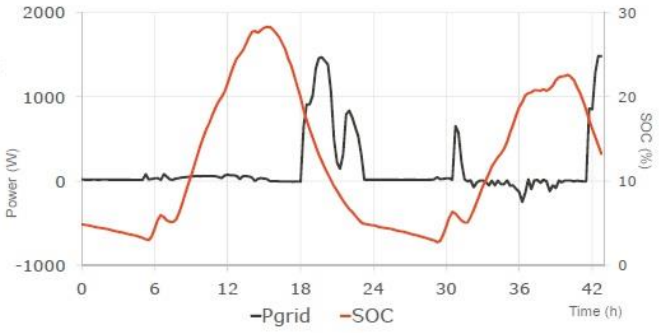

For more information see also poster "Performance Characterization of a Vanadium Redox Flow Battery".

Performance Characterization of a Vanadium Redox Flow Battery

Luis Fialho[1], Tomás Fartaria[1], Manuel Collares Pereira[1]
[1] ST Renewable Energies Chair, Universidade de Évora, Portugal

Vanadium Redox Flow Battery

Specification	Value
Number of cells	40
Tank volume	2x1800 l
Maximum current	200 A
Nominal Power	5 kW
Storage capacity	60 kWh
Battery inverters nominal power	3x2.4 kW

Test 1 – Full Cycle Charge/Discharge Efficiency cell

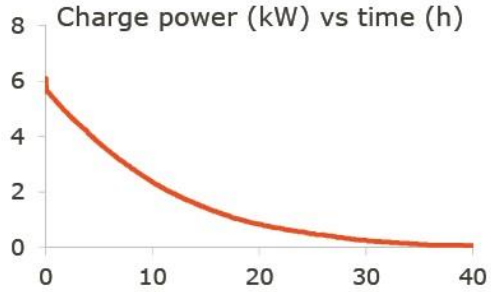

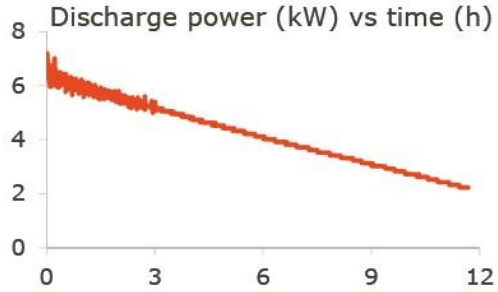

Test 2 – State of Charge (SOC) vs Voltage of reference

Conclusions:

The tests performed are in accordance with the specifications provided by the battery manufacturer.

The inverters voltage range limit the battery capacity to 60 kWh.

The reference cell voltage is not affected by the battery charge/discharge state. The reference cell allowed a precise SOC measurement.

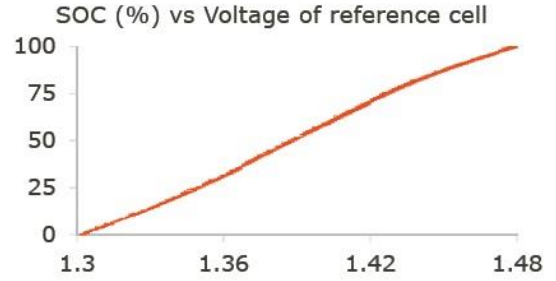

For more information see also poster "Validation of a Energy Management Strategy for a BIPV System with a Vanadium Battery Demonstrator".

Scientific poster presented at the 2018 NREL/SNL/BNL PV Reliability Workshop

PEARL PV

EU COST Action PEARL-PV:

Performance and Reliability of Photovoltaic Systems: Evaluations of Large-Scale Monitoring Data

WG5: PV in grids

Marios Theristis[a], Carolina Senabre[b], Emilio Gómez[c], Sonia Pinto[d], Luis Fialho[e], Emilio Muñoz[f], Jonathan Leloux[g]

a) PV Technology Laboratory, University of Cyprus, Nicosia, Cyprus, b) Universidad Miguel Hernández de Elche, Elche, Spain, c) Renewable Energy Research Institute, Universidad de Castilla-La Mancha, Albacete, Spain, d) DEEC, Instituto Superior Técnico, Lisbon, Portugal, e) Department of Physics, Universidade de Évora, Évora, Portugal, f) IDEA Research Group, Universidad de Jaén, Jaén, Spain, g) Universidad Politécnica de Madrid (UPM), Madrid, Spain

Introduction The EU COST Action PEARL-PV was initiated at the end of 2017. PEARL-PV is the abbreviation for "Performance and Reliability of Photovoltaic Systems: Evaluations of Large-Scale Monitoring Data". The Action entails the formation of an inclusive network of PV researchers/experts and the **largest-ever agglomeration of PV systems performance data in Europe** that will be analyzed in order to include more-nuanced evidence-based reliability of PV system evaluation methods, simulation and design tools. To execute the research proposed, 5 Working Groups have been set up that will conduct research using a shared data bank, simulation tools and models in order to analyze and compare these data. The 5 Working Groups are focused on (WG1) **PV monitoring**, (WG2) **PV simulation**, (WG3) **Reliability and durability of PV**, (WG4) **PV in the built environment** and (WG5) **PV in grids**.

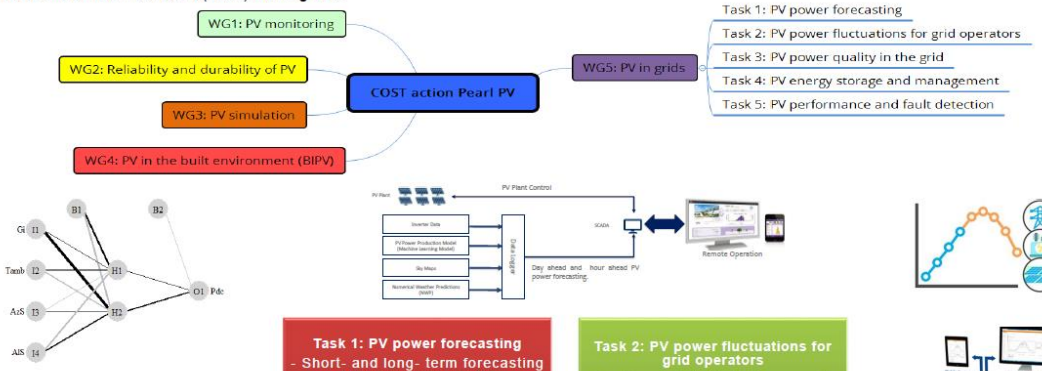

WG Objectives

- Improve PV grid integration
- Enhance PV performance
- Understand the behaviour
- Use information from WG1 - WG4

Task 1: PV power forecasting
- Short- and long- term forecasting of PV power generation
- Numerical weather predictions, satellite and sky images
- Machine learning techniques
- Application to different climates

Task 2: PV power fluctuations for grid operators
- Feeding distributed PV power into grids under variable conditions
- Impact of PV power fluctuations
- Correlation of PV fluctuations between neighbouring installations

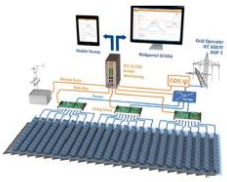

Task 3: PV power quality in the grid
- Power quality indicators
- Harmonics, frequency, voltage, current intensity, power factors

Task 4: PV energy storage and management
- Matching electricity demand with supply
- Electric vehicles and other storage solutions

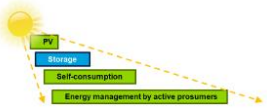

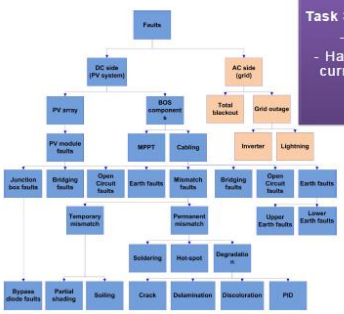

Task 5: PV performance and fault detection
- Failure detection and classification techniques
- Micro- to macro-scale failure detection
- Machine learning techniques
- Peer-to-peer approach
- Bulk data handling of real applications installed in EU

Acknowledgements

We would like to thank all 23 participants of PEARL PV WG5 for their enthusiasm and efforts.
This poster is based upon work from COST Action PEARL-PV CA16235, which is supported by COST (European Cooperation in Science and Technology).
COST (European Cooperation in Science and Technology) is a funding agency for research and innovation networks. Our Actions help connect research initiatives across Europe and enable scientists to grow their ideas by sharing them with their peers. This boosts their research, career and innovation, see www.cost.eu.

Contact

WG5 Chair: Jonathan Leloux at jonathan.leloux@upm.es
WG5 Vice Chair: Marios Theristis at theristis.marios@ucy.ac.cy
www.pearlpv-cost.eu and
www.cost.eu/COST_Actions/ca/CA16235

cost EUROPEAN COOPERATION IN SCIENCE & TECHNOLOGY

PEARL PV

UNIVERSIDADE DE ÉVORA
INSTITUTO DE INVESTIGAÇÃO
E FORMAÇÃO AVANÇADA

Contactos:

Universidade de Évora

Instituto de Investigação e Formação Avançada - IIFA

Palácio do Vimioso | Largo Marquês de Marialva, Apart. 94

7002-554 Évora | Portugal

Tel: (+351) 266 706 581